THE COATING BEHAVIOR AND SYNTHESIS PROCESS OF PERFLUOROCARBON EMULSION

by

Chun-Jen Wu

A dissertation submitted to the faculty of
The University of Utah
in partial fulfillment of the requirements for the degree of

Doctor of Philosophy

Department of Materials Science and Engineering

The University of Utah

December 2013

The University of Utah Graduate School

STATEMENT OF DISSERTATION APPROVAL

The dissertation of **Chun-Jen Wu**

has been approved by the following supervisory committee members:

Agnes Ostafin	, Chair	**10/24/2013** Date Approved
John Morrison Veranth	, Member	**10/28/2013** Date Approved
Ling Zang	, Member	**10/24/2013** Date Approved
Ashutosh Tiwari	, Member	**10/31/2013** Date Approved
Jennifer Shumaker-Parry	, Member	**10/24/2013** Date Approved

and by **Feng Liu**, Chair of

the Department of **Materials Science and Engineering**

and by David B. Kieda, Dean of The Graduate School.

ABSTRACT

In this dissertation, the surface coating method/characteristics and a novel synthesis method for perfluorocarbon (PFC) emulsions were studied. These materials have relevance in a wide range of industrial and biomedical areas. Electrostatic coating of emulsions with poly-L-lysine (PLL) and chitosan (CS) was used to enhance the stability of the emulsions against phase separation. The ionic surfactant, 1,2-dioleoyl-sn-glycero-3-phosphate, DOPA, was used as an additive to the nonionic surfactant lecithin in order to increase the surface charge of the emulsion surface and facilitate accumulation of coating materials on the emulsion surface. Analysis of zeta potential versus pH was used to establish the best conditions for the coating process. The particle size and zeta potential was used to follow the coating progress. To characterize the final product, colorimetric determination was used to measure the bound/unbound fraction of PLL and CS and this was compared with a model-based analysis of zeta potential as a function of coating. Through this comparison and accounting for experimental error, a discrepancy in the effective particle number was revealed that was interpreted in terms of the compression and expansion of coating molecules on the surface as it assembles. Fluorescence quenching measurements using pyrene and fluorescein-doped emulsions supported the compression/expansion concept, resulting in more quenching when expansion of the coating took place. Thermodynamic analysis also supported these conformation changes and indicated a lowering of surface free energy for expanded coating.

The second part of the dissertation reports a novel cosolvent method to synthesize PFOB emulsion with high yield production, in contrast to traditional extrusion methods that generate a large amount of water-filled liposomes as a side product. It was found that the selection of best cosolvent is related to its polarity relative to that of perfluorooctyl bromide (PFOB). Fourier transform infrared spectroscopy (FTIR) analyses were used to measure the retention of PFOB and revealed that nonpolar hexane has the best PFOB retention ability compared to methanol, ethanol, and chloroform. Moreover, phase transition temperatures (PTT) of the hexane/PFOB/lecithin system were observed at 13~19 °C and 22~24 °C by monitoring both the change in transparency by UV-Vis spectrophotometry and PFOB retention by FTIR. If emulsions are produced above the PTT (at 30 ^{o}C), PFOB is not retained. Quantitative measurement using FTIR for the best conditions gave 72% PFOB retention using the cosolvent method. Fluorescent and density analysis by centrifugation indicated that the traditional method for emulsion synthesis (directly emulsified) produced significantly more low-density water-filled liposomes than the cosolvent method. Higher density PFOB emulsion made with the cosolvent method can be easily separated and concentrated by centrifugation. The image of emulsions made by the traditional and cosolvent method could be viewed by cryogenic transmission electron microscopy.

TABLE OF CONTENTS

LIST OF FIGURES

LIST OF TABLES

ACKNOWLEDGEMENTS

The dissertation would not have been possible without the help of many people in many ways. I would like to express my deepest appreciation to my advisor, Professor Agnes Ostafin, who always gives me the useful inspiration and the meaningful thought. She patiently showed me how to think about the questions scientifically and solve them logically. Also, Dr. Hiroshi Mizukami and Dr. Michael Batenjany also provided a lot of great idea for my experiment. In my lab, I really had a good time with Yen-Chi Chen, Kyu-Bum Han, and Curtis Takagi, and they helped me a lot on my studies and experiment. Samia Awan and Shukaria Rajabi also helped me do the experiment together.

I also would like to thank my committee, Dr. Ling Zang, Dr. Ashutosh Tiwari, Dr. Jennifer Shumaker-Parry, and Dr. John Veranth Morrison. They gave me precious suggestion for my qualified exam and research. Also, Dr. David Belnap helped me with TEM pictures.

Finally, I would like to thank my parents and my sister, who give me the endless support and love for my life. My fiancée, Rita Hsiang, also takes care of me. I want to show my gratitude to all of them.

CHAPTER 1

INTRODUCTION

1.1 Overview

For several decades, blood substitutes have enjoyed generous investment and intensive research. Although blood transfusion is still the mainstream clinical treatment, there are some unavoidable issues like limited lifetime of blood storage (35 to 42 days, at 2-6 °C), shortage during emergency demand (war, trauma, and disaster), and blood donations declining for all types of blood [1]. A side-effect of transfusion is that recipients could experience reduced immune response, so-called immunosuppressive effect [2-4]. Another critical issue is that blood transfusion still has the potential risk of blood-borne disease such as hepatitis C [5], HIV [6], Cruetzfeld-Jacob [7], and SARS [8]. Hence, blood substitutes in the form of synthetic nonhuman/animal materials are vital and necessary for the future welfare of humans to meet the acute need for blood transfusion [9].

The first development of blood substitutes dates back to the early 1600s when sheep's blood was transfused to the wounded soldiers [10]. After that, ale, wine, and opium were attempted in the mid-1600s [11]. In the 19^{th} century, milk from cows, goats, and humans was used as well [12]. Of course, these blood substitutes did not work well due to severe reactions. Until 1949, an experimental hemoglobin saline solution was used to treat

patients with postpartum hemorrhage after exhausting available compatible banked blood, but the patients died due to renal failure [13]. It was reported in 1966 that mice immersed in perfluorocarbon liquid saturated with oxygen could survive up to 10 min [14]. The idea of polymerized hemoglobin-based oxygen carriers (HBOCs) was first proposed in 1978 to avoid the serious systemic toxicity problems when stroma-free hemoglobin solution is infused into patients [15]. Although not available commercially, perfluorocarbons (PFCs) and hemoglobin-based oxygen carriers remain the two main blood substitute candidates [16-18].

Schmidt revisited perfluorocarbon as the base material on which to design a blood substitute, coating it with an inorganic rigid layer [19-23], but since then, our research group has encountered problems in the production and stability. The focus of this work is to produce a reinforced, perfluorocarbon-based blood substitute using layer-by-layer deposition of biological polymers at high reaction yields. The challenges in this area include: 1) poor understanding of the relation of polymer structure to emulsion phase stability, 2) dynamic changes of the conformation of lipids/polymers on the emulsion surface and how it affects gas exchange and interactions with other molecules in the blood, and 3) how to produce materials with high yield.

In this project, we focus on two issues: 1) how to characterize the emulsion coating process and characteristics of the coating, and 2) how to produce high yield of emulsion.

For the first issue, we chose two different molecules, poly-L-lysine (PLL) and chitosan, to coat the surface emulsion. Both molecules have the ability to modulate their surface charges for layer-by-layer deposition via pH titration due to amino acids in PLL and amine groups in chitosan. In this thesis, PLL with molecular weight between 500~2000 and

chitosan with molecular weight 150,000 were used for emulsion coating. PLL and chitosan have 8.6 and 837.2 repeat units in their structure so it can be expected that PLL is a short-chain molecule and chitosan is a long-chain molecule.

We developed a method to characterize the process of coating of an emulsion with PLL and chitosan that utilized a combination of calculation and zeta potential measurement, and used it to quantify the degree of emulsion coating and the properties of the coating at various time points in the coating process. For the second issue, we demonstrate an improvement in production efficacy of emulsion using a method of cosolvent addition. The concept has been tried in other emulsion systems [24, 25], but not reported in the literature for perfluorocarbon-based systems.

This work should be helpful for the synthesis and further development of the perfluorocarbon-based system as an artificial oxygen carrier (AOC). In addition, it is a new approach for the study and prediction of the conformation of polymeric coating materials on emulsions and other microparticles. This is important in the design of drug delivery particles and active thin film coatings. The cosolvent method could be used to synthesize at high yield a variety of oil-in-water (O/W) systems for drug delivery, cosmetics, and food industry.

1.2 Background

1.2.1 Blood substitutes: HBOCs and PFCs

HBOC production starts from purified cell-free hemoglobin (Hb), which is derived from human or animal blood by lysing red blood cells (RBCs) and removing pieces of cell membrane and other proteins [26]. Cell-free Hb, also called stroma-free hemoglobin

(SFHb), is supposed to have no antigenicity, better immunologic and allergic responses compared to RBC, and a prolonged lifetime [27, 28]. However, it needs modification to express similar properties as Hb still inside in RBCs because outside the cell, SFHb shows irreversible high oxygen affinity, contributes to elevated oncotic pressure via reaction with NO, and experiences rapid intravascular clearance, thus reducing its duty time [26, 27]. Modified SFHb can fix some of these issues but still has serious problems of renal toxicity [27, 29, 30], hypertension and vasoconstriction [31-33], gastrointestinal distress [32, 34], neurotoxicity [35-37], free radicals [38-40], and platelet and coagulation effects [41-43]. HBOCs that have made it to various stages of clinical trials include poly-SFHb-P (PolyHeme®) [44, 45], HBOC-201 (Hemopure®) [46-48], rHb1.1 and rHb2.0 (Optro™) [49-51], Hb-raffimer (HemoLink™) [52, 53], and DCLHb (HemoAssist™) [54, 55]. Although these products have excellent oxygen affinity and shelf time, they still have many obstacles to overcome in order to be a safe and effective HBOC product [26].

Perfluorocarbons (PFCs), another candidate for blood substitutes, are derived from hydrocarbons by replacing all the hydrogen atoms with the fluorine atoms. PFCs used as an HBOC are colorless liquids with high density (usually up to twice that of water) and low viscosity (due to low intermolecular attraction forces). The first PFCs were developed as a part of Manhattan project during War World II to use as an insulating material [56]. In mid-1960, it was later discovered that the synthetic PFCs could dissolve and transport a large quantity of nonpolar gas such as nitrogen and oxygen [57, 58]. Due to the strongest carbon fluorine bond in organic compound, PFCs are inert and fairly chemically stable in human body, suggesting they should be quite safe for blood substitutes [59]. However, PFCs cannot be used directly since they are immiscible with aqueous solutions, like plasma.

Emulsification before introduction into blood stream is necessary. Fluosol® was the first approved PFC-based artificial blood substitute by the US Food and Drug Administration (FDA) [16, 60]. Details about related PFC products will be illustrated more in Section of 1.2.2.

In this study, PFCs were used as the starting point of blood substitutes because they are much less toxic than HBOCs.

1.2.2 Perfluorocarbon-based products

Many biomedical applications for PFCs can be listed, such as anticancer agents [61-63], perfusates for isolated organs [64], cell culture media supplements [65, 66], liquid ventilation fluids [14, 67, 68], surgery tools in ophthalmology [69, 70], and diagnostic imaging agents [71-73]. In this section, perfluorocarbon-based products utilized mainly for blood substitutes are listed and discussed in greater detail.

For the first generation of PFC emulsion, Fluosol® by Green Gross, Japan was the first proposed commercially in 1989 and approved by FDA [16]. It was originally used clinically as an oxygen-carrying adjunct to coronary balloon angioplasty for patients with high risk. This product ceased production in 1994 for economic reasons as it was seldom used by cardiologists during angioplasty [74]. Other limitations of Fluosol® included storage problem (unstable in room temperature), relatively poor O_2 carrier efficacy (compared to hemoglobin), and activation of Pluronic F68 by the complement system activating and altering white blood cell function. Another product Oxypherol also from Green Gross, Japan was not used clinically due to long retention half time (> 500 days) of PFC in the human body [75]. Perftoran®, produced in Russia, is used as a temporary

intravascular oxygen carrier for haemorrhagic shock patients and perfusate for isolated human organs from Russia was approved in 1995-1996 by the Russian health regulatory authorities [76].

The second generation of PFC emulsion was improved by focusing on biocompatibility and excretion in the human body via the molecular weight selection of PFCs, prolonging the shelf-life by adding perfluorinated stabilizers and surfactants, and manufacturing concentrated emulsions with larger PFC molecules but with lower viscosity [75, 77]. Oxygent™, with 4 days of retention half time proposed from USA, can be stored more than one year at 5 to 10 °C and it has completed phase III in Europe, May 2000 [75, 78-80]. Similarly, Oxyfluor™ with added safflower oil and egg yolk phospholipids as the stabilizer and surfactants was developed in USA [81-83]. For now, it mainly has been the commercial product as an oxygen scavenging enzyme [84-86]. Other products like Fluxon and Oxycyte® (Oxygen Biotherapeutics, Inc.) were also synthesized for the improvement of the stability or appropriate retention half time [75, 87, 88]. However, the current status of Fluxon is not clear. As for Oxycyte®, it is approved currently for phase II-b trials in the United States, and for phase II-b clinical trials in Switzerland and Israel for use in treating traumatic brain injury (TBI) [89, 90]. It has been targeted as an oxygen therapeutic rather than a blood substitutes [91].

1.2.3 PFC candidate - perfluorooctyl bromide (PFOB)

The development of second-generation PFC emulsions in the West described in the previous section has focused on linear perfluorocarbon molecules such as perfluorooctyl bromide (C8F17Br) or perfluorodecyl bromide (C10F21Br) [75, 78-80]. In this dissertation,

perfluorooctyl bromide (PFOB), also referred to as 1-bromoperfluorooctane and perflubron, was chosen for the following research. The principal consideration for the selection of this PFC relates to its retention half time in human body and its efficacy of oxygen solubility and delivery.

The organ retention half time of PFCs in human body primarily depends on the molecular weight, and molecular structure and the presence of heteroatoms or cycles have minimal influence [92]. It is usually acceptable for PFCs with molecular weight around 460 to 500 g/mol, which have organ retention half time around 10 to 50 days [93]. From animal studies, the retention half time of PFOB (molecular weight: 499 g/mol) is approximately 4 days [93, 94]. Then, PFOB becomes vapor gradually and leaves from the human body through the lung [95]. PFOB can be manufactured with a high degree of purity, which means unwanted side products can be avoided. In the past, physiological side effects have often been attributed to partially fluorinated contaminants [96]. Compared to perfluoro-2-methyloctane, perfluoro-2-methyl-3-isopropylpentane, perfluorodecane, perfluoro-2,7-dimethyloctane, 1-bromoperfluorohexane, 1-bromoperfluoroheptane, 1-bromoperfluorodecane, 1-iodoperfluorodecane, and perfluorotributylamine (FC-47), PFOB shows excellent values of oxygen capacity in room air (1.0 ± 0.4 ml O_2/100ml emulsion) and saturated with 97% O_2 / 3% CO_2 (5.3 ± 0.2 ml O_2/100ml emulsion) as it was emulsified by a nonionic surfactant, Pluoronic® F-68 [97]. The terminal bromine atom on the PFOB molecule confers relative lipophilicity, which improves its ability to be emulsified by surfactants [98, 99]. Hence, this is the reason that PFOB could be an excellent candidate in this work.

1.2.4 PFOB emulsion and colloidal system

Due to their high lipophilicity, surfactants are necessary to emulsify PFOB so it can be used in an aqueous system for biomedical applications. As a second-generation injectable blood substitute, egg yolk phospholipids (EYP) were successfully utilized to emulsify perfluorocarbon [81-83]. From thermodynamics, an emulsion is an unstable system because of Ostwald ripening, which is the basic mechanism by which small droplets grow into large droplets through the process of molecular diffusion [100-102]. During the process, small PFOB droplets diffuse through the continuous aqueous phase toward large droplets at the expense of the former [103]. For this reason, emulsions usually have a storage problem at room temperature. Some reports related to the second-generation PFC emulsions show that a small amount of additive can significantly retard the process of Ostwald ripening [75, 77, 104]. In this work, PFOB was emulsified by surfactants and coated with additional molecules. This should also reduce the possibility of Ostwald ripening, in addition to reinforcing the mechanical stability of the particle. Details about emulsion coating will be illustrated later.

The main emulsification lipids used for biomedical applications are phospholipids. They have components of one hydrophilic head group and one or two hydrophobic tails. Once the surfactants are in the boundary of oil and water, the tails insert into oil and the head group orients toward the water. Once equilibrium has been reached, the interfacial tension between two liquids is lowered and the surfaces in this system experience less driving force to change, so the system is stable. The geometry or structure of the emulsion particles is strongly dependent on the amount and structure of the emulsifier, temperature, and presence of impurities. As surfactants (or lipids) are added in increasing amount into

an emulsion, different phases such as reverse emulsions, liposomes, micelles, and reverse micelles can be formed [105-107] (Figure 1.1).

To use PFOB emulsions as a blood substitute, an oil-in-water (O/W) emulsion with highest volume of PFOB is desired, as shown in Figure 1.1 (a). In Figure 1.1 (d), a micelle with limited diameter around 20 nm can only carry a small amount of PFOB. If the ratio of oil to water increases to a certain level, the oil-in-water emulsion tends to become water-in-oil emulsion, shown in Figure 1.1 (b), doing so by passing through a complex bicontinuous phase. In some situations, reverse micelles in Figure 1.1 (e) would form in the oil-in-water system. Liposomes are sometimes generated in the system of oil, water, and surfactant because of the presence of extra surfactant in water relative to the oil. Liposomes are usually synthesized by adding lipid in water [108-110].

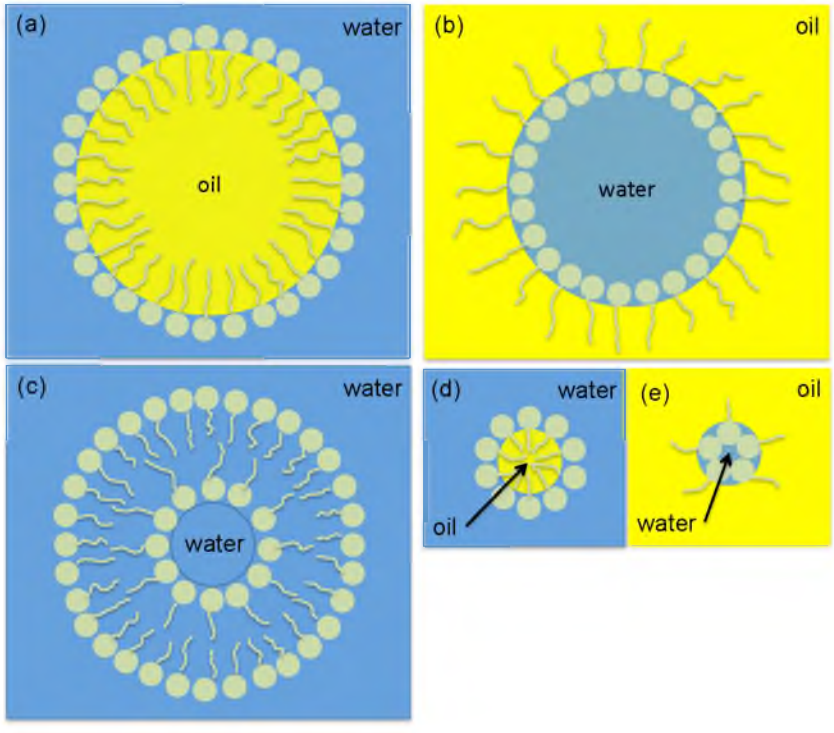

Figure 1.1 The structures of various colloid systems: (a) oil-in-water (O/W) emulsion, (b) water-in-oil (W/O) emulsion, (c) liposomes, (d) micelle, and (e) reverse micelle

1.2.5 The other biomedical applications of PFOB emulsion

In this section, other biomedical applications of PFOB emulsions (except for blood substitutes or high oxygen capacity related applications such as perfusates for isolated organs, cell culture media supplements, liquid ventilation fluids, and surgery tools in ophthalmology) are introduced.

1.2.5.1 Contrast agents for ultrasound imaging

In order to use ultrasound in diagnosis, a good sound reflector should be used. The optimal reflector, or contrast agent, for ultrasound are tiny gas bubbles, that can be highly compressed by the sound waves [111-113]. The key to good contrast is that the bubble compress much more (absorbing more energy) than the surroundings that may contain cells such as red blood cells. However, there are no ideal injectable gas bubbles because the diameter of bubbles cannot be controlled and the circulation time is not be long enough for imaging (the air in gas bubbles tends to diffuse out due to the combination of surface tension (Laplace pressure) and blood pressure). For osmotic stabilization, the partial vapor pressure of PFC can be applied in gas bubble to counterbalance the surface tension and blood pressure so osmotic stabilization in gas bubbles can be achieved [73, 114, 115]. Imavist™ has been developed as an ultrasound contrast agent based on PFOB emulsion [116, 117].

1.2.5.2 Contrast agents for magnetic resonance imaging (MRI)

For MRI, superparamagnetic iron oxide nanoparticles (SIONs) with high sensitivity are used widely, but they cannot be detected directly, so excretion and tissue retention can

deplete MRI signal in the human blood stream to influence the final result of imaging [118-120]. It would be very difficult to interpret if darker areas are from nanoparticles or from other inhomogeneities by anatomic proton (^{1}H) MRI [119]. PFC can be used alternatively as an MRI contrast agent because of the presence of its natural fluorine isotope ^{19}F, which has similar sensitivity to ^{1}H [121, 122]. Basically, ^{19}F has 100 % natural abundance because no other isotopes exist in significant quantities due to their unstable property [123]. The lack of ^{19}F background in the human body results in high imaging specificity. This isotope can also be applied to measure tissue oxygen tension and to map oxygen in tissue via the ability of nearby paramagnetic oxygen molecules (O_2) to perturb the signal of ^{19}F MRI [124, 125]. In various reports, myocardial vascular volume [126], local cerebral volume [127], and tumor imaging [128] were studied by utilizing PFC contrast agents for ^{19}F MRI.

1.2.5.3 Contrast agents for computed tomography (CT) and sonography

PFOB can be used as a contrast agent in CT because it is radiopaque [129]. Thus, it has the unique ability to enhance the signal of blood vasculature, whereas other contrast agents only enhance imaging of the liver and spleen [130, 131]. This is because PFOB emulsions introduced by IV injection, unlike water-soluble contrast media, do not diffuse into the interstitial space. This can prolong the circulation time in blood vasculature since it is less likely to be filtered by the kidneys [132]. Due to the limitations of water-soluble contrast enhancers, PFC emulsion is a potential substitute [133].

1.3 Emulsion manufacture and challenges

1.3.1 Introduction of homogenizers

It is essential to add a surfactant in order to emulsify PFOB in aqueous solution. To acquire a uniform emulsion consisting of specifically-sized particles homogenization, using intense mechanical agitation is needed [134, 135]. There are several types of homogenizers such as high-speed blender, high-pressure homogenizer, colloid mill, high shear disperser, ultrasonic disruptor, and membrane homogenizer [136, 137]. A high-speed blender with a stirring vessel is fairly inexpensive, so it is widely used for synthesis or mixing [138-140]. A broad size distribution and large particle size of the products results, therefore, a high-speed blender usually is used for the premix production. A high-pressure homogenizer is the most commonly used method for producing fine (submicron) emulsions in food industry [141]. In this device, the emulsions collapse into smaller ones as coarse emulsions enter into the homogenizer valve and eject from the exit [142]. This technique also has been used extensively for emulsion manufacture [143-145]. A colloid mill is used in the food industry to make emulsions with medium or high viscosity [146]. Emulsion rather than the separate oil and aqueous solution is fed into a narrow channel between the rotor (a rotating disk) and the stator (a static disk). The shear stress in the channel can reduce the particle size of the emulsion [134, 147]. The emulsion size can be controlled by the speed of the rotor and the thickness of the channel. The basic design principal of a high shear disperser is similar with a colloid mill, which both have the system of rotor and stator [148]. The coaxial intermeshing rings with radial openings in a high shear disperser could generate high shear forces and turbulent flow to disrupt the emulsion into smaller droplets [149]. An ultrasonic disruptor used sound waves exceeding a frequency of 20k Hz that is

generated by piezo-electric or magneto-restrictive transducers. The generated waves could disrupt the emulsion by inducing cavitation in which smaller local pressure is less than the vapor pressure of the solvent [150, 151]. A membrane homogenizer can produce narrow particle size distribution of the emulsion by pushing the disperse phase or emulsion through the microporous membrane against high pressure [152, 153]. This process is called extrusion, and the resulting particle size mainly depends on the membrane pore size, applied pressure, and materials. For high dispersed phase concentrations, recirculation could make it a time-consuming process. In this study, membrane homogenization (or extrusion) is the preferred method to homogenize PFOB emulsion for a smaller size and a narrow size distribution.

1.3.2 Selection of surfactants

Typically, surfactants have one hydrophilic side called a head group and one hydrophobic or lipophilic side called a tail. Most surfactants have similar tails made of linear, branch, or aromatic hydrocarbons and usually have either one or two tails in their structure. Hence, most surfactants could be classified into various types by means of their polar head groups, such as nonionic surfactant, ionic surfactant (anionic and cationic surfactant), and zwitterionic surfactant [154]. Because the coating of the emulsion by electrostatic forces will be conducted for our emulsion design, ionic surfactants can provide more surface net charges for coating than the nonionic one in this work. However, charge lipids are general more expensive than neutral lipids, and the cost considerations of large-scale emulsion manufacture suggested that the combination of ionic and non-ionic surfactants may be preferred. The nonionic surfactant, L-α-phosphatidylcholine (lecithin),

and anionic surfactant, 1,2-dioleoyl-sn-glycero-3-phosphate (sodium salt) (DOPA), were used in this work. In eukaryotic cells, phosphatidylcholine (lecithin) is the major phospholipids in cell membrane [155-157], which serves as a reservoir of several lipid messengers [158]. The toxicity of lecithin was reviewed in previous studies, and it has been applied in many biomedical applications such as drug delivery, gene delivery, vaccination, diagnosis, and so on [159-163]. In addition, lecithin from soy has huge potential for large-scale production owing to its low cost and large production volume. DOPA is a synthetic phospholipid that could provide highly negative charge at most working pH, but it is expensive. Only a small amount was used to improve the surface potential of lecithin emulsion by integrating it with lecithin.

1.3.3 The challenge of emulsion manufacture

Emulsions may be transiently or permanently stabile. The kind of surfactant is the ingredient that leads to the formation of an ideal, stable, and uniform emulsion from the oil and aqueous solution. However, depending on the thermodynamics of the system, the emulsion could break completely (known as coalescence) and form two separated layers of oil and water solutions during a period of time. This process could occur by four possible mechanisms such as creaming, Brownian/sedimentation flocculation, and disproportionation [164-168]. The first three are primary mechanisms that destabilize emulsion and all the four mechanisms could occur simultaneously and in any order [169, 170].

During the process of creaming, the emulsion does not actually break but instead there is a separation of the emulsion into two emulsions, each of which have a different ratio of

oil to aqueous solution. Creaming, typically the precursor to coalescence, is the main process to form a disperse phase separated from an emulsion. According to Stoke's equation, creaming is caused mainly by the density difference of oil and aqueous solution [166, 171, 172]. The equation can be shown:

$$\upsilon = 2\, r^2\, (\rho - \rho_0)\, g / 9\, \eta \qquad (1.1)$$

where

υ is the creaming (setting) rate,

r is the emulsion radius,

ρ is the density of emulsion,

ρ_0 is the density of dispersion medium,

g is the acceleration of gravity,

η is the viscosity of dispersion medium

From the above equation, it is clear that the creaming rate is reduced for small radius size emulsions, small density differences between oil and aqueous materials, and high viscosity. For biomedical applications of PFOB emulsion, a small particle size is desired, but high viscosity of emulsion suspension should be avoided. The large density difference between PFOB and water is unavoidable. So the stability of PFOB emulsions against creaming could be a challenge for two out of three reasons.

Flocculation generally is defined as the aggregation of emulsions. Emulsions can keep their integrity without coalescence, but they can attract each other to form clusters by various mechanisms such as Van der Waals forces [173, 174]. Separately, Brownian

flocculation is viewed as random movement of emulsions and sedimentation flocculation is viewed as vertical movement. Both flocculations occur simultaneously in an emulsion and the behaviors can be expressed by the following equation [175],

$$\Gamma_{max} = 2 \pi (\rho - \rho_0) g r^4 / 3 k_b T \quad (1.2)$$

where

Γ_{max} is the relative rate of each type of flocculation,

ρ is the density of emulsion,

ρ_0 is the density of dispersion medium,

g is the acceleration of gravity,

r is the emulsion radius,

k_b is Boltzmann constant,

T is absolute temperature (Kelvin)

If the value of $\Gamma_{max} > 10$, Brownian flocculation can be negligible. If the value of $\Gamma_{max} < 0.1$, sedimentation aggregation is negligible. A simple calculation can be done by applying $\rho = 1.93$ g/ml (PFOB), $\rho_0 = 1$ g/ml (water), g = 9.8 m/s^2, r = 200 nm, and T = 300K. The value of relative rate for flocculation is then around 7.4×10^{-3}, which means there should be Brownian flocculation, but no sedimentation aggregation. It should have some influence for the stability of emulsion by Brownian flocculation.

Disproportionation is a process related to Ostwald ripening. Smaller emulsions tend to diffuse toward and mix with larger emulsions at the expense of smaller emulsions due to

the vapor pressure difference of large and small emulsion. The difference in pressure provides the driving force, shown by the Kelvin equation [176, 177],

$$\ln (P_0 / P) = 2 \gamma V_m / r R T \quad (1.3)$$

where

P_0 is the vapor pressure of the dispersion medium,

P is the vapor pressure of emulsion,

γ is the surface tension of the dispersion medium,

V_m is the molar volume of the disperse phase,

r is the emulsion radius,

R is gas constant,

T is absolute temperature (Kelvin)

From the Stokes-Einstein equation, the diffusion rate (D) depends on the viscosity of the disperse phase and the particle size of emulsion [178, 179]. It can be shown as the following:

$$D = k_b T / 6 \pi \eta r \quad (1.4)$$

where

k_b is Boltzmann constant,

T is absolute temperature (Kelvin),

η is the viscosity of dispersion medium,

r is the emulsion radius

For the PFOB emulsions we are trying to produce, the viscosity of the dispersion medium cannot be too high [180] and the particle size should be around hundred nanometers. This means the Ostwald ripening diffusion rate between emulsion particles could be relative high.

A final challenge of emulsion manufacture is that liposomes could be accidentally generated during the emulsion production. It is inevitable to have liposomes by the method of blending oil, aqueous solution, and surfactants [181, 182].

1.4 Design of coating on emulsion surface

1.4.1 Overview: Why is coating necessary?

The purpose of emulsion coating can be listed as the enhancement of emulsion structure strength, the reduced possibility of biological removal and blood vessel penetration (the increment of blood circulation period), and the feasibility of other biomedical applications. It will be introduced in the following section.

1.4.1.1 The enhancement of emulsion structure strength

In the previous section, creaming, Brownian/sedimentation flocculation, and disproportionation (Ostwald ripening) could worsen the stability of the emulsion especially in fluid shearing conditions [183]. Many studies have reported that the shear stress in human blood vessel is relatively high [184-189]. Based on hemodynamics, laminar shear stress of blood vessel is normally about 2.5~46 dyn/cm^2 [190, 191]. Thus injected PFOB emulsions could be easily destroyed or disrupted during blood circulation.

1.4.1.2 The increment of blood circulation period

Emulsion size is another critical issue to point out. Because the smallest diameter of vascular capillaries in body is ~4 μm [192], emulsions that are very large or flocculate significantly could be dangerous because they may be retained/caught by the capillary bed of the lungs [193, 194]. Moreover, macrophages of the mononuclear phagocytosis system (MPS) will try to immediately eliminate intravenously administered emulsions because they are recognized as foreign in the human body [195-197]. However, if the particles are smaller than 4 μm, they are instead eliminated quickly by cells of the reticuloendothelial system (RES) [193, 195]. The RES can capture particles, like 60~90 % particles taken up by in the liver and 3~10 % particles by macrophages in the spleen [198-200]. It is often said that particles up to 100 nm would be phagocytosed by Kupffer cells and particles larger than 200 nm tend to be filtered by spleen [201]. If particles applied intravenously have size between 30 and 100 nm, larger particles tend to be eliminated faster from bloodstream than the smaller ones. Therefore, the larger the particle is, the shorter is its bloodstream half-life period [202].

Because of premature, size-dependent removal by the body's defenses, only part of the administered particles can even reach target cells and tissues by blood circulation. Another bottleneck is the permeability of the vascular capillary wall [203]. There are four types of blood capillaries: tight junction capillaries (such as the blood brain barrier, BBB), continuous capillaries, fenestrated capillaries, and sinusoid capillaries. Tight junction capillaries with connection of their endothelial lining cells, in the central nervous system, are usually hard to penetrate [204, 205]. Continuous capillaries, in major tissues like muscle, skin, lung, and connective tissue, have a limitation for permeation, generally ≤ 6

nm in diameter [206, 207]. Larger particles (50~60 nm) can be excreted from the kidney through its fenestrated capillaries [208, 209]. If particles are larger than 60 nm, they only can be cleared by reticuloendothelial system (RES), which has sinusoid capillaries [210, 211]. These capillaries have usually over 100 nm pores, witch are classified as the open pore capillary.

The particle size of PFOB emulsion should be designed for the desired purpose and duration of use, and remain mainly in blood circulation. In this study, biomaterials coated on emulsion surface for protection were designed to improve the structure strength of the emulsion particles. Besides, coating materials on emulsion surface can provide steric stabilization away from cell absorption such as the elimination of macrophages [212, 213].

1.4.1.3 The feasibility of other biomedical applications

The advantage of coating materials on the PFC emulsion is that the new surface can be tailored for specific biomedical applications like anticancer agents [61-63], tissue engineering [214-217], and drug or gene delivery [80, 218-222]. The new emulsion surface could be designed to improve biocompatibility, increase the dispersion in water, and prolong the circulation time in the blood stream by avoiding protein absorption or macrophage elimination. For the purpose of binding applications, the coated PFC emulsion also can be conjugated to itself or coated with ligands/receptors that can perform specific targeting. Hence, coating of an emulsion surface not only improves emulsion stability but also creates more biomedical opportunities.

1.4.2 Coating materials

In this study, two biomaterials, poly-L-lysine (PLL) and chitosan, were chosen for coating of the PFOB emulsion surface. PLL has charged lysine amino acids and chitosan has amine groups in their molecular structures so each would have net positive charge as pH is lowered and net negative charge as pH is raised. Having these molecules on the surface provides a means for us to control the surface charge or zeta potential of emulsion particles by pH titration.

1.4.2.1 Polylysine (PLL)

Lysine is the essential α-amino acid for human with the chemical formula $HO_2CCH(NH_2)(CH_2)_4NH_2$. Lysines have two types of stereoisomers: L-lysine and D-lysine. Synthetic D-lysine can be converted from L-lysine [223, 224], which is rich in nature. In this work, poly-L-lysine (PLL) was used for one of coating materials on emulsion surface. The chemical structure of PLL is shown in Figure 1.2. Due to amine groups in the structure, the positive or negative charge of PLL would be adjusted by pH titration. If emulsion surface has the opposite electrical charge to that of the coating material, the coating process would be achieved by electrostatic attraction forces.

PLL has been used in various applications. It is usually applied as a food preservative owing to its low cytotoxicity [225-228]. Polylysine has the ability to inhibit the microorganism growth, and can also generate antimicrobial activity, specifically against yeast, fungi, and bacteria [229]. In January 2004, polylysine was certified as "generally recognized as safe" (GRAS) in United States [230, 231]. It also has been widely used as the capsules of the vehicles for gene delivery due to its ability to bind to negatively charged

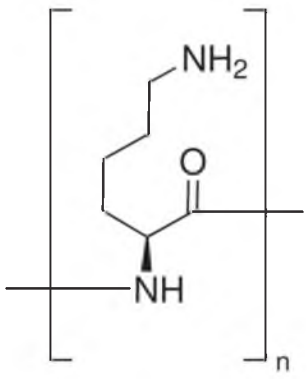

Figure 1.2 The chemical structure of poly-L-lysine. Adapted from Sigma-Aldrich. http://www.sigmaaldrich.com/catalog/product/sigma/p8954?lang=en&region=US

DNA [232-235]. PLL with the excellent biodegradability can also be utilized as the scaffold in tissue engineering [236-241], as well as polymer capsules or carriers in drug delivery [236, 242-244].

1.4.2.2 Chitosan

Glucosamine, which is an amino sugar with chemical formula $C_6H_{13}NO_5$, is part of the structure of polysaccharide chitosan. It is found in the exoskeletons of crustaceans and other arthropods, cell walls in fungi, and other higher organism [245, 246]. The amine groups in its chemical structure take on positive charge at lower pH and negative charge at higher pH. It is similar to PLL in that tunable net electric charge of chitosan would be convenient to tune the process of electrostatic emulsion coating. The chemical structure of chitosan is shown in Figure 1.3.

Chitosan has also been used in various areas such as the automobile industry [247, 248], wastewater treatment [249-251], health care [252-254], and agriculture and horticulture [255, 256]. One of the more famous biomedical applications of chitosan is to use it as a

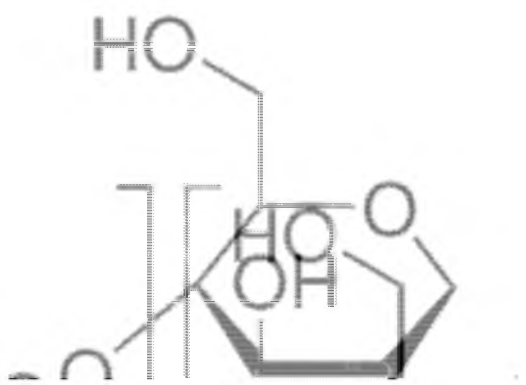

Figure 1.3 The chemical structure of chitosan. Adapted from Sigma-Aldrich. http://www.sigmaaldrich.com/catalog/product/aldrich/740500?lang=en&region=US

hemostatic, mixing chitosan salt with organic acids like succinic or lactic acid [257-261]. Numerous biomedical applications like formation of hydrogels [262, 263], bio-composites [264, 265], or scaffolds for tissue engineering [266-269] were reported. It is characterized by biocompatibility, biodegradability, nontoxicity, and antimicrobial ability [270-272].

In this study, we used PLL with molecular weight between 500~2000 (average molecular weight is around 1250) and chitosan with molecular weight about 150,000 for emulsion coating. Because the unit number of PLL and chitosan can be calculated respectively as 8.6 and 837.2 repeat units in their structure, it can be expected that PLL is a small molecule and chitosan is a huge molecules.

1.4.3 The behavior of coating materials

As mentioned, we can expect improvement in the stability and performance of FOB emulsions if they are coated with something. However, it is fairly difficult to characterize the behavior of the coating materials on the emulsion surface because the measurement is complicated and technique is limited. The conformation or morphology of coating

materials would influence the function of the coating, and this would be affected by coating details, including surface concentration, temperature, and molecular weight of coating material. For example, similar complexity can be in many references wherein the function of surface-attached antigens is different when their conformation changes [273-277]. The conformation of coating materials, especially of protein-based molecules, is critical to their function because some functional domain could be blocked due to the altered conformation. Some insight into the behavior of emulsion coating materials could be gleaned from thin films and Langmuir-Blodgett films [278-282], but being on a curved, submicron surface is significantly more complicated.

Since understanding of the conformation of coating materials is important to predict their performance/function in biology, pharmaceutics, and biomedical applications, in this study, we developed a model to measure/predict the conformation (expansion or compression) of coating materials using simple size and zeta potential measurements and basic calculation.

1.5 Techniques and theories in this work

1.5.1 Extrusion

Extrusion is the process of homogenization by membrane homogenizer to enable an emulsion to be formed with the desired particle size and uniform size distribution [283-285]. The suspension of oil, aqueous solution, and surfactants is forced to pass through a membrane with the specific and uniform pore size by high pressure. In this study, emulsions were extruded by a 10 ml Thermobarrel LIPEX extruder (Northern Lipids, Burnaby, BC, Canada) and the membrane is a 100 nm pore size 25 mm diameter Millipore

polycarbonate extrusion filter (Millipore). The suspension in the extruder connected to an air tank was under 100~500 psi at 22°C and against the membrane, 200 nm to form the emulsion. The extrusion process for the suspension was repeated 5 to 10 times until the emulsion reached the required size by verifying dynamic light scattering (DLS). It is worth remembering that membrane breaking could happen during extrusion if the pressure in extruder increases rapidly or the units of extruder are not installed properly.

1.5.2 Dynamic light scattering (DLS)

1.5.2.1 Size measurement

Dynamics light scattering (DLS), also known as photon correlation spectroscopy (PCS), is the device to measure Brownian motion and to relate this to the particle size [286-288]. Using a laser, DLS particles in a colloidal suspenion are illuminated and the fluctuations of the scattered light are analyzed to extract a particle size measurement. Particles suspended in a liquid randomly move in various directions due to Brownian motion. It can be assumed that larger particles move more slowly and smaller particles move more quickly. The relation of the particle size and their diffusional speed due to Brownian motion can be defined by Stokes-Einstein equation [178, 179], which has been illustrated in the section 1.3.3. The diffusion rate (D) depends on disperse liquid viscosity and the particle size. It can be shown as the following,

$$D = k_b T / 6 \pi \eta r \qquad (1.5)$$

where

k_b is Boltzmann constant,

T is absolute temperature (Kelvin),

η is the viscosity of dispersion medium,

r is the particle size

Hence, DLS can measure the diffusion rate (D), and analyze the particle size(r) by setting two parameters: temperature (T) and disperse liquid viscosity (η). Because scattered light refracting from suspended particles varies according to the dispersant medium, particle composition, and particle concentration, the parameters of refractive index (RI) and absorbance (Abs.) of the dispersed medium and particles should be set in advance before size measurement. In this study, the Zetasizer Nano instrument ZEN3600 (Malvern Instruments) was used. The device enables us to measure particle size from 0.6 nm to 6 μm and detects the scattered light from the front of the cuvette at an angle of 7° (173° backscatter mode). Disposable sizing cuvettes were used for size measurement, and they were cleaned by E-pure water and wiped carefully. In order to avoid the phenomenon of multiple scattering, it is suggested that the sample has to be very diluted. According to the Malvern's manual of DLS, the sample concentration over which the sample can be measured is approximately 50 – 1000 ppm. Hence, 10 µl sample typically produced in this project was diluted by 1 ml E-pure water to form 1000 ppm approximately for size measurement. It also has a temperature extension option to 120 °C. The input parameters for DLS in this study could be shown in Table 1.1 [289-293].

The DLS instrument provides three types of size distribution curves, which are respectively, intensity distribution, volume distribution, and number distribution. The much light is scattered by the particles in different sizes. The volume distribution describes the

Table 1.1 The parameters for DLS size measurement intensity distribution shows how

Measured particles

Material	RI	Abs.
PFOB	1.3	0.010

Dispersed medium

Material	Temperature (°C)	Viscosity (cP)	RI
Water	25	0.8872	1.330
Hexane	10	0.3442	1.375
Hexane	20	0.3131	1.375
Hexane	30	0.2892	1.375

total volume of particles in different sizes. The number distribution presents the total number of particles in different sizes. The three distributions are distinct but all relate to particle size. Considering that all particles are spherical and there are N_A particles with size a, N_B particles with size b, N_C particles with size c…, the relative contribution of intensity distribution is

$$\%I_A = \frac{100N_A a^6}{N_A a^6 + N_B b^6 + N_C c^6 + \cdots} \quad (1.6)$$

The relative contribution of volume distribution is

$$\%V_A = \frac{100N_A a^3}{N_A a^3 + N_B b^3 + N_C c^3 + \cdots} \quad (1.7)$$

And the relative contribution of number distribution is

$$\%N_A = \frac{100N_A}{N_A+N_B+N_C+\cdots} \quad (1.8)$$

The sixth power of particle size used in the intensity distribution could over-emphasize the larger size objects in the sample, and similarly the size factor of number distribution could over-emphasize the smaller size group in the sample and ignore the larger size group. All the presentations of particle distribution are correct but they just have different physical meaning. Mie scattering gives a more complete explanation of the complicated scattering behavior. This theory is related to how the light is scattered from particles with various sizes while the optical properties like refractive index and absorbance of particles are known. Intensity distribution is not only just proportional to the size power of the particle size but corrected by a size-related Mie function *M*(a) [286, 294]. Generally, the presentation of intensity distribution is shown as,

$$\%I_A = \frac{100N_AM(a)}{N_AM(a)+N_BM(b)+N_CM(c)+\cdots} \quad (1.9)$$

Intensity distributions modified by Mie scattering are basically used in DLS measurements, so for mono-disperse specimens, it is usually more accurate to use the result of intensity distribution (it is also suggested by Malvern's manual). Because the volume and number distribution of particle size are converted from intensity distribution later, the large group size of particles could be ignored during the distribution conversion. Therefore,

intensity distribution was utilized to record as the particle size in this study. In the case of nongaussian particle distributions, one of the other presentations may be more useful.

1.5.2.2 Zeta potential measurement

Electrically charged colloidal particles that suspend in a dispersed solution attract ions in their surroundings. This results in the formation of electrical double layers around the particles, which are respectively, a Stern layer and a slipping layer (Figure 1.4). Ions that are strongly bound to the core charged particle form the Stern layer, and the potential between the stern layer and a point in bulk fluid away from the interface is called the Stern potential. The outer layer is referred to as the slipping plane where ions are less associated firmly. Zeta potential is the potential between the slipping plane (hydrodynamic plane of

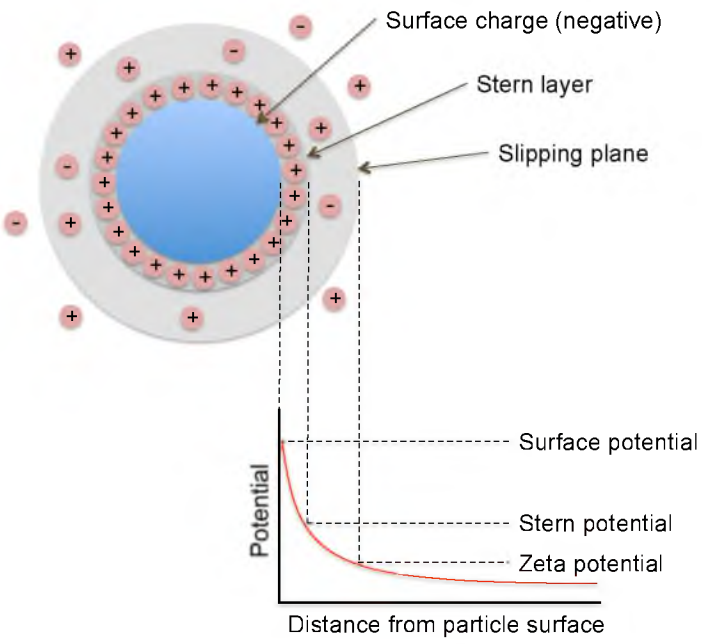

Figure 1.4 The notion of double layers and corresponding potentials of a charged particle.

shear) versus a point in bulk fluid away from the interface. When the charged particle moves, the ions outside the slippage boundary would stay with the bulk dispersion medium while the others move with the particle [295, 296].

In electrokinetics, zeta potential could be meaured by means of electrophoresis, which is the movement of a charged particle relative to the liquid. The particle is suspended under the influence of an applied electric field. The behavior of electrophoretic mobility is determined by the Henry equation [297],

$$U_E = \frac{2\varepsilon z f(\kappa a)}{3\eta} \tag{1.10}$$

where

U_E is the electrophoretic mobility,

ε is the dielectric constant of dispersion medium,

z is zeta potential,

$f(\kappa a)$ is Henry's function,

η is the viscosity of dispersion medium

In Henry's function, $f(\kappa a)$, a is the particle radius and the reciprocal of κ (1/κ) is called Debye length (λ_d) [298, 299], which is the thickness of double layers. The equation can be shown as the following:

$$\lambda_d = \sqrt{\sum \frac{\varepsilon \varepsilon_0 kT}{Z_i{}^2 e^2 n_{i_0}}} \tag{1.11}$$

where

ε is the dielectric constant of medium (ε_{water} = 78.5)

ε_0 is the vacuum permittivity

k is the Boltzman's constant

n_{i_0} is the bulk concentration of ions with charge Z_i

e is one electron charge

Henry's function can be viewed as the ratio of particle radius to double layer thickness. Furthermore, Henry's function of polar media like water can be simplified approximately to 1.5 by Smoluchowski's formula [300, 301]. There are two assumptions: 1) the Debye length is much smaller than the surface radius of curvature and 2) the zeta potential is small (ion distributions are only slightly disturbed). Zeta potential can then be acquired by measuring the electrophoretic mobility of particles if the viscosity of dispersion medium and the dielectric constant of dispersion medium are already known.

Zeta potential is also an important parameter that indicates the likely stability of colloidal system. If particles have high enough electrical charge on surface, the electrical repulsion will prevent them from flocculation. Generally, particles with zeta potential less than ± 30 mV would not be stable and would tend to aggregate [302, 303]. In this study, zeta potential was measured by Zetasizer Nano instrument ZEN3600 (Malvern Instruments). It is also used for size measurement. Based on Malvern's manual, the sample for zeta potential has to be diluted prior measurement. Similarly, 10 µl of sample was diluted by 1 ml E-pure water to form 1000 ppm approximately for zeta potential measurements and a clear, disposable zeta cell was used. The parameters for DLS in this study are shown in Table 1.2.

Table 1.2 The parameters for zeta potential measurement

Measured particles

Material	RI	Abs.
PFOB	1.3	0.010

Dispersed medium

Material	Temperature (°C)	Viscosity (cP)	RI	Dielectric constant
Water	25	0.8872	1.330	78.5

1.5.3 Acid dissociation constant and Henderson-Hasselbalch equation

The chemistry reaction of acid dissociation represents the strength of an acid solution, and it can be quantified by the acid dissociation constant K_a (also known as acid-ionization constant or acidity constant) [304, 305]. The equilibrium of the reaction can be written as,

$$HA \rightleftarrows H^+ + A^- \tag{1.12}$$

So the equilibrium constant or acid dissociation constant can be written as,

$$K_a = \frac{[H^+][A^-]}{[HA]} \tag{1.13}$$

Owing to the large orders of magnitude of K_a, a logarithmic representation of acid dissociation constant is more commonly used. Hence, logarithmic acid dissociation constant can be written as,

$$pK_a = -logK_a \tag{1.14}$$

In chemistry or biology, the Henderson-Hasselbalch equation is usually used to estimate the pH of a buffer solution and to find the equilibrium pH of acid-base reaction [306-308]. The derivation of the Henderson-Hasselbalch equation can be shown as the following,

$$K_a = \frac{[H^+][A^-]}{[HA]} \tag{1.15}$$

$$logK_a = log\frac{[H^+][A^-]}{[HA]} \tag{1.16}$$

$$logK_a = log[H^+] + log\frac{[A^-]}{[HA]} \tag{1.17}$$

$$-pK_a = -pH + log\frac{[A^-]}{[HA]} \tag{1.18}$$

$$pH = pK_a + log\frac{[A^-]}{[HA]} \tag{1.19}$$

In practice, pK_a can usually be found in previous references so the ratio of the concentration of dissociation acid (A^-) and undissociation acid (HA) could be known by measuring the pH of the acid solution. If the acid dissociation rate is 50%, which means the concentrations of dissociation acid (A^-) and undissociation acid (HA) are equal, the measured pH value would be the logarithmic acid dissociation constant (pK_a). In this work, the concept was applied to verify the pKa of phosphate groups on lipids during the measurement of zeta potential versus pH.

1.5.4 Colorimetric determination of polylysine and chitosan

Colorimetric determination is a method of analyzing the concentration of a chemical compound or chemical element in a solution by means of color reagent. The detected sample could be an organic or inorganic compound, and the determination could be involved in an enzymatic reaction or not. In this study, the concentration of polylysine and chitosan in solution were determined by colorimetric analysis. The different absorbance at a specific wavelength was verified by UV-Vis spectrometry after a colored reagent was added. The details are provided below.

1.5.4.1 UV-Vis spectrometry

Ultraviolet-visible (UV-Vis) spectrometry is an instrument to measure the absorption or reflectance spectra in the range of ultraviolet-visible wavelength by using the light in the visible and adjacent (near-UV and near-infrared) range. In the visible range, the absorption refers to the perceived color of the chemicals involved. In this range of the electromagnetic spectrum, molecules have electron transitions from the ground state to the excited state.

This technique is complementary to fluorescence spectroscopy, which measures electron transitions from the excited state to the ground state. In both, electrons can be excited to higher antibonding molecular orbitals if molecules with π-electrons or nonbinding electrons (n-electrons) can absorb the energy in the form of ultraviolet or visible light [309-311].

UV-Vis spectroscopy is extensively utilized for the qualitative and quantitative determination in analytical chemistry. The Beer-Lambert law quantitatively connects absorbance to concentration [312-314]. The basic equation of the Beer-Lambert law can be shown as,

$$A = \varepsilon b c \qquad (1.20)$$

where

A is the absorbance of the sample

ε is the extinction coefficient or the molar absorptivity

b is the pathlength through the sample

c is the concentration of the sample

The absorbance of the sample is proportional to the concentration of the sample because the extinction coefficient (ε) and the pathlength through the sample (b) are fixed. Generally, the extinction coefficient can be acquired from some reference and the pathlength through the sample can be known by measuring the cuvette length so the concentration of the sample can be found out if the absorbance is measured.

In this work, colorimetric determination of PLL and chitosan were conducted using a UV Mini 1240 spectrophotometer (Shimadzu Scientific Instruments) and a 1 cm pathlength quartz cuvette. Another colorimetric experiment exploring phase transition temperature was completed using a more advanced Cary 100 UV-Vis spectrophotometer (Agilent technologies, CA), with temperature control kit and a 1 cm pathlength quartz cuvette.

1.5.4.2 Colorimetric determination of polylysine

Trypan blue (TB) is a dye with negative charges that is electrostatically attracted to positive PLL, and can be used for quantitative determination of PLL concentration. TB is attracted by PLL and precipitates the blue intensity of unbound TB in the supernatant solution would decrease [315-317]. The scheme of this chemical reaction for PLL determination is shown in Figure 1.5. The basic procedure of PLL colorimetric determination is to mix the PLL-containing sample with TB reagent and to place the mixture in a warm incubator (37 °C) for one hour. After that, the mixture is centrifuged to collect the precipitate and the supernatant solution is analyzed by UV-Vis spectrometry. Soluble TB (not precipitated) usually has an absorbance peak at 578 nm. If a standard curve of the absorbance of supernatant after TB is reacted with PLL and precipitated versus the concentration of PLL is created in advance, the concentration of PLL in solution can be easily measured by UV-Vis spectrometry. We similarly measure the emulsion bound concentration of PLL by measuring the amount of free PLL remaining in the supernatant after the emulsion particle have been removed by centrifugation.

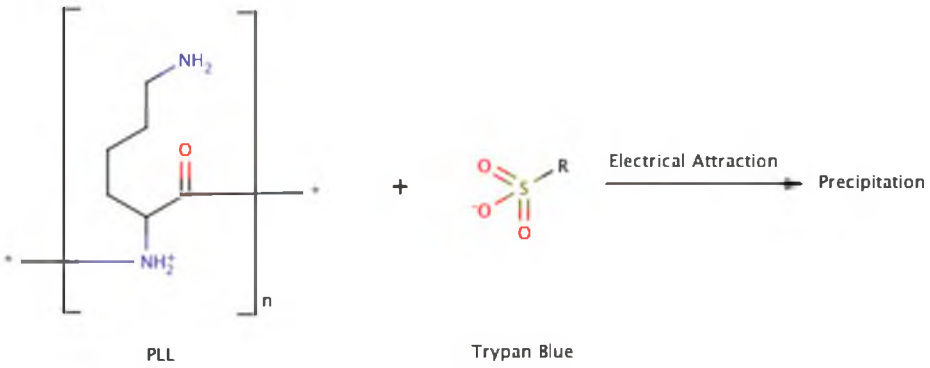

Figure 1.5 The precipitation mechanism of PLL and Trypan blue.

1.5.4.3 Colorimetric determination of chitosan

Cibacron Brilliant Red 3B-A, also known as Reactive Red 4, is the dye to utilize for chitosan quantitative determination because the dye with negative charges and the chitosan with positive charges on their amine groups tend to attract each other by electrostatic force. The scheme of chemical reaction of chitosan determination can be found in Figure 1.6. The basic procedure is to mix chitosan solution (dissolved by acetic acid so chitosan has positive charges in acid condition) with Cibacron Brilliant Red 3B-A in buffer solution. If the mixture solution is analyzed by UV-Vis spectrometry, it would cause bathochromic shifts (or called as red shift) so a sharp peak around 575 nm could be found [318-321]. Bathochromic shift is a change of spectral band position in absorption of a molecule to a longer wavelength, which means lower frequency. As the concentration of chitosan increases gradually, the phenomenon of bathochromic shift occurs obviously and the peak height at 575 nm is larger. If the standard curve of the absorbance of the bathochromic shift peak versus the concentration of chitosan is plotted in advance, the concentration of

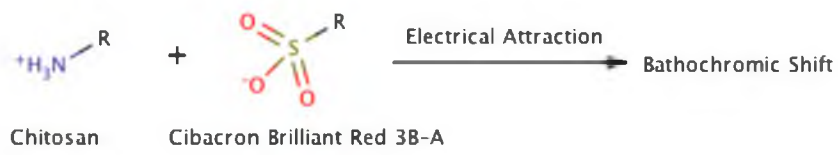

Figure 1.6 The bathochromic shift mechanism of chitosan and Cibacron Brilliant Red 3B-A.

chitosan solution could be known when the absorbance is measured by UV-Vis spectrometry.

1.5.5 Fluorescent spectrophotometer

Fluorescence is the method of spectrochemical analysis where the molecules are excited from the ground state to the excited state in various vibrational states, by illuminating at a specific wavelength, and allowing them to relax by emitting radiation of a longer wavelength [322-324]. The lifetime of electron relaxation is fairly short, usually about 10^{-8} sec [325]. The emitted light's wavelength depends on the band gap between the ground state and the excited state minus any energy that is lost to vibration and thermal loss. In this work, fluorescence spectra were examined using a Cary Eclipse fluorescence spectrophotometer (Varian). The applied light is wavelength tuned to maximize absorption and therefore emission intensity. For stable measurements, the sample in the cuvette is covered with a lid on the top.

1.5.6 Fluorescence quenching

Any process that refers to the reduction of fluorescence intensity can be called fluorescence quenching. It can be the result of a variety of molecular interactions such as excited-state reactions, molecular rearrangements, energy transfer, ground-state complex formation, and collision [322]. Quenching often depends on pressure and temperature [326]. In this section, collisional or dynamic quenching between a fluorophore and quencher is described as it is used in the project.

In collisional quenching, the fluorophores have to encounter the diffused quenchers during the lifetime of their excited state. After contact, the fluorophores return to the ground state from their excited state, but no photon emission happens. In this process, the molecule of the quencher generally has no permanent change, which means there is no photochemical reaction. In contrast, the process of static quenching happens as the fluorophore and quencher contact and form a nonfluorescent complex [327, 328]. Molecular oxygen (O_2), iodide ions (I^-), and acrylamide (C_3H_5NO) are the best-known collisional quenchers [329-332]. The mechanism of quenching by oxygen, which has been debated, is likely that the fluorophore undergoes intersystem crossing to triplet state due to the paramagnetic oxygen [333, 334]. Another type of quenching mechanism is due to heavy atoms such as halogens: iodide or bromide. These halogen atoms cause intersystem crossing to an excited triplet state, promoted by spin-orbit coupling of singlet fluorophores and the halogens [335]. Due to slow emission from the triplet state, it would be highly quenched by other processes. A donation of an electron from fluorophore to the quencher happens because these halogen atoms are sensitive uniquely to quench by chlorinated or by

electron scavengers like protons. In this work, iodide ions were applied to quench the fluorescent dye pyrene [336-338].

Collisional quenching of fluorescence (and phosphorescence) can be quantitatively described by the Stern-Volmer relationship [339]. The effect of quencher on steady-state fluorescence of a fluorophore can be simply described as the Stern-Volmer equation [340]:

$$\frac{I_0}{I} = 1 + K_{S-V}[Q] \qquad (1.21)$$

where

I_0 is the initial fluorescent intensity of pyrene in absence of iodide ions

I is the fluorescent intensity of pyrene quenched by iodide ions

$K_{S\text{-}V}$ is the Stern-Volmer constant (M^{-1})

[Q] is the iodide ion concentration (M)

The dynamic Stern-Volmer constant is equal to the product of the bimolecular quencher rate constant (k_q) times the excited state lifetime in absence of the quencher (τ_0), shown in the following equation:

$$K_{S-V} = k_q \tau_0 \qquad (1.21)$$

where

k_q is the bimolecular quenching rate constant

τ_0 is the excited state lifetime in absence of the quencher

The bimolecular quencher rate constant, k_q, is also equal to the product of the quenching efficiency, γ, times the diffusion-limited bimolecular rate constant for collision, *k*, which is calculated theoretically by using the Smoluchowski equation [341-343]. It can be shown as the following equation:

$$k_q = \gamma k = \frac{4\pi D r N_A}{1000} \quad (1.22)$$

where

γ is the quenching efficiency

k is the diffusion-limited bimolecular rate constant for collision

D is the diffusion rate

r is the molecular radius

N_A is Avogadro's number

The diffusion rate (D) for different species can be predicted by the Stokes-Einstein equation. The viscosity (highly dependent on temperature and pressure [344]) and working temperature influences the fluorescent quenching. In this project, it needs to be remembered that a different results in the experimental measurement of pyrene quenching by iodide ions could occur due to the different viscosities of PLL and chitosan-coated emulsion suspension and need to be taken into consideration.

1.5.7 Fourier transform infrared spectroscopy (FTIR)

As a molecule absorbs the energy of ultraviolet or visible light, it undergoes electron transitions between different energy states but also vibrational and rotational energy transitions. The atoms in a molecule have quantized vibrational energy levels as they

vibrate around their equilibrium positions. The spacings of energy levels are related to photon energies in the infrared region. Vibrations, generally, have several types like symmetric stretching, antisymmetric stretching, in-plane bending, and out-of-plane bending. Similarly, the atoms in the molecules also have quantized rotational energy levels whose spacings are related to photon energies in the microwave region [345-347]. The atoms in a molecule only stretch, bend, or rotate at specific frequencies corresponding to specific energy levels. In this way, infrared spectrum has been used extensively for identification of organic compounds [348-351]. It is more convenient to plot a frequency spectrum (the intensity versus various frequency) for the analysis of organic or biochemical, but the interferogram signal cannot be interpreted directly. Fourier transformation can be applied to calculate and convert individual frequencies of interferograms into a spectrum. Fourier transform infrared spectrometer (FTIR) has been one of the important devices in organic chemistry analysis by infrared spectrum.

The infrared region of the electromagnetic spectrum covers the region from above the visible (7.8×10^{-7} m) to approximately 10^{-4} m, but organic chemists only use the midregion from 2.5×10^{-6} m to 2.5×10^{-5} m. In chemistry or biochemistry, frequencies are usually given in wavenumber, which is the reciprocal of the wavelength in centimeters. Hence, the unit of wavenumber can be expressed as cm^{-1} and the useful infrared region is from 4000 to 400 cm^{-1}. In the region from 4000 to 2500 cm^{-1}, the absorptions are caused by N-H, C-H, and O-H single-bond stretching motions. N-H and O-H bonds absorb during the range of 3300 to 3600 cm^{-1} and C-H bonds absorb during the range near 3000 cm^{-1}. In the region of 2500 to 2000 cm^{-1}, the triple-bond stretching like nitriles or alkynes absorbs. In the region from 2000 to 1500 cm^{-1}, all kinds of double bonds such as C=O, C=N and C=C absorb here.

Carbonyl groups usually absorb in the range of 1680 to 1750 cm^{-1}, and alkene groups absorb during the range of 1640 to 1680 cm^{-1}. The region below 1500 cm^{-1} is the fingerprint region of infrared spectrum, which has various absorptions from the vibration of C-C, C-O, C-N, and C-X single bonds [352-354].

In this work, an FTIR (Excalibur 3100) with attenuated total reflectance (ATR) kit was used to verify the existence of PFOB in the emulsion. ATR is a technique used to enable the sample to be examined directly in solid or liquid state without sample preparation [355-359]. In previous references, the carbon-fluorine bond stretching was identified to occur in the infrared region of 1360 to 1000 cm^{-1} [360, 361]. The wide region is because the stretching frequency is very sensitive to the location of substituents in the molecule. Mono-fluorinated chemical compounds exhibit a band between 1000 to 1110 cm^{-1} but multifluorinated compound can have two broad bands, which arise from symmetric and anitsymmetric vibrations [362].

Infrared spectroscopy is not only a powerful tool for the identification of organic chemicals (qualitative analysis) but is also a common technique for quantitative measurement [363-367]. The basic theory of FTIR quantitative measurement is based on the Beer-Lambert law, which has been illustrated in a previous section. Assuming the same pathlength through the sample and a constant, known extinction coefficient, the measured absorbance of a specific vibrational band is proportional to the concentration of measured chemical. To control the fixed pathlength through the sample, a demountable liquid cell (PIKE technology, WI) was used in this work. The schematic liquid cell is shown in Figure 1.7 (acquired from the website of PIKE technology). Liquid sample was injected into the center space of the spacer with a thickness of 0.015 mm (the pathlength through the

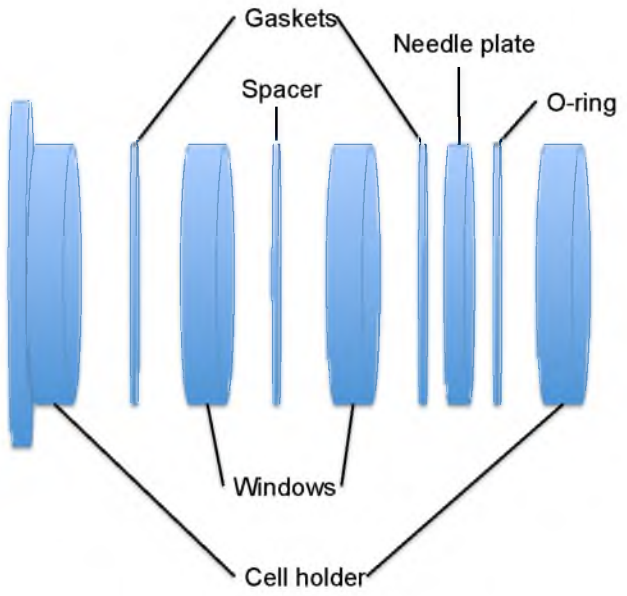

Figure 1.7. The demountable liquid cell assembly layout

sample). According to the Beer-Lambert law, the concentration of the measured sample can be calculated by knowing the absorbance of the sample at the specific band. It is worth remebering that the absorbance could be slightly different due to the method of baseline determination. In this work, the baseline for FTIR quantitative measurement was taken as a fitted line straight line between the two lowest sides of the specific peak. The absorbance was defined as the height from the highest point of the peak to the sloping baseline. This approach has a slight error, but relative measurement between specimens should be accurate.

1.5.8 Cryogenic transmission electron microscopy (Cryo-TEM)

The basic principle of transmission electron microscopy (TEM) operation is similar to optical microscopy but uses electrons instead of light. The electron beam is applied such that it transmits through an ultrathin sample and interacts with the sample's electrons as it

passes through. Due to de Broglie wavelength of electrons, electrons can provide high imagining resolution [368-370]. The wavelength of electrons of TEM depends on the energy of the accelerated electrons, which is related to the process known as thermionic emission from a filament. Theoretically, the resolution is limited by the wavelength of light or electron source according to Rayleigh criterion [371, 372]. The spatial resolution of TEM, basically, can be from nanometer to subangstrom so it can supply the morphology images of fine sample and plot the molecular structure from a diffraction pattern [373, 374]. However, the mean free path of electron gas interaction reduces and the electrical arc is generated if the electrons from filament go through the air directly [374, 375]. It is necessary to evacuate air in the TEM chamber to relative low pressure or vacuum, which means it is impossible to image the living or liquid samples without pretreatment via TEM [376-378].

A derivative technology, known as cryo-electron microcopy (cryo-EM) or electron cryomicroscopy, was proposed by Adrian et al. in 1984 [379]. In this method, the samples are studied at cryogenic temperature (generally liquid nitrogen temperature) without contrast agents to enhance electron density. This method of specimen preparation can preserve the sample in a state close to its original state. It can prevent damage of biological samples during preparation and the dehydration of particles in suspension. The sample should be rapidly plunged into liquid ethane with a high freezing rate greater than 1,000,000 K/sec [380-382], and then is observed by electron microscopy. It is commonly used in the study of structural biology.

In this study, the emulsion could suffer from PFOB evaporation and structural rupture during TEM observation if emulsion is fixed directly on the TEM grid and air-dried. For all

samples, approximately 3.5 μL of solution was placed on a holey-carbon-coated copper grid, blotted, and plunge-frozen in liquid ethane using an FEI Vitrobot (Hillsboro). Samples were transferred to a Gatan 626 cryoholder (Pleasanton) cooled with liquid nitrogen. Cryo-TEM images were recorded at 200 kV in a FEI Tecnai F20 transmission electron microscope (Hillsboro).

1.6 The work in the thesis

This thesis is mainly focused on the improvement of perfluorocarbon emulsion (PFOB emulsion is the primary material in this work) in terms of its structural stability and synthesis efficiency so that these materials can have greater potential in the area of artificial blood substitutes, MRI imaging, and drug delivery applications. Electrostatic coating of biomaterials on emulsion surfaces is fairly simple and can provide mechanical strength protection in blood vessels. The conformation prediction of coating biomaterials on the emulsion surface could be significant for future applications such as predicting the release rate of oxygen/ carbon dioxide and surface modification for specific targeting. In addition, a novel method of emulsion synthesis was developed by taking advantage of cosolvent to promote the emulsion uniformity without the generation of liposomes.

In the beginning of Chapter 2, PFOB was emulsified by various compositions of ionic and nonionic surfactants. The size and zeta potential of PFOB emulsion were measured to determine the optimal composition for PFOB emulsion. Later, the change of zeta potential of emulsion and coating materials at different pH was plotted, respectively, in Chapter 2. Emulsions coated by PLL and chitosan were then also described respectively using the change of size and zeta potential of coated PFOB emulsion at various concentrations of

coating materials and temperatures. By colorimetric determination of free PLL and chitosan, the concentration of coated materials on the emulsions could be calculated. A model for conformation prediction was established to compare PLL and chitosan coating on PFOB emulsion. Interestingly, the model used indicated these two molecules behaved oppositely. Finally, this result was verified experimentally by fluorescence quenching and the analysis of thermodynamics.

In Chapter 3, a new synthesis process for producing PFOB emulsions using cosolvents was described and four types of emulsions were characterized by FTIR for PFOB retention. A phase transition temperature for the synthesis of PFOB emulsion was discovered and characterized via UV-Vis spectrophotometry. PFOB retention efficiency for the cosolvent synthesis of emulsion was obtained from quantitative measurement of the FTIR results. The emulsion uniformity without liposomes was confirmed using fluorescent dyes trapped in oil phase of the emulsion and centrifugation to separate emulsion particles from any formed liposomes.

Chapter 4 outlined the main conclusion of this thesis project and directions for future study.

CHAPTER 2

POLY-L-LYSINE AND CHITOSAN-COATED PERFLUOROCARBONS (PFCs) EMULSIONS: PROCESS AND CONFORMATION ANALYSIS OF COATING MATERIALS

2.1 Abstract

A technique for evaluating the conformation of poly-L-lysine (PLL) and chitosan (CS) on perfluorocarbons (PFCs) emulsions was developed. By means of the size and zeta potential of the coated emulsion, a change in the specific volume of PLL and CS molecules attached to the emulsion surface as their concentration increases was detected. Compression of PLL coatings and expansion of CS coatings on the emulsions was further verified by fluorescent quenching and supported by thermodynamic analysis. The approach developed is a convenient method for micro- and nanoparticulate coatings that cannot be easily probed by conventional optical or surface methods.

2.2 Introduction

Stability and performance control of surfactant-stabilized nanoemulsions in drug delivery, imaging, and other applications is enhanced when they are coated with other molecules that can provide chemical responsiveness [383-386], diffusional gating [387-

389], or target recognition function [390-393]. Little is known about the characteristics of these coatings at the molecular level. Typically, coatings are applied such that they maximally cover the surface, and it is assumed that the coating molecules retain their shape and physico-chemical characteristics as are found in solution. This assumption is probably incorrect as there are many examples of surface and concentration-dependent denaturation of molecules, such as polymer, proteins, and enzymes [394-397]. Naked and coating-reinforced nanoemulsions, liposomes, and other submicron-structures are highly investigated for biomedical applications, and the exact nature of the coating molecules is critical for understanding their biological and physiological behavior. For example, native and denatured conformations of a molecule may have widely varying ability to activate the immune system, bind complement, or interact with blood and tissues [398-402].

Molecular conformations of individual molecules in dilute solution can be probed indirectly in a variety of ways such as dynamic light scattering [403-405], neutron scattering [406-408], and Fourier transform infrared spectroscopy [409-412]. These indirect methods are difficult to apply to molecules tethered to nanoparticles. This is because both the molecule of interest and the nanoparticle have complex scattering signatures, single particle spectroscopic detection at the required resolution is difficult, and nanoparticle suspensions are usually at low concentration. Here, we present a simple method based on zeta potential measurements that permits following the assembly of a molecular coating on the surface of a nano- or microparticle, i.e., a submicron-sized spherical oil-in-water emulsion particle, and evaluating the changing conformation of the coating molecules as surface capacity is reached.

2.3 Experimental method

2.3.1 Materials

L-α-phosphatidylcholine (lecithin) from soybean and 1,2-dioleoyl-*sn*-glycero-3-phosphate (sodium salt) (DOPA) were purchased from Avanti®. Perfluorocarbon 1-bromoperfluorooctane (PFOB) was purchased from Oakwood Products, Inc. Sodium phosphate monobasic ($NaH_2PO_4 \bullet H_2O$) and sodium phosphate dibasic, heptahydrate ($Na_2HPO_4 \bullet 7H_2O$) were acquired from Fisher Scientific and Mallinckrodt, respectively. Chitosan (M_r~150,000 g/mol) was acquired from Fluka and poly-L-lysine with average molecular weight from 500 g/mol to 2000 g/mol was acquired from Sigma-Aldrich®. Acetic acid (Mallinckrodt) and ethanol (Pharmco-AAPER) were used. 18.20 MΩ-cm E-pure water was acquired from the machine Barnstead MicroPure ST (Thermo Scientific). MES buffer, Trypan Blue assay, Cibacron Brilliant Red 3B-A assay, and glycine were obtained from Sigma-Aldrich®. NaCl was obtained from VWR, and both HCl and NaOH were acquired from Mallinckrodt.

2.3.2 Synthesis procedure

Various compositions of DOPA-lecithin emulsions were synthesized according to the details listed in Table 2.1. DOPA mole percentage of total surfactants (DOPA and lecithin) is listed specially in the bottom of the table.

For a typical synthesis, Lecithin or Lecithin/DOPA solutions were first prepared in phosphate buffer (2ml of 0.2M $NaH_2PO_4 \bullet H_2O$ and 298.68ml of 0.2M $Na_2HPO_4 \bullet 7H_2O$ in 859.25ml E-pure water, 18MΩ cm resistivity). To this was added an amount of PFOB and the mixture stirred in a 20ml vial at 1200 rpm stirring for 30 min to disperse into a coarse

Table 2.1 Various compositions of DOPA-lecithin emulsions (The MW of DOPA and lecithin are close. $MW_{lecithin}$=775.0 g/mol, MW_{DOPA}=772.5 g/mol)

Sample	1	2	3	4	5	6	7
Lecithin (10^{-3} moles)	2.33	2.31	2.28	2.23	2.21	1.16	0
DOPA (10^{-3} moles)	0	0.02	0.05	0.10	0.12	0.17	2.33
PFOB (ml)	1.60	1.60	1.60	1.60	1.60	1.60	1.60
Buffer (ml)	4.24	4.24	4.24	4.24	4.24	4.24	4.24
DOPA (%) of total surfactants	0.00	1	2	4	5	50	100

emulsion. The emulsions were then extruded through a 200 nm pore size polycarbonate membrane (Nuclepore Track-Etch membrane, Whatman) using a 10ml Thermobarrel LIPEX extruder (Northern Lipids, Burnaby, BC, Canada) for 5 times at 500 psi in room temperature. For comparison, mixtures of DOPA-only and lecithin-only emulsions were prepared at the following mole percentages spanning the range indicated for samples 2 through 6 in Table 2.1.

For coating of the emulsions, 30 μM CS and 4000 μM PLL solutions were prepared, respectively. A solution of 30 μM CS chitosan was made by adding 100 mg chitosan, 1ml acetic acid (Mallinckrodt), and 200μl ethanol (Pharmco-AAPER) into 18.8ml water. Solid chitosan can dissolve easier in water with the existence of acetic acid and ethanol. A solution of 4000 μM PLL solution was made by adding 100mg poly-L-lysine into 19.9ml water. The final pH of CS and PLL solution were about 3.5 and 6.5 without any pH titration.

2.3.3 Coating

Five hundred µl of sample 3 emulsion (2D98L) in Table 2.1 titrated to pH 3.51, 3.57, 3.62, 3.71, 6.95, 7.02, 7.08, 7.12, 7.19 were prediluted to 2.5 times of its original volume using E-pure water at room temperature. These nine samples were prepared for size and zeta potential measurement at several temperatures: 273, 278, 283, 288, 293, 298, and 310K. For coating of emulsions, 500µl of sample 3 emulsion were prediluted to 2.5 times of it original volume using E-pure water and then mixed at room temperature (unless otherwise indicated) with varying amounts of 4000 µM PLL or 30 µM CS solution, as indicated in Table 2.2, and stirred at 150 rpm for 30 minutes. These nine samples of coated emulsion were titrated to pH 7.2. Another set of coatings with varying amounts of 4000 µM PLL or 30 µM CS solution but no pH titration were applied at several temperatures: 273, 278, 283, 288, 293, 298, and 310K. The temperature was also held constant all the time during size and zeta potential measurements. This examined temperature range (from 0°C to 30°C) would be useful in future bio-applications and allows us to scrutinize coating-relevant coating characteristics. The resulting set of mixtures is numbered from T1 to T7. Their composition is shown in Table 2.3. The reasoning behind use of sample 3 (2D98L) for coating studies will be explained in the results and discussion of emulsion synthesis.

2.4 Characterization

2.4.1 Dynamic light scattering (DLS)

Zetasizer Nano instrument ZEN3600 (Malvern Instruments, Malvern, Worcestershire, UK) and disposable sizing polystyrene cuvettes were used. The range for particle diameter measurement is from 0.6 nm to 6 µm. For diameter measurements, 10 µl sample was

Table 2.2 Various compositions of coated emulsions.

Coating	Sample	Final coating concentration (μM)
PLL	P1	1000
	P2	800
	P3	600
	P4	400
	P5	200
CS	C1	10.4
	C2	8.3
	C3	6.3
	C4	4.2

Table 2.3. Various coating temperatures of coated emulsions.

Temp. (K)	273	278	283	288	293	298	310
PLL	P1T1	P1T2	P1T3	P1T4	P1T5	P1T6	none
	P2T1	P2T2	P2T3	P2T4	P2T5	P2T6	
	P3T1	P3T2	P3T3	P3T4	P3T5	P3T6	
	P4T1	P4T2	P4T3	P4T4	P4T5	P4T6	
	P5T1	P5T2	P5T3	P5T4	P5T5	P5T6	
CS	C1T1	C1T2	C1T3	C1T4	C1T5	C1T6	C1T7
	C2T1	C2T2	C2T3	C2T4	C2T5	C2T6	C2T7
	C3T1	C3T2	C3T3	C3T4	C3T5	C3T6	C3T7
	C4T1	C4T2	C4T3	C4T4	C4T5	C4T6	C4T7

diluted by 1 ml E-pure water. It would contain 4×10^{11} emulsion particles in a 1 ml dilution sample, which is calculated from theoretical emulsion concentration later. The parameters of PFOB refract index and absorbance are 1.3 and 0.01, and of water viscosity and refract index are 0.8872 and 1.330. Both uncoated emulsion and coated emulsion were measured at 273, 278, 283, 288, 293, 298, and 310K, respectively, by the temperature control of DLS. Some samples were concentrated/viscous so extra care was taken to ensure samples were pipetted well and distributed uniformly.

2.4.2 Zeta Potential

Zetasizer Nano instrument ZEN3600 (Malvern Instruments, Malvern, Worcestershire, UK) was also used for zeta potential measurement. The disposable zeta potential cell made of polycarbonate with gold-plated beryllium copper electrodes was cleaned by E-pure water, and filled with 10 μl of the sample diluted by 1 ml E-pure water. The parameters used for zeta potential measurement were the same with size measurement. Only the water dielectric constant was additionally needed. Diluted PLL/CS solution was pH titrated before zeta potential measurement. Both emulsion and coated emulsion were measured at 273, 278, 283, 288, 293, 298, and 310K by the temperature control of DLS.

2.4.3 pH

Titrations of pH of 5 ml PLL/CS solution, emulsion, and coated emulsion in a 20ml vial were performed by dropwise addition of 1M HCl or 1M NaOH. After pH titration, the liquid was stirred at 300 rpm for 1 minute. The added volume was 2-4 μl and much smaller

than the bulk solution so the change of concentration could be ignored. The pH meter (Nist ACCMT AR60) and electrode used to measure pH were both from Fisher Scientific.

2.4.4 UV-Vis

UV Mini 1240 spectrophotometer (Shimadzu Scientific Instruments Columbia, MD) was used for colorimetric determination. All the samples measured were prepared in 1.5ml aliquots without dilution in 1 cm pathlength quartz cuvette. Samples were isolated from light during preparation using aluminum foil. The wavelength range of measurement was from 400 nm to 700 nm.

2.4.5 Modeling

MarvinSpace (ChemAxon, Hungary) was used to model the assumed structure of the emulsions used by this dissertation. Assumptions include: 1) the two hydrophobic tails of DOPA and lecithin stretch into PFOB core, 2) only the size of the lipid head group determines the thickness of the lipid layer, as well as the number of lipids needed to stabilize a PFOB droplet of given size, 3) there is only one lipid layer, and 4) the lipids are closely packed. The head group size of DOPA is approximately close to 5Å (Figure 2.1(a)) and that of lecithin is about 8Å (Figure 2.1(b)) so the thickness of one lipid layer is assumed to be 8Å. Knowing the average emulsion particle size from DLS, the volume of PFOB in one particle can be calculated. Knowing the total amount of PFOB used and experimental sample (2D98L) described later is 68.4 nmol (The composition of sample is shown in Table 2.1).

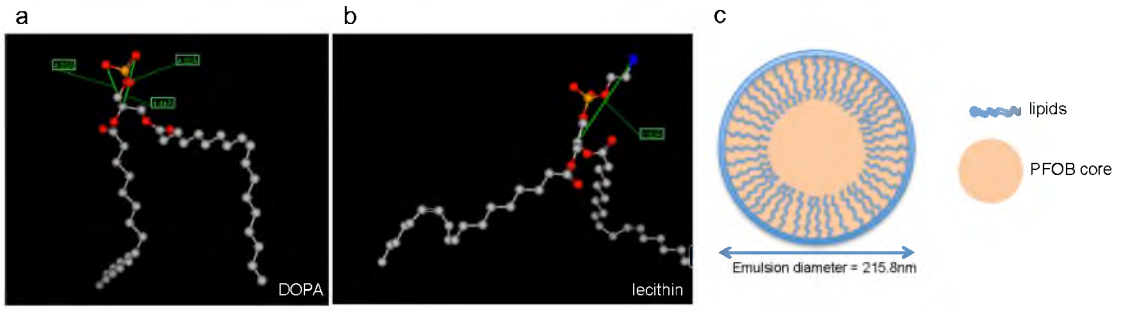

Figure 2.1 Model of single lipid structure calculated by MarvinSpace. No lipid compression consideration. (a) The head group of DOPA is around 5Å. (b) The head group of lecithin is around 8Å. (c) The cartoon of emulsion shows that the hydrophobic tails of lipids would stretch into PFOB core. While calculating the diameter of PFOB core, the thickness of the lipid layer can be viewed as the size of the lipid head group.
assuming no loss, the theoretical concentration of emulsion particles used in each

2.4.6 Colorimetric determination

Spectrophotometric determination of PLL was performed using the Trypan blue (TB) assay [315, 316]. The negatively charged dye interacts with positively charged PLL to form a precipitate via the reaction shown in Figure 2.2(a). (From our result, the pH of PLL solution and PLL-coated emulsion was around 6.5 to 7.2 so PLL had positive charges.) After centrifugation, the loss in intensity of blue color at 578 nm is used as a measure of the amount of free PLL in the suspension mixture and the amount attached to the nanoparticles is calculated assuming that no dye was adhered to the walls of 1.7ml microcentrifuge tubes. The system was calibrated using PLL solutions prepared in 0.1M MES with 0.15M NaCl at pH 6.5 that were serially diluted. The diluted concentrations of PLL solution were from 0 to 14.4 μM. The assay solution consisting of 1.1 mM Trypan Blue in 0.1M MES buffer was mixed with the analyte solution, placed at 37°C for one hour, and then centrifuged at 8000 rpm for 20 min. The absorbance at 578 nm in the supernatant

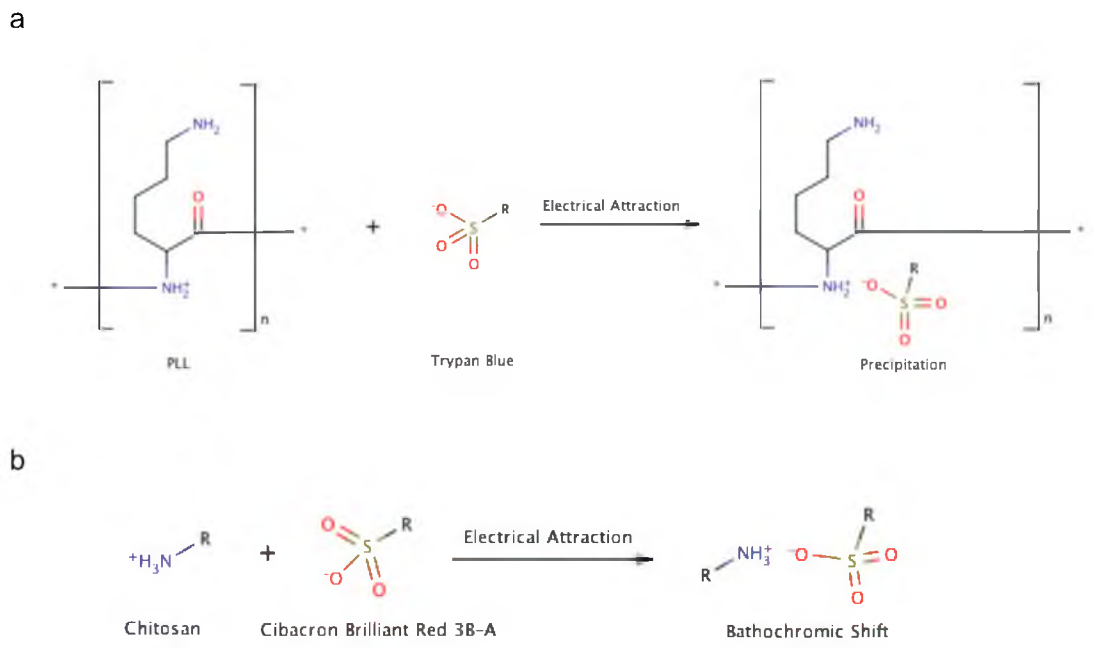

Figure 2.2 The chemical reaction of colorimetric determination. (a) The mechanism of PLL and Trypan blue precipitation. (b) The bathochromic shift mechanism of chitosan and Cibacron Brilliant Red 3B-A.

solution was measured by UV/Vis spectrometry and correlated to the concentration of PLL solution.

The dye Cibacron Brilliant Red 3B-A (also called Reactive Red 4) was utilized for the quantitative determination of the chitosan. The reaction of negatively charged dye and positively charged amine groups of chitosan (in Figure 2.2(b)) causes a bathochromic (i.e., red) shift of the absorption peak to 575 nm from 536 nm [318-320]. To calibrate, an assay solution consisting of 5 ml 0.75 μM Cibacron Brilliant Red 3B-A solution was mixed with 95ml buffer solution (81ml solution of 0.1M glycine and 0.1M NaCl with 19ml 0.1M HCl at pH 3.5). The diluted concentrations of CS solution from 1.7 to 2.7 μM were used for standard curve, and the peak shift correlated with the CS.

Experimental samples of PLL- and CS-coated emulsions prepared with various concentrations of PLL and CL were centrifuged at 3000 rpm for 20 min at 273, 278, 283, 288, 293, 298, and 310K, then the supernatant collected. (The centrifuging temperature is the same with the coating temperature.) The pellet material consisted mainly of coated emulsions because PFOB has the density close to 2 g/ml [413]. The supernatant solutions from PLL-coated emulsion samples were diluted to 50 times by ultrapure water and for CS-coated emulsion samples, C1, C2, C3, and C4, diluted to 4, 3, 2, and 1 times by ultrapure water to accommodate the narrow analysis range of the Cibacron Brilliant Red 3B-A assay.

2.4.7 Thermodynamics analysis

To understand the relation of coating concentration/temperature and coating material conformation, the analysis via thermodynamics was achieved. The following thermodynamics equation can be shown,

$$\Delta G = -RT\ln K = \Delta H - T\Delta S \qquad (2.1)$$

where

R is the gas constant (8.314 $kJ/mol^{-1}K^{-1}$)

T is absolute temperature)

H is the enthalpy (kJ/mol)

S is the entropy (kJ/mol/K)

K is the equilibrium constant of coating reaction

Using unbound PLL/CS unbound concentration from the colorimetric determination, an equilibrium constant for the coating reaction can be acquired and Gibbs free energy calculated. Various coated emulsions (shown in Table 2.3) were analyzed thermodynamically.

2.4.8 Fluorescent quenching

To evaluate the conformation of coating materials on the emulsion surface, the method of fluorescent quenching was applied. Pyrene (λ_{ex}=337 nm and λ_{em}=394nm) is a fluorescent dye that can slightly dissolve in perfluorocarbon liquids [414] but only trace amounts in water [415]. Hence, we can assume the intensity from encapsulated pyrene is much higher than that from uncapsulated pyrene. Pyrene-labeled emulsions were prepared by mixing pyrene at a concentration of 4 mM with PFOB during sample 3-emulsion formation according to Table 2.1.

PLL- and CS-coated emulsions prepared with the emulsion 3 composition (the surfactant with 2% DOPA and 98% lecithin) and containing a total concentration of 1 mM pyrene were mixed with 5, 10, 20, and 50 mM KI solution to form mixtures that contained a final iodide concentration of 3.75, 7.5, 15, and 37.5 mM. Fluorescent measurements of 1.5 ml samples at 394 nm were taken before the addition of KI (I_0) and at 30 min after mixing with KI (I). Data were also plotted according to the Stern-Volmer equation as I_0/I versus [Q] to determine the efficiency of fluorescent quenching [360].

$$I_0/I = 1 + K_{S\text{-}V}\,[Q] = 1 + k_q\tau_0\,[Q] \qquad (2.2)$$

where

I_0 is the initial fluorescence intensity of pyrene in absence of iodide ions

I is the fluorescent intensity of pyrene quenched by a known amount of iodide ions

K_{S-V} is the Stern-Volmer constant (M^{-1})

k_q is the bimolecular quenching rate constant ($M^{-1}S^{-1}$)

τ_0 is the excited state lifetime in absence of the quencher

[Q] is the iodide ion concentration (M)

The figures with the ratios of I_0/I versus [Q] for PLL- and CS-coated emulsion were respectively plotted and the trend lines for the data points were fitted by linear regression.

2.5 Results and discussion

2.5.1 Emulsion synthesis

Stable emulsion systems may be formed using charged or neutral lipids [416, 417]. Coating of emulsions by the controlled precipitation of secondary molecules has been demonstrated, but the mechanism involved varies [418-420]. In most cases, the emulsion particle acts as a sort of seed crystal onto which molecules at low concentration in the surrounding fluid attach. The driving force is the reduction in particle surface free energy. This process is accentuated if there is an accumulation of ions or coating precursors at the particle periphery. This results in a local concentration increase that then may exceed the solubility of the molecules and lead to rapid deposition onto the seed particle. Surface charge driven ion/molecule accumulation is particularly effective. Because lecithin is neutral, a phosphatidic acid lipid, DOPA, was added to the emulsion to increase the negative charge of the particles.

The zeta potential of the resulting DOPA-lecithin emulsion particles was used to optimize the surface charge Figure 2.3(a). The zeta potential curve of emulsions prepared using a mixture of lecithin and DOPA was found to be nonlinear (Red squares Figure 2.3(a)). In contrast, simple admixtures of lecithin-only and DOPA-only emulsions (Blue squares Figure 2.3(a)) yield a linear change in zeta potential as a function of DOPA weight percent. The results suggest that less than 5% of DOPA is needed to make a significant increase in zeta potential in the mixed lipid emulsion.

The unusually rapid change in zeta potential with DOPA loading suggests complex phenomena are involved. Small amounts of DOPA appear to dramatically alter the interaction between emulsion particles via the electro-viscous effect [421, 422], as evidenced by a rapid increase in viscosity of the DOPA-lecithin emulsion as the amount of DOPA used increases. There is no evidence for emulsion-breaking and the primary particles retain a relatively constant diameter as measured with DLS (Figure 2.3(d)). It is likely that the zeta potential measurement is artificially increased to be more negative since

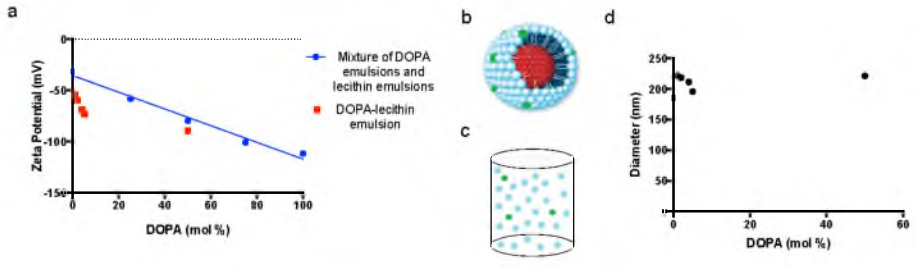

Figure 2.3 Zeta potential and size of DOPA-lecithin emulsion. (a) The zeta potential of emulsions prepared with lecithin and DOPA lipids: mixed lipids (red squares), admixtures of single lipid emulsions (blue squares). Only a small amount of DOPA can make the surface charge of DOPA-lecithin emulsion more negative. (b) The concept of DOPA lipids (green) integrated into lecithin emulsion (blue). (c) The concept of mixture of DOPA emulsions (green) and lecithin emulsions (blue). (d) The size of various compositions of emulsions shows no obvious change.

as the viscosity increases, the electrophoretic mobility decreases and given the dielectric constant and Henry's constant is unchanged, the measured zeta potential also must be larger, according to equation 1.10.

For the purpose of this project, 2 % DOPA and 98 % lecithin (2D98L) emulsion (Sample 3 in Table 2.1) was chosen to balance between high zeta potential and low viscosity.

2.5.2 Coating

The isoelectric points of PLL and CS were determined by measuring the zeta potential as a function of titration with acid and base (Figure 2.4). PLL is electrically neutral at pH 7 and CS at pH 8. Due to gel formation of chitosan at the isoelectric point [423], a lower electrophoretic mobility results (according to equation 1.10), that effects measurement of the zeta potential at the high pH end of the chitosan curve in Figure 2.4(b). The zeta potential curve versus pH is not complete during the pH titration range. Hence, the shape of the titration curve of chitosan is different from PLL. The titration curve of 2D98L

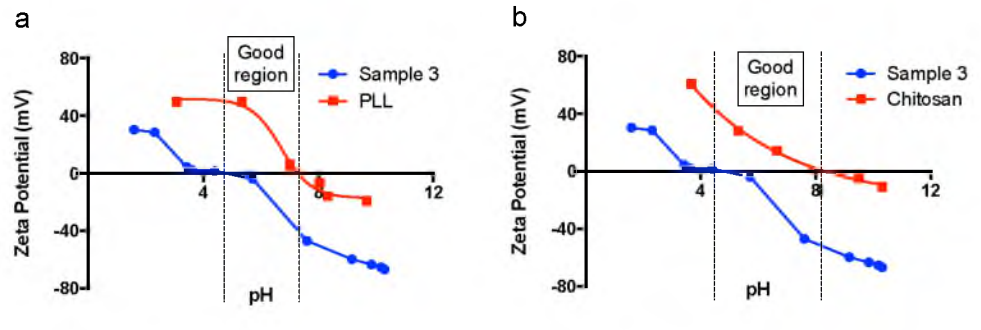

Figure 2.4 Good region for coating. (a) The zeta potential versus pH curves of sample 3 (2D98L emulsion) and PLL show opposite electric charge from pH 5.0 to pH 7.5. (b) The zeta potential versus pH curves of sample 3 (2D98L emulsion) and CS show opposite electric charge from pH 5.0 to pH 8.5.

emulsion is more complex. The phosphate group of lecithin has one titratable proton, while DOPA has two (Figure 2.5). Hence, the first drop in the 2D98L emulsion curve can be viewed as the first titratable proton release from phosphate groups of both DOPA and lecithin. The midpoint of the first drop is at pH 2.86 close to the pK_{a1} 2.12 of phosphoric acid. The midpoint of the second drop between a pH value 7.06 is close to the pK_{a2} 7.21 of phosphoric acid and represents the second titratable proton of DOPA. The equilibrium reactions of phosphoric acid can be seen:

$$H_3PO_4 \leftrightarrow H^+ + H_2PO_4^- \qquad K_{a1} = \frac{[H^+][H_2PO_4^-]}{[H_3PO_4]} = 7.5\times10^{-3} \quad (pK_{a1} = 2.12)$$

$$H_2PO_4^- \leftrightarrow H^+ + HPO_4^{-2} \qquad K_{a2} = \frac{[H^+][HPO_4^{-2}]}{[H_2PO_4^-]} = 6.2\times10^{-8} \quad (pK_{a2} = 7.21)$$

$$HPO_4^{-2} \leftrightarrow H^+ + PO_4^{-3} \qquad K_{a3} = \frac{[H^+][PO_4^{-3}]}{[HPO_4^{-2}]} = 2.14\times10^{-13} \quad (pK_{a3} = 12.67)$$

The emulsion and PLL have opposite electrical charge between pH 5.0 to pH 7.2 and CS between pH 5.0 to pH 8.5 with the greatest charge difference at around pH 7.2.

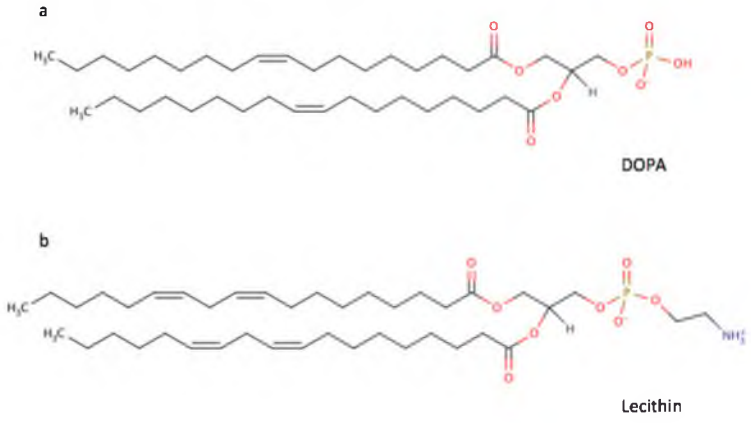

Figure 2.5 Chemical structures of DOPA and lecithin. (a) The phosphate group in the hydrophilic head of DOPA shows two available protons to release. (b) The phosphate group in the hydrophilic head of lecithin shows one available proton to release. Both are drawn by the software MarvinSketch.

Thus, this is the pH at which best coating should take place. Therefore, PLL and CS solutions at pH 6.5 and 3.5, respectively, were added to the 2D98L emulsion (Sample 3 from Table 2.1) prepared at pH around 7.5 with an estimated concentration of 8.2×10^{12} particle/ml, containing roughly 46.2 micrograms of lipids. The pH of each sample after mixing was then adjusted to 7.2 and held for 5 min for equilibrium. Samples were then characterized with DLS and zeta potential (Figure 2.6). The average particle diameter increased linearly as a function of PLL added, largely due to aggregation at the highest PLL concentrations, but exhibited saturation behavior for CS without apparent aggregation (Figure 2.6(a) and 2.6(b)). Figure 2.6(c) and 2.6(d) show the zeta potential decreasing to below -10 mV at the highest PLL concentrations.

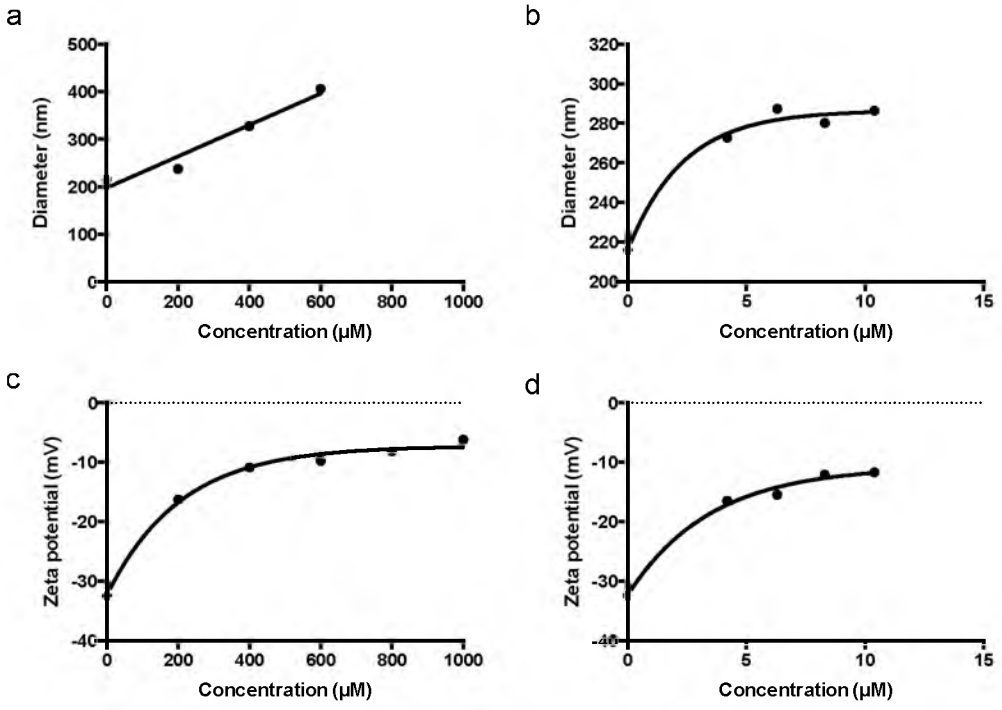

Figure 2.6 Coated emulsions at pH 7.2. (a) PLL-coated emulsion diameter. (b) CS-coated emulsion diameter, (c) PLL-coated emulsion zeta potential, and (d) CS-coated emulsion zeta potential. At higher PLL concentrations, particles tend to aggregate because their zeta potential falls below -10 mV.

The results above, while suggestive, are not a direct proof that coating has been applied. Therefore, we developed a different approach in which we compared the zeta potential as a function of pH for uncoated (Figure 2.7) and coated 2D98L (Figure 2.8) emulsions. A significant jump in zeta potential is seen between pH 3 and pH 7 because proton concentration changes the surface charge of uncoated emulsion (Figure 2.4).

The size and zeta potential of 2D98L emulsion particles in Figure 2.7 did not change much as pH changed and temperature increased. For convenience, the average size and zeta potential of uncoated emulsions were used to plot in Figure 2.8. The temperature-dependent data were recorded in two pH groups avoiding the steep transition region (first group pH_a is pH 3.51, 3.57, 3.62, and 3.71, and second group pH_b is pH 6.95, 7.02, 7.08, 7.12, and 7.19). For PLL, the size and zeta potential measured at the same temperature in the second pH group were averaged for Figure 2.8(a) and 2.8(b). For the CS part, they were from the first pH group for Figure 2.8(c) and 2.8(d). Also, the pH difference of ionic strength for these samples can be ignored because the factor of phosphate buffer in emulsion would dominate mainly and all the samples have the same concentration of phosphate buffer.

For PLL-coated emulsions, the diameter of the resulting particle increases with the amount of coating material used with aggregation of particles at the highest coating concentration. Higher temperatures result in less aggregation. The corresponding zeta potential of the coated particles becomes less negative with the amount of coating material used and with temperature. For CS-coated emulsions, the size of the emulsion particles also increases with coating material used and with increasing temperature, while the zeta potential becomes increasingly positive with coating amount at lower temperature, but less

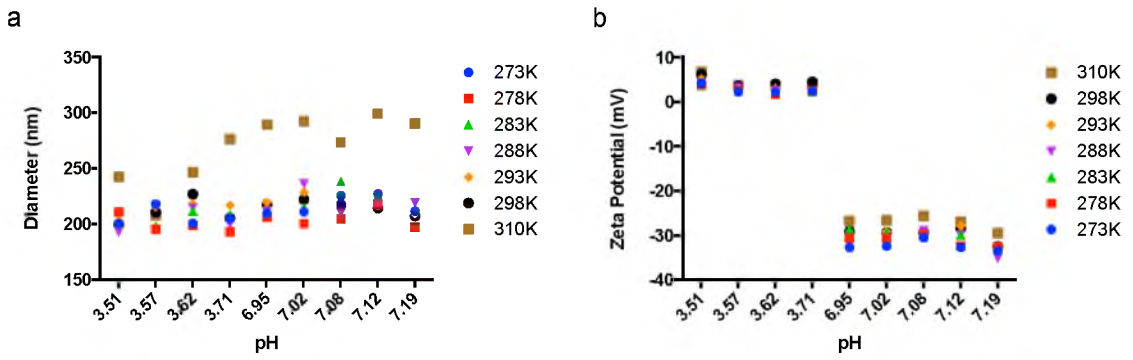

Figure 2.7 Nine emulsion samples at various pH. (a) The size of 2D98L emulsion versus pH, and temperature. In the fixed temperature (except 310K), emulsion size stayed similar with varying pH. (b) The zeta potential of 2D98L emulsion versus pH, and temperature. In the same pH range (around pH 3.6 and 7.1), zeta potential did not change much at the fixed temperature. For convenience, the average size and zeta potential were used for following experiments.

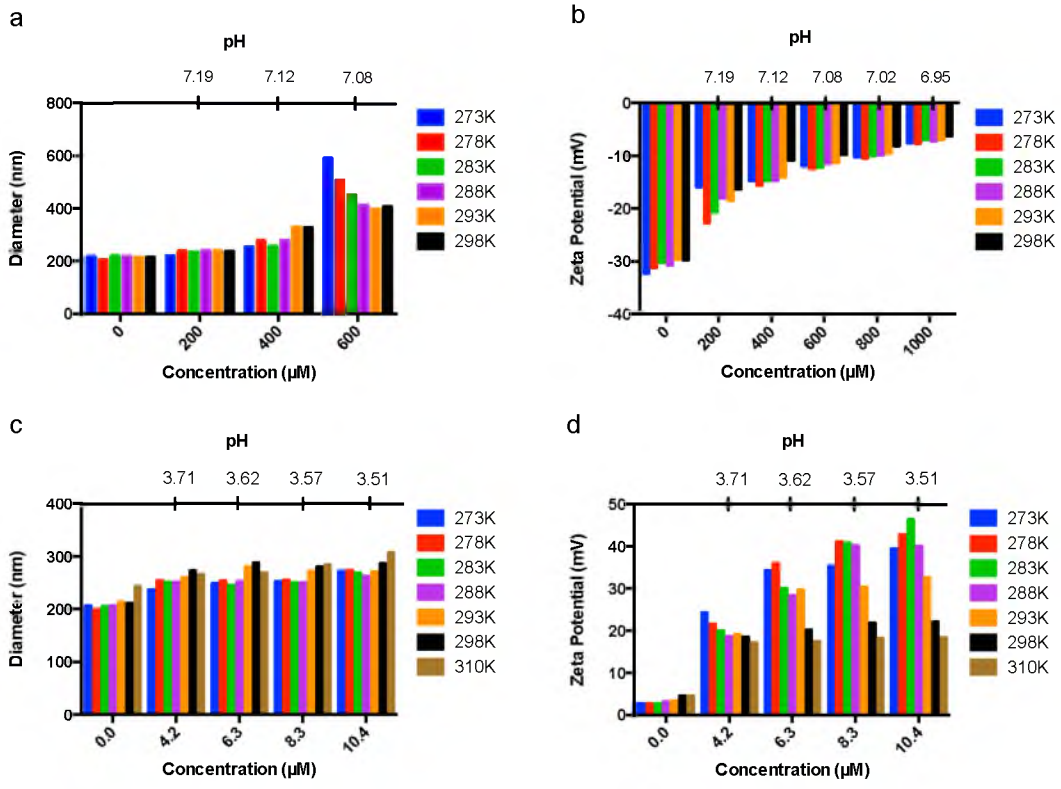

Figure 2.8 Coated emulsions at various pH. (a) The diameter of PLL-coated emulsion. (b) The zeta potential of PLL-coated emulsion. (c) The diameter of CS-coated emulsion. (d) The zeta potential of CS-coated emulsion. No obvious trend for various coating concentration and temperature to size and zeta potential could be concluded at this point. Further data are necessary to find out the bound material concentration.

dramatically increasing at higher temperatures. This suggests that thetemperature-dependent properties of CS in this system are different from those of PLL.

In the analysis above, all data are plotted with respect to the amount of coating material used to make the sample. In order to be able to attribute the differences highlight in Figure 2.8 to the coating, it is necessary to correlate the results to the actual amount of coating material bound to the particles. The amount bound was calculated from the amount added and the direct colorimetric measurement of the amount unbound.

2.5.3 Colorimetric determination

The result of unbound and bound PLL and CS concentration was measured and calculated by colorimetric determination. In Figure 2.9, it shows the concentration of PLL/CS-bound coating materials versus coating concentration. The concentration of emulsion-bound PLL increases as the coating concentration increases but decreases for CS molecules. The amount of bound coating material as a function of applied coating amount

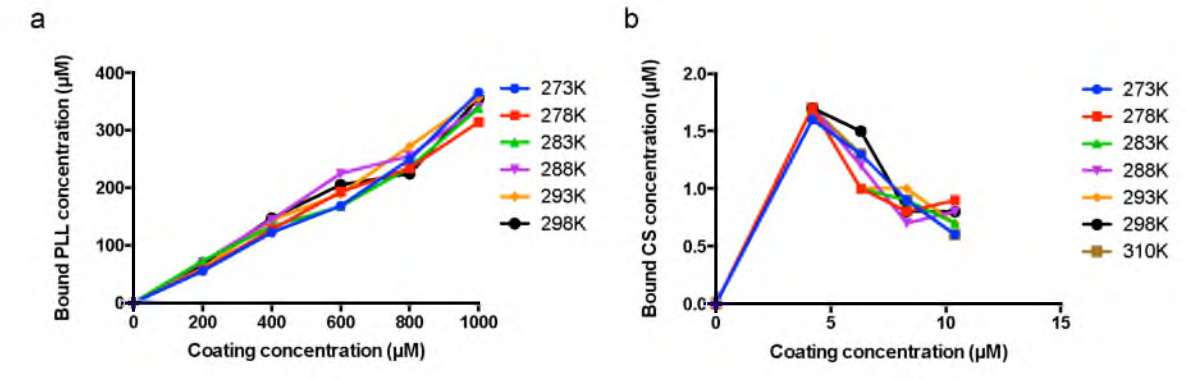

Figure 2.9 The bound PLL/CS concentrations are shown with various coating concentrations and different temperatures. From colorimetric determination results, the bound material concentration is temperature independent. The unexpected behavior of CS-bound concentration could be related to conformation changes.

is temperature independent. Hence, we hypothesize that the unexpected behavior of bound CS concentration could be associated with concentration-dependent conformational changes of the molecules.

2.5.4 Modeling

Zeta potential measurements were used as an alternate means to determine the amount of coating. In a colloidal system, the electric potential as the function of the distance from particle is extremely complicated. It can be illustrated as the following equation [299] ,

$$\frac{d^2\psi}{dl^2} = -\frac{e}{\varepsilon}\sum_i Z_i n_{i_0} exp\left(\frac{Z_i e\psi}{kT}\right) \quad (2.3)$$

where

ψ is the potential at the distance l from the particle surface

ε is dielectric constant of medium

n_{i_0} is the bulk concentration of ions with charge Z_i

e is one electron charge

k is the Boltzman's constant

T is the absolute temperature

If the colloidal system has low charge density, the quantity ($Z_i e\psi/kT$) would be less by one and the above equation can be simplified as [299],

$$\psi(l) = \psi_\delta e^{-\kappa l} \quad (2.4)$$

where

ψ_δ is the Stern potential

κ is the reciprocal of Debye length

As the distance from the particle surface is equal to Debye length, the electric potential would be the zeta potential. In other words, the Stern potential is 2.7 times to the zeta potential, according to equation 2.4 (as *l* is equal to Debye length). Because the Stern plane is really close to the particle surface, we assume that the value of the Stern potential should be near to the surface potential. Moreover, surface charge density can be calculated from the surface potential by applying the following equation,

$$\sigma = \frac{\varepsilon\varepsilon_0\psi_0}{\lambda_d} \tag{2.5}$$

where

σ is the surface charge density

ε is the dielectric constant of medium (ε_{water} = 78.5)

ε_0 is the vacuum permittivity

ψ_0 is the surface potential

λ_d is the Debye length (or κ^{-1})

The surface charge can be obtained by using the area of particle surface so the surface charge change can be calculated after coating. Finally, by using the surface charge change and the charge of each coating material, the amount of coating materials on one emulsion can be derived. Before that, the Debye length is defined as the following equation,

$$\lambda_d = \sqrt{\sum \frac{\varepsilon \varepsilon_0 kT}{{Z_i}^2 e^2 n_{i_0}}} \qquad (2.6)$$

The following calculation of Debye length, Stern potential (viewed as surface potential), surface charge density, surface charge (Q), and surface charge change (ΔQ) can be arranged in Table 2.4.

The calculated number of bound molecules per single emulsion particle is estimated by dividing the change in surface charge by the charge of a single coating molecule. PLL with average molecule weight 1250 has 8.6 repeat units per molecule, and CS has 837.2 repeat units per molecule. Hence, assuming each unit has one unit of electrical charge, then one PLL and one CS molecule would have a total charge of 1.37×10^{-18} C and 1.34×10^{-16} C, respectively. The results can be viewed in Figure 2.10. The number of PLL molecules per emulsion particle is much larger than that of CS. This can be readily explained by the difference of molecule weight of PLL and CS. As more PLL is added to the emulsions, the calculated number of PLL per particle increases independent of temperature. Because of its size, steric, and local charge hindrance, far fewer CS molecules need to interact with the emulsion surface to neutralize the charge. The reason for the difference of bound number is that the PLL we used is small molecules and CS is much bigger. A similar temperature dependence is seen for CS as in Figure 2.10(b) since the calculated results are derived from those measurements.

Since the surface charge density and number of surface charges occupied by a coating molecule are known, it is possible to back estimate the number emulsion particles involved. Based on the amount of material used and MarvinSpace estimates each identical emulsion sample used in this study should contain about 68.4nmol. Based on the following equations,

Table 2.4 The profile of Debye length, stern potential, surface charge density, surface charge, and surface charge change of emulsion and PLL/CS-coated emulsion

Sample	λ_d (nm)	ψ_δ (mV)	σ (C/m^2)	10^{-15} Q (C)	10^{-15} ΔQ (C)
E (pH$_b$, T1)	0.746	-88.0	-0.818	-12.1	0
P1T1	0.746	-20.6	-0.019	-2.8	9.3
P2T1	0.746	-27.7	-0.026	-3.8	8.3
P3T1	0.746	-32.4	-0.030	-4.4	7.7
P4T1	0.746	-40.2	-0.037	-5.5	6.6
P5T1	0.746	-43.2	-0.040	-6.0	6.1
E (pH$_b$, T2)	0.753	-84.8	-0.078	-10.3	0
P1T2	0.753	-20.8	-0.019	-2.5	7.8
P2T2	0.753	-20.8	-0.026	-3.4	6.9
P3T2	0.753	-34.0	-0.031	-4.1	6.2
P4T2	0.753	-42.4	-0.039	-5.2	5.1
P5T2	0.753	-61.7	-0.057	-7.5	2.8
E (pH$_b$, T3)	0.760	-82.2	-0.075	-11.4	0
P1T3	0.760	-19.1	-0.017	-2.7	8.7
P2T3	0.760	-27.1	-0.025	-3.8	7.6
P3T3	0.760	-33.2	-0.030	-4.6	6.8
P4T3	0.760	-40.2	-0.037	-5.6	5.8
P5T3	0.760	-56.3	-0.051	-7.8	3.6
E (pH$_b$, T4)	0.767	-83.7	-0.076	-11.4	0
P1T4	0.767	-19.6	-0.018	-2.7	8.7

Table 2.4 Continued

Sample	λ_d (nm)	ψ_δ (mV)	σ (C/m^2)	10^{-15} Q (C)	10^{-15} ΔQ (C)
P2T4	0.767	-26.8	-0.024	-3.7	-7.7
P3T4	0.767	-31.3	-0.028	-4.3	7.1
P4T4	0.767	-40.0	-0.036	-5.4	6.0
P5T4	0.767	-48.9	-0.044	-6.7	4.7
E (pH$_b$, T5)	0.774	-80.5	-0.072	-10.6	0
P1T5	0.774	-18.8	-0.017	-2.4	8.2
P2T5	0.774	-26.0	-0.023	-3.4	7.2
P3T5	0.774	-30.7	-0.028	-4.1	6.5
P4T5	0.774	-38.1	-0.034	-5.0	5.6
P5T5	0.774	-50.3	-0.045	-6.6	4.0
E (pH$_b$, T6)	0.780	-80.8	-0.072	-10.5	0
P1T6	0.780	-16.9	-0.015	-2.2	8.3
P2T6	0.780	-22.2	-0.020	-2.9	7.6
P3T6	0.780	-26.6	-0.024	-3.5	7.0
P4T6	0.780	-29.6	-0.026	-3.9	6.6
P5T6	0.780	-44.3	-0.039	-5.8	4.7
E (pH$_a$, T1)	0.746	7.6	0.007	0.9	0
C1T1	0.746	107.4	0.100	13.4	12.5
C2T1	0.746	96.0	0.089	11.9	11.0
C3T1	0.746	93.2	0.086	11.6	10.7
C4T1	0.746	66.1	0.061	8.2	7.3

Table 2.4 Continued

Sample	λ_d (nm)	ψ_δ (mV)	σ (C/m^2)	10^{-15} Q (C)	10^{-15} ΔQ (C)
E (pH$_a$, T2)	0.753	7.4	0.007	0.8	0
C1T2	0.753	116.3	0.107	13.5	12.7
C2T2	0.753	111.7	0.103	12.9	12.1
C3T2	0.753	97.9	0.090	11.3	10.5
C4T2	0.753	58.7	0.054	6.8	6.0
E (pH$_a$, T3)	0.760	7.3	0.007	0.9	0
C1T3	0.760	126.1	0.115	15.2	14.3
C2T3	0.760	111.2	0.102	13.4	12.5
C3T3	0.760	81.6	0.075	9.8	8.9
C4T3	0.760	54.4	0.050	6.5	5.6
E (pH$_a$, T4)	0.767	8.63	0.008	1.0	0
C1T4	0.767	108.7	0.099	13.1	12.1
C2T4	0.767	109.3	0.099	13.2	12.2
C3T4	0.767	76.9	0.070	9.3	8.3
C4T4	0.767	50.6	0.046	6.1	5.1
E (pH$_a$, T5)	0.773	9.2	0.008	1.2	0
C1T5	0.773	88.9	0.080	11.4	10.2
C2T5	0.773	82.6	0.074	10.6	9.4
C3T5	0.773	80.7	0.073	10.4	9.2
C4T5	0.773	51.9	0.047	6.7	5.5
E (pH$_a$, T6)	0.780	12.6	0.011	1.6	0

Table 2.4 Continued

Sample	λ_d (nm)	ψ_δ (mV)	σ (C/m^2)	10^{-15} Q (C)	10^{-15} ΔQ (C)
C1T6	0.780	60.1	0.054	7.5	5.9
C2T6	0.780	59.5	0.053	7.4	5.8
C3T6	0.780	54.9	0.049	6.8	5.2
C4T6	0.780	50.3	0.045	6.3	4.7
E (pH$_a$, T7)	0.795	12.5	0.011	2.0	0
C1T7	0.795	50.0	0.044	8.1	6.1
C2T7	0.795	49.5	0.043	8.0	6.0
C3T7	0.795	47.6	0.042	7.7	5.7
C4T7	0.795	46.8	0.041	7.6	5.6

*E: uncoated emulsion

$$Emulsion\ concentration$$

$$= \left(\frac{Total\ number\ of\ bound\ materials\ on\ total\ emulsions}{Total\ number\ of\ bound\ materials\ on\ one\ emulsion}\right) \quad (2.7)$$

$$= \left[\frac{Total\ number\ of\ bound\ materials\ on\ total\ emulsions}{\left(\frac{Surface\ coarge\ coange\ after\ coating}{One\ coating\ material\ charge}\right)}\right] \quad (2.8)$$

The total number of bound materials on total emulsion could be acquired by knowing the number of bound materials for one emulsion (Figure 2.10) and theoretical emulsion concentration (68.4nmol). In Figure 2.11, bound PLL and CS concentrations converted from total number of bound materials on total emulsions were plotted versus coating material concentration.

The apparent change in bound coating material concentration is quite large and is not easily explained by loss of emulsion particles. Rephasing of the emulsion system to form multilamelar lipid layers would have to result in breaking of the emulsion or expansion of the emulsion size, which is not true for the subset of data points in Figure 2.11. A likely explanation is expansion or compression of the coating molecules as they accumulate on the emulsion surface. A compression and expansion ratio (CER) can be defined as,

$$CER = \frac{Bound\ concentration\ by\ colorimetric\ determination}{Bound\ concentration\ by\ theoretical\ calculation} \quad (2.9)$$

The numerator and the denominator are from Figure 2.9 and 2.11, respectively. If CER is larger than one, it means the coating materials on the emulsion surface compress. If CER is smaller than one, it means the coating materials on the emulsion surface expand. In Figure

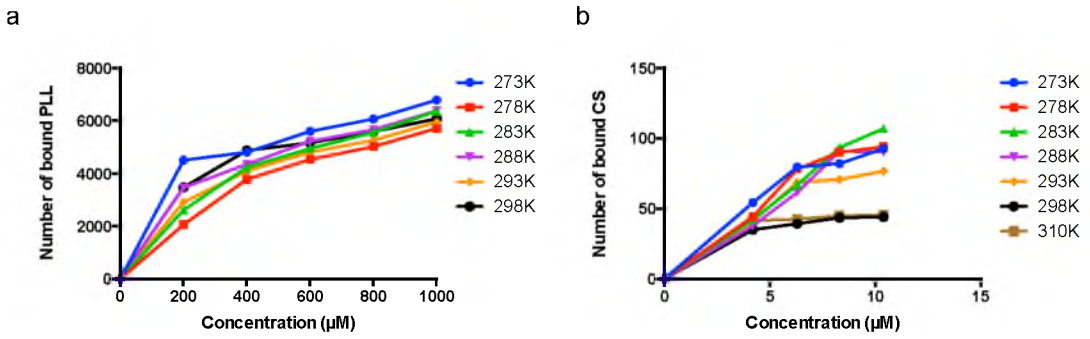

Figure 2.10 The number of bound PLL/CS. (a) The curve of the number of bound PLL per one emulsion versus coating concentration at various temperatures. (b) The curve of the number of bound CS per one emulsion versus coating concentration at various temperatures. There is no obvious trend of coated emulsions within various temperatures. The large molecule weight gap of PLL and CS makes the number of coating materials different in these two figures.

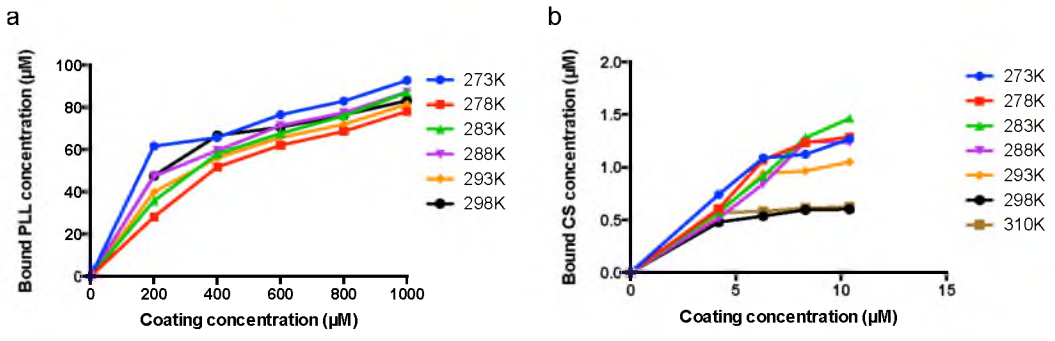

Figure 2.11 The bound coating material concentration was obtained via theoretical calculation. (a) The bound PLL concentration versus PLL coating concentration at various temperatures. (b) The bound CS concentration versus CS coating concentration at various temperatures.

2.12, the CER values for PLL- and CS-coated emulsions are plotted against the amount of PLL and CS used in the coating procedure. In Figure 2.12(a), it shows PLL on coated emulsions would become more compressed and increases packing density as PLL concentration goes higher. However, CS on coated emulsions would become more expanded when increasing CS concentration. In Figure 2.12(b), CS emulsions coated at high temperature do not have as much CS molecules on the emulsion surface as those

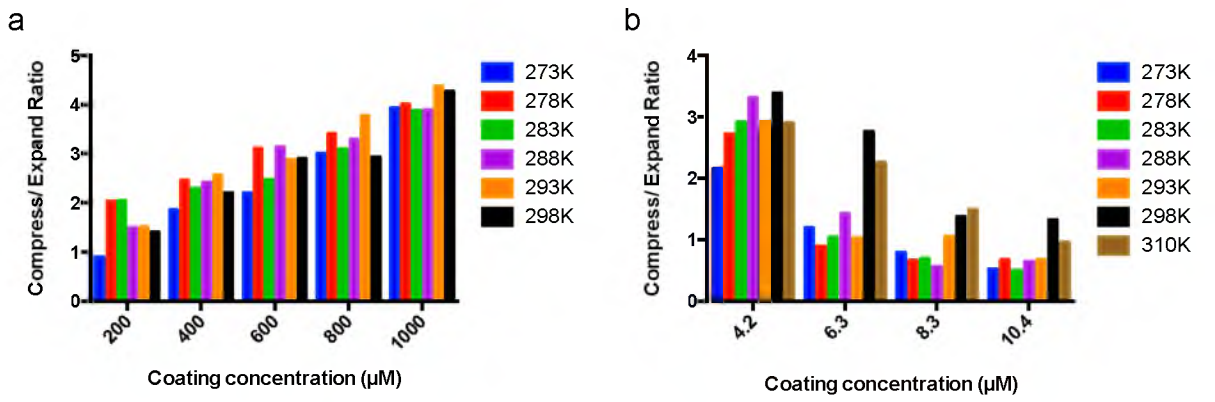

Figure 2.12 CER values. (a) The curve of CER versus PLL-coating concentration at various temperatures. (b) The curve of CER versus CS-coating concentration at various temperatures. With the increase of PLL concentration, PLL molecules on the emulsion surface become more compressed. Reversely, CS molecules on the emulsion surface become more expanded as CS concentration increases.

coated at lower temperature. This is why CS molecules on emulsion coated at higher temperature can be more compressed than those coated at lower temperature.

2.5.5 Thermodynamic analysis of coating process

Emulsion with varying coating concentration and temperature could be complex due to the conformation change of coating materials. One way to evaluate the tendency of favorable or unfavorable coating is via thermodynamic analysis. By means of colorimetric determination of PLL and CS, the binding constant (K_b) can be known (equation 2.10).

$$K_b = \frac{[Bound\ coating\ materials]}{[Unbound\ coating\ materials][Unbound\ emulsions]} \qquad (2.10)$$

The concentration of bound coating materials and unbound coating materials was determined colorimetrically. In the initial emulsion concentration (68.4nmol), the

concentration of bound coating materials and the calculated number of coating materials on one emulsion could decide the concentration of unbound emulsions. In Figure 2.13, the K_b is shown at various coating concentration and temperature. Binding constants of PLL keep steady until the last high PLL coating concentration. The increment K_b at highest concentration means more PLL was attached to the nearly neutral coated emulsion surface. For CS, the lower coating concentration is, the higher binding constants they show. However, there is no specific trend of binding constant change at various temperatures.

Based on equation 2.1, the Gibbs surface free energy during the coating reaction at various temperatures is shown in Figure 2.14(a) and 2.14(b). The change of Enthalpy (ΔH, kJ/mol) and entropy (ΔS, kJ/mol/K) can be deduced by linear regression. The free energy represents the electrostatic binding of coating material to the emulsion surface during the coating. The negative slopes of the lines mean ΔS is a positive quantity consistent with a spontaneous process (ΔS>0) so increasing the coating tends to move the system to a more stable energy state. In Figure 2.14(a), the samples with PLL coating concentrations of 200,

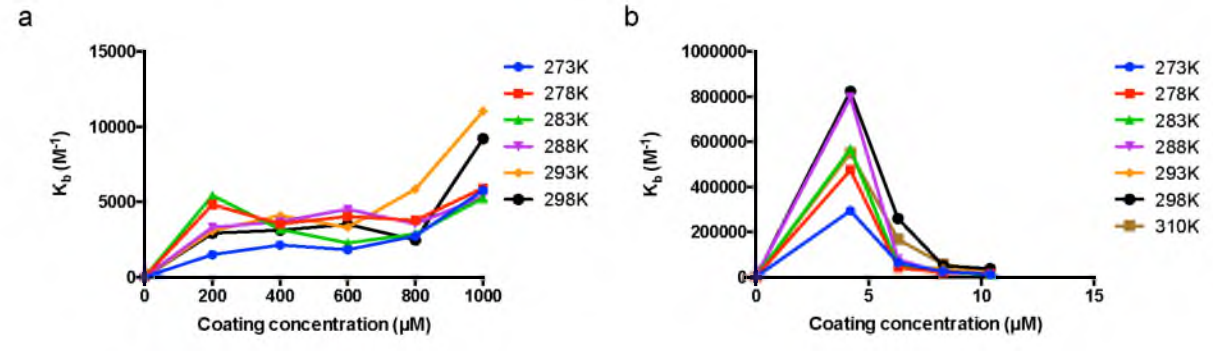

Figure 2.13 Binding constants. (a) Binding constant of PLL at various coating concentration and temperature. The binding constant of PLL increased as higher PLL coating concentration was applied. (b) Binding constant of CS at various coating concentration and temperature. The binding constant of CS decreased as higher CS coating concentration was applied. It is still difficult to realize the physical relation between binding constant and temperature from the above two diagrams.

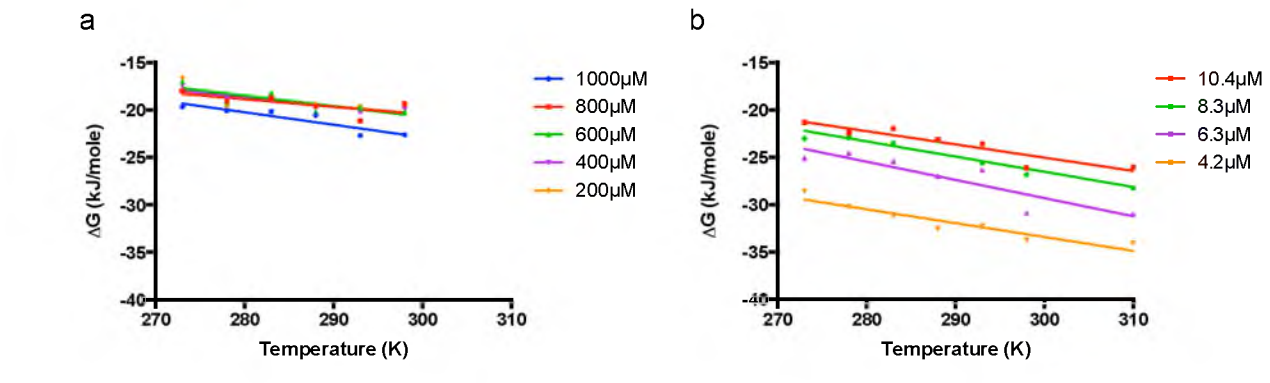

Figure 2.14 Free energy. (a) Emulsion coated by PLL concentration 1000 μM had lowest Gibbs surface free energy because the conformation of PLL became more compressive (b) The Gibbs surface free energy of CS-coated emulsion was lower as coating concentration was lower due to the compressive CS conformation.

400, 600, and 800μM have the same slope (ΔS) and intercept (ΔH), but the samples with PLL coating have a concentration of 1000 μM (higher concentration is different, with ΔG more negative). This result suggests that the emulsion surface is highly attractive to PLL, which reduces its surface energy initially, until a steady state surface energy is reached. Presumably, if we were to add additional PLL, the coating process would continue. The phenomenon in protein in which specific volume contracts during protein concentration increases is found in previous reference [424, 425]. The idea of macromolecular crowding is also similar, in which high concentration of protein alters its own conformation [426, 427].

In contrast, ΔG is more negative at lower CS coating concentration, suggesting that coating is more favored as more CS is bound to the emulsion. This can only be explained if the conformation of CS on the surface is changing in such a way as to increase the affinity for more binding. That some sugar expands or swells during the increment of its concentration is also found due to extra water uptake [428].

2.5.6 Fluorescent quenching

To prove that the packing density of coating molecules on the emulsions is a function of coating concentration, fluorescence quenching was used. Pyrene-doped PFOB emulsions were coated with PLL and CS and exposed to 5, 10, 20, and 50mM KI to form mixtures with final concentrations of 3.75, 7.5, 15, and 37.5mM. When the emulsion coating is in an expanded state, the iodide ions should be able to pass through the coating and interact with the pyrene at the emulsion/coating interface (Figure 2.15). The solubility of pyrene in water is relative slight (about 1~3μM) due to its hydrophobic aromatic structure [429, 430]. Hence, the fluorescent from pyrene in water is neglectable, which is compared to the pyrene doping concentration in PFOB (4mM). Although it would be difficult for iodide ions to pass through the PFOB core, they could quench pyrene accumulated near the surface of the PFOB core at least.

The fluorescent quenching of uncoated pyrene-doped emulsion in water as the control group is shown in Figure 2.16 to see if air affects the fluorescent quenching much because oxygen is one kind of quencher. It can be found that oxygen would cause fluorescent quenching slightly. Hence, it can be considered that all the fluorescent quenching is caused only by iodide ions in the following experiments. Because iodide is negatively charged, its efficiency for quenching pyrene depends on accessibility to pyrene. The emulsion surface charge, the density of the coating layer, and the overall viscosity of the suspension will affect the diffusion rate of ions. If the rate of diffusion is lower than the relaxation time of the dye, then there will be no quenching during the lifetime of the dye, except when a large concentration of ions is used. In this case, static, rather than dynamic quenching is possible.

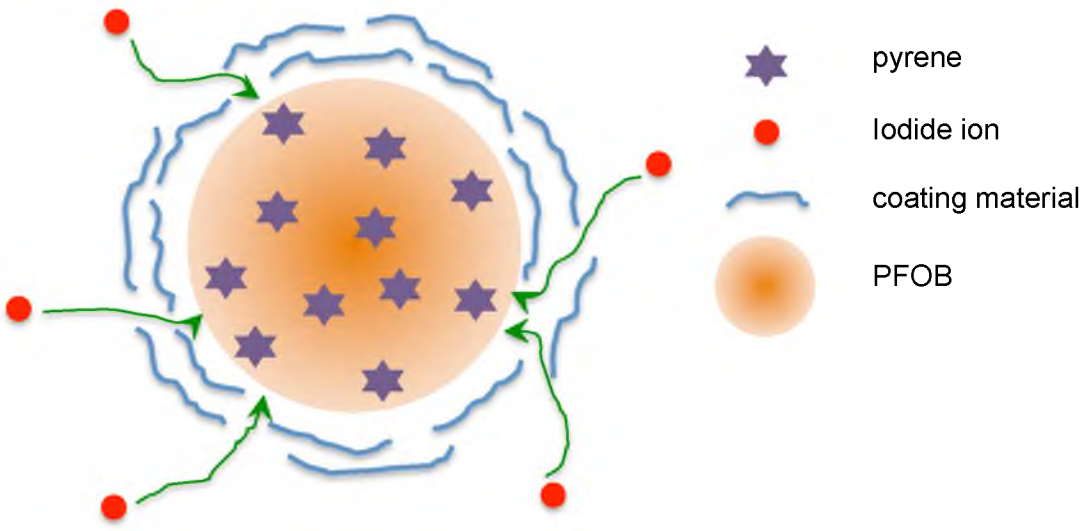

Figure 2.15 The proposed scheme for the reaction of iodide ions and pyrene is shown. The iodide ions can pass through the diffuse coating layers and quench the pyrene at the PFOB core oeripher (green lines indicate the routes).

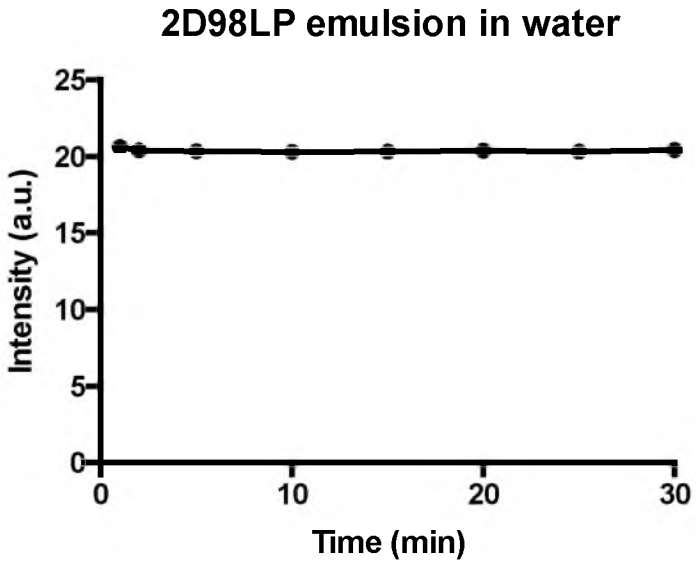

Figure 2.16 The fluorescent quenching of uncoated pyrene-doped emulsion by oxygen in the air is shown. All the measurement was done in the glass cuvette with the lid so the factor about oxygen quenching is limited.

Figure 2.17(a) shows that the ratio of I_0/I for pyrene in the PLL-coated emulsions increases linearly with iodide quencher concentration, but that there is more quenching for lower coating concentrations. This behavior is normally what would be expected for increasing coating density. In Figure 2.17(b), it is shown that for CS-coated emulsion, there is also more quenching when higher quencher concentration is used, but there is more quenching when a larger amount of CS is attached to the particles. This represents an unusual behavior, but does make sense in the context of the results of the previous section where it was inferred that CS molecules expand on the emulsion surface as their concentration increases. Considering the quencher concentration, as the KI concentration increases, the viscosity of the suspension increased so that the diffusion of iodide ions is slowed so there is less dynamic quenching possible. A Stern-Volmer constant (K_{S-V}) (Table 2.5) can be acquired from the slopes of the trend lines (linear regression) in Figure 2.17. The trend lines of the ratio of I_0/I versus [Q] for the CS-coated emulsion only are determined by the KI concentrations: 3.75, 7.5, and 15mM. The bimolecular quenching rate constant (k_q) can also be deduced using the pyrene fluorescent excited state lifetime (τ_0) in air-equilibrated water, 126ns [431]. The reason may be that the CS-coated emulsion surface has positive charges to attract the negatively charged iodide ions, but the PLL-coated emulsion surface has negative charges, shown in Figure 2.8(b) and 2.8(d).

Based on the result of defined CER ratio calculation shown in Figure 2.12 (as CER is larger than 1, the conformation of the coating material tends to be more compressed; as CER is smaller than 1, the conformation of the coating material tends to be more expanded) and the experiment about fluorescent quenching results, we can propose a concept for PLL and CS molecule conformation on coated emulsion (Figure 2.18). The coated PLL

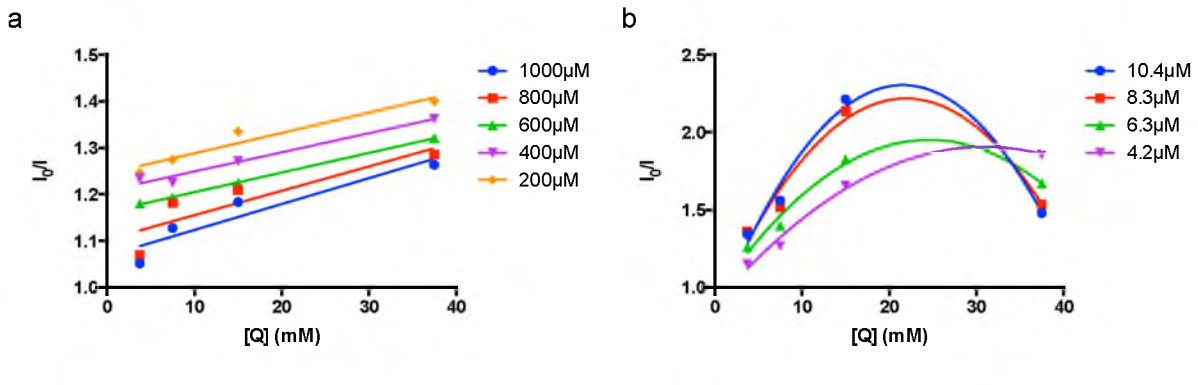

Figure 2.17 Fluorescent quenching results. (a) The ratio of the initial fluorescent intensity to the final fluorescent intensity versus the quencher concentration for PLL-coated emulsion is shown. As I_0/I is higher, it means iodide ions can pass easier through the more expanded coating layer at lower PLL concentration. (b) The ratio of the initial fluorescent intensity to the final fluorescent intensity versus the quencher concentration for CS-coated emulsion is shown. As I_0/I is higher, it suggests iodide ions can pass easier through the more expanded coating layer coated by higher CS concentration. When considered as a function of quencher concentration, regardless of the coating levels, quenching is reduced because the higher ion concentration causes a dramatic increase in suspension viscosity and reduction of dynamic (collisional) quenching.

Table 2.5 Stern-Volmer constants (K_{S-V}) and bimolecular quenching rate constant (k_q) of coated emulsion in various concentrations of KI solution

Conc. (μM)	Trend line slope	R^2	K_{S-V} (M^{-1})	10^{-9} k_q($M^{-1}S^{-1}$)
1000	0.00556	0.8788	5.6	0.044
800	0.00523	0.7780	5.2	0.042
600	0.00421	0.9995	4.2	0.033
400	0.00411	0.9745	4.1	0.033
200	0.00437	0.9369	4.4	0.035
10.4	0.08018	0.9918	80.2	0.636
8.3	0.07078	0.9806	70.8	0.562
6.3	0.05123	0.9899	51.2	0.407
4.2	0.04614	0.9870	46.1	0.366

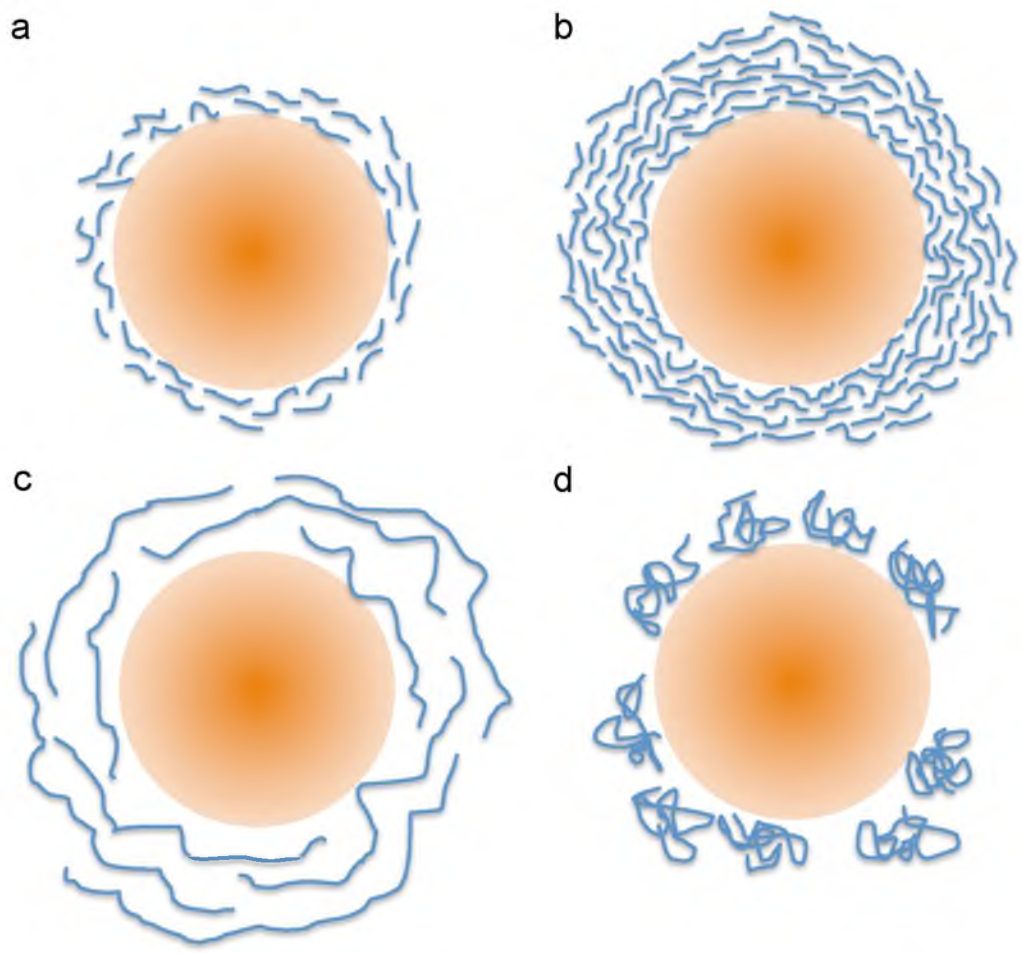

Figure 2.18 The conformations of the coating materials. (a) PLL-coated emulsion has more expanded surface during low coating concentration. (b) PLL-coated emulsion has more compressed surface during high coating concentration. (c) CS-coated emulsion has more compressed surface during low coating concentration. (d) CS-coated emulsion has more expanded surface during high coating concentration.

molecules on the emulsion surface pack loosely when the coating concentration is lower, as shown in Figure 2.18(a). Once PLL coating concentration increases, PLL molecules pack more tightly via electrostatic attraction on the emulsion surface in Figure 2.18(b). In contrast, CS molecules on the emulsion surface pack tightly in Figure 2.18(c) at lower CS coating concentration but rephase to looser packing at the higher concentration (Figure 2.18(d)). Hence, it can be concluded that PLL molecules on the emulsion surface become

more compressed and CS molecules on the emulsion surface become more expanded while the coating concentration increases. The reversed result of conformation change could be possibly related to the large difference between the molecular weight of PLL and CS.

2.6 Conclusions

This work shows an analysis of an emulsion coating process that in addition to providing information about the thermodynamics of coating reveal something fundamental about the characteristics of the coating molecules as the particles are formed. The ionic surfactant DOPA was used to create a negative surface charge on an emulsion make from 98% nonionic surfactant lecithin. One formulation with maximum surface charge and minimum modification (2% DOPA and 98% lecithin PFOB emulsion prepared at pH 7) is for measurement of binding equilibrium as a function of temperature and coating formation, and for zeta potential measurements as a function of coating formation. PLL and CS exhibited different coating characteristics explained by concentration and pH-dependent conformational differences. By using the measurements to back calculate the bound coating material concentration, it is possible to discern a change in the specific volume of the coating molecules that follows the expected trend for protein and sugar molecules in concentrated solution. The trend is rationalized due to the high local concentration of these molecules as they accumulate and attach to the emulsion surface. PLL molecules tend to compress on the coated emulsions as the coating concentration increases. Conversely, CS molecules tend to expand as the concentration increases. The effect of compression versus expansion was further validated by means of fluorescent quenching. The ratio of initial fluorescent intensity to final intensity is higher for lower PLL coating concentration and

higher CS coating concentration, supporting the hypothesis that at these two extreme concentration ranges, both conformations of the coating materials are expanded and create a more porous coating that can be easily permeated by small charged ions. Thermodynamic calculations also support this picture.

CHAPTER 3

METHOD TO IMPROVE THE ENCAPSULATION OF PERFLUOROCARBONS (PFCs) IN OIL-IN-WATER (O/W) EMULSIONS USING COSOLVENT

As pointed out elsewhere, the purpose of this project is to produce a reinforced, perfluorocarbon-based blood substitute via electrostatic layer-by-layer coating of biological polymers with high production yield. In Chapter 2, the relation of polymer structure to emulsion phase stability and dynamic changes of the polymer conformation on emulsion surface were introduced. The next challenge is to manufacture emulsions at high yield. Here, a novel method of emulsion synthesis would be proposed.

3.1 Abstract

Perfluorocarbon oil-in-water (O/W) emulsions are challenging to produce in high yield due to the large hydrophobicity of perfluorocarbons and the high affinity of emulsifier for water and production of liposomes. Therefore, traditional emulsification processes are inefficient, and the result is a mixture of emulsion, liposomes, and excess oil/surfactants. To improve yields, various cosolvents were tested along with a low temperature vacuum drying method. FT-IR was used to relatively quantify the amount of perfluorocarbon

remaining in the mixture after this process and the result compared with standard mixing/extrusion methods. Hexane as the cosolvent had the best ability to product high-yield perfluorocarbon emulsions. Fluorescence methods were used to show that this method also reduces the formation of liposomes. Emulsions made by the direct-emulsified method and our new method (cosolvent method) had different sediment behaviors consistent with the higher density of the more pure emulsion preparation. The novel method exactly provides the possibility of high yield of emulsion synthesis.

3.2 Introduction

Oil-in-water (O/W) emulsions have been widely used in cosmetics, health care, food industry, firefighting, and pharmaceutical applications [432-441]. Using a ternary phase diagram or hydrophilic-lipophilic balance (HLB) rule, the ratio of oil, water, and surfactant can be easily selected to optimize the formation of O/W emulsions [442, 443]. However, these approaches obscure the reality that the demarcation of phases is blurry and that mixtures of phases exist throughout. For many applications, it is critical to have highly efficient production of the desired phase and minimize side products.

Perfluorocarbons (PFCs) O/W emulsions are an example of a system that is difficult to produce in concentrated, purified form because the available emulsifiers have difficulty mixing with the highly hydrophobic oil. Most PFC-based O/W emulsions are mixed phases. Mechanical methods such as extrusion are often insufficient to create a pure O/W phase. Here, we explore a cosolvent method to increases the yield of O/W emulsion and compare it to conventional methods such as extrusion.

3.3 Experimental method

3.3.1 Materials

Surfactant, 95% L-α-phosphatidylcholine (lecithin) from soybean was acquired from Avanti®. perfluorocarbon 1-bromoperfluorooctane (PFOB) (partial pressure P_{PFOB}: 6.5mmHg at 20°C) was purchased from Oakwood Products, Inc. Four organic liquids: ≥99.9% methanol (partial pressure $P_{methanol}$: 140.1mmHg) from Sigma-Aldrich, ≥99.5% ethanol (partial pressure $P_{ethanol}$: 58.7mmHg) from Sigma-Aldrich, ≥99.8% chloroform (parital pressure $P_{chloroform}$: 198.1mmHg) from Mallinckrodt chemicals, and ≥99.0% hexane (partial pressure P_{hexane}: 153.5mmHg) from Sigma-Aldrich were obtained [444]. Pure water (18.2 MΩ-cm) was produced using a Barnstead E-Pure (Barnstead/Thermolyne) ultrapure water system.

3.3.2 Cosolvent selection

For emulsions made using the cosolvent method, 10 ml of cosolvents were respectively mixed with 1 ml PFOB, and 1 g lecithin added while stirring magnetically at 1000 rpm for 30 min at room temperature (20°C). The molar ratio of lecithin to PFOB is about 1 to 4. The mixtures were allowed to rest in a closed container overnight then placed into a vacuum chamber at 4°C for 10 hours to evaporate the cosolvent. After this, 10ml of E-pure water was added to the mixture and stirred with 300 rpm at room temperature for 10 min. FTIR was applied to verify if PFOB retained.

3.3.3 Emulsion with cosolvent method

For emulsions made using the cosolvent method, 10 ml of hexane was mixed with 1 ml PFOB, and 1 g lecithin added while stirring magnetically at 1000 rpm for 30 min at 4 °C. The mixtures were placed into a vacuum chamber at 4 °C for 10 hours to evaporate the cosolvent. After this, 10 ml of E-pure water was added to the mixture and stirred at 300 rpm at room temperature for 10 min. The emulsion made by the cosolvent method is denoted as HPL emulsion. Where indicated, the emulsions were then extruded through a 600 nm pore size polycarbonate membrane (Nuclepore Track-Etch membrane) using a 10 ml Thermobarrel LIPEX extruder (Northern Lipids) 5 times at 500 psi in room temperature.

3.3.4 Emulsion with direct-emulsified method

For emulsions produced via extrusion method, 1ml PFOB, 1 g lecithin added, and 10ml water were mixed at the same time and stirred in 20 ml vial at 1200 rpm stirring for 30 min. The emulsions were then extruded through a 600 nm pore size polycarbonate membrane (Nuclepore Track-Etch membrane) using a 10 ml Thermobarrel LIPEX extruder (Northern Lipids) 5 times at 500 psi in room temperature. For the convenience, the emulsion made by direct-emulsified method is denoted as DE emulsion.

3.4 Characterization

3.4.1 Fourier transform infrared spectroscopy (FTIR)

An Excalibur 3100, Varian Inc. FTIR recording measured at 4 cm^{-1} resolution and averaging 64 scans were used to measure the relative PFOB content of the emulsions. Samples were placed in attenuated total reflectance (ATR) kit for measurement.

The region for C-F stretch is found between 1000 cm^{-1} and 1360 cm^{-1} and is diagnostic for the presence of PFOB in the samples. For molecules with one fluorine, one strong signal between 1000-1110 cm^{-1} is seen, and for molecules with multiple fluorine atoms, this peak splits into one symmetric peak and another asymmetric peak [346].

Spectral analysis was used to quantify the relative amount of PFOB remaining in the samples produced after the vacuum drying step. To do this, hexane was added to resuspend the emulsion instead of water. A demountable liquid cell (PIKE technology, WI) was used in this work. Liquid sample was injected into the center space of the spacer with a thickness of 0.015 mm (the pathlength through the sample). According to the Beer-Lambert Law, $A= \varepsilon bc$, where A is the absorbance, ε is the absorptivity co-efficient (L mol^{-1} cm^{-1}), b is the pathlength of light in the sample (cm), and c is the concentration of the sample (mol/L), the absorbance of the specific peaks on FT-IR spectra should be proportional to the functional group concentration in the sample when measured under the same conditions. The specific peak of carbon-fluorine bond at 1242 cm^{-1} was applied, and the peak height was acquired by drawing a baseline between the left and right lowest points of the specific peak. Hexane and PFOB mixtures were used to establish a calibration curve and the PFOB content in the experimental samples determined from this curve.

3.4.2 Phase transition temperature (PTT)

The optical clarity of the PFOB/hexane/lecithin mixture before vacuum drying was measured using the total amount of scattered light at 525 nm from 0 °C to 30 °C using a Cary 100 UV-Vis spectrophotometer with temperature control (Agilent). The particle sizes of lecithin in hexane and PFOB at 10 °C, 20 °C, and 30 °C were measured by dynamic

light scattering (DLS) using a Zetasizer Nano ZEN3600 from Malvern Instruments. Table 3.1 shows the required parameters for size measurement of the study [289-293].

Two emulsions made using hexane as the selected cosolvent were prepared for the remaining studies) at 0 °C (opaque) and 30 °C (transparent), respectively. FTIR was used to measure the amount of PFOB retained.

3.4.3 Fluorescence

To compare the ratio of liposomes generated in PFOB emulsion, emulsion was synthesized by direct-emulsified and cosolvent methods. Two fluorescent dyes, fluorescein (0.6 mM) and pyrene (4.0 mM), were added into prepared PFOB emulsions. Fluorescein with carboxyl and hydroxyl groups in its structure has slight solubility in water

Table 3.1 The parameters for DLS size measurement of PTT

Measured particles

Material	RI	Abs.
PFOB	1.3	0.010

Dispersed medium

Material	Temperature (°C)	Viscosity (cP)	RI
Water	25	0.8872	1.330
Hexane	10	0.3442	1.375
Hexane	20	0.3131	1.375
Hexane	30	0.2892	1.375

[445] but not in PFOB. Nonpolar pyrene with flat aromatic can slightly dissolve in water (1~3 μM) [429, 430] but has much higher solubility in nearly nonpolar PFOB. Hence, fluorescence from fluorescein in the sample can be viewed as the existence of liposomes. The presence of a large pyrene emission should indicate a large quantity of PFOB emulsion. First, 0.6 mM solutions of fluorescein in 10 ml water and 10 ml PFOB were made, respectively. Next, 4.0 mM solutions of pyrene in 10 ml water and 10 ml PFOB were made, respectively. The undissolved pyrene would be removed during extrusion (600 nm), and undissolved fluorescein was removed before resuspending vacuum-dried solid by 0.2 μm syringe filter (Whatman). The fluorescence of four samples doped with fluorescein or pyrene was analyzed. The detailed information about the four samples is shown in Table 3.2.

For DE emulsion, two samples were produced. One sample contained mixed 1.0 g lecithin, 1 ml PFOB, and 10ml water with 0.6 mM fluorescein and was extruded through a 600nm membrane. Another contained 1.0 g lecithin, 1 ml PFOB with 4.0 mM pyrene, and 10 ml water. Each were mixed and extruded through a 600 nm pore size membrane. Both samples were dialyzed against E-Pure water after extrusion using membrane tubing with molecular weight cut-off (MWCO) 3500 g/mol, from VWR Scientific. For HPL emulsion, two PFOB emulsion samples were also synthesized. One sample was a mixture of 1.0 g lecithin, 1 ml PFOB with 4.0 mM pyrene, and 10 ml hexane. Another one was a mixture of 1.0 g lecithin, 1 ml PFOB, and 10ml hexane. Each was vacuum-dried at at 4 °C for 10 hours. For resuspension, the sample with pyrene was added 10 ml water and the sample without pyrene was added 10 ml 0.6 mM fluorescein solution. Both samples were later extruded through a 600 nm pore-size membrane and dialyzed against E-Pure water. For

Table 3.2 The information of fluorescence-doped emulsion samples

Sample Denotation	Emulsion	Dope Fluorescence	Dope Conc. (mM)	Excitation wavelength (nm)	Expected emission peak (nm)
S1	DE	fluorescein	0.6	480	518
S2	DE	pyrene	4.0	337	394
S3	HPL	fluorescein	0.6	480	518
S4	HPL	pyrene	4.0	337	394

each of the four samples, fluorescence emission was recorded for the PFOB emulsion before extrusion, after extrusion/before dialysis and after dialysis.

In this work, fluorescence spectra were measured using a Cary Eclipse fluorescence spectrophotometer (Varian). Fluorescence measurements were performed using a photomultiplier tube detector set at a voltage of 400 volts. All samples were measured in a 1 cm pathlength quartz cuvette covered by a lid at room temperature. For the samples with fluorescein, the excitation wavelength was set at 480 nm and the expected emission peak would be at wavelength 518 nm. For the samples with pyrene, the excitation wavelength was set at 337 nm and the expected emission peak would be at wavelength 394 nm.

3.4.4 Centrifugation

To prove the difference of PFOB emulsion amount by cosolvent and direct-emulsified methods, centrifugation by density was applied (r_{PFOB}=1.93 g/ml). Centrifugation of the prepared samples (HPL emulsion with 600 nm extrusion and DE emulsion) was done at

2000 rpm for 10 min using a 5417C Eppendorf microcentrifuge. Emulsions with significant PFOB content should be easier to pellet by centrifugation, leaving behind empty liposomes and other low-density debris. HPL emulsions prepared by the cosolvent method, extruded, and for which FTIR indicated high PFOB content should be easiest to pellet. In contrast, DE emulsion with low PFOB content would not pellet easily. Particle sizes of DE and HPL emulsions after extrusion were verified by DLS to be similar (534nm and 548nm). FTIR was used to determine the PFOB content of HPL emulsion in pellet and supernatant.

3.4.5 Cryogenic transmission electron microscopy (Cryo-TEM)

To verify the morphology of HPL emulsion made above/below PTT and DE emulsion, TEM image were applied. Due to the fragility of the emulsion, Cryo-TEM can prevent emulsion from PFOB evaporation and structural rupture. For the samples of DE and HPL emulsion (with extrusion), approximately 3.5 μL of solution was placed on a holey-carbon-coated copper grid, blotted, and plunge-frozen in liquid ethane using an FEI Vitrobot (Hillsboro). Samples were then transferred to a Gatan 626 cryoholder (Pleasanton) cooled with liquid nitrogen. Cryo-TEM images were recorded at 200 kV in an FEI Tecnai F20 transmission electron microscope (Hillsboro) with the assistance of Dr. David Belnap, who helped prepare Cryo-TEM sample pretreatment procedures and acquired images.

3.5 Results and discussion

3.5.1 Miscibility of cosolvent with PFOB

To determine miscibility of cosolvent and PFOB, 1:1 mixtures of cosolvent/PFOB were prepared. In Figure 3.1, it can be seen there is a clear separation between methanol-PFOB

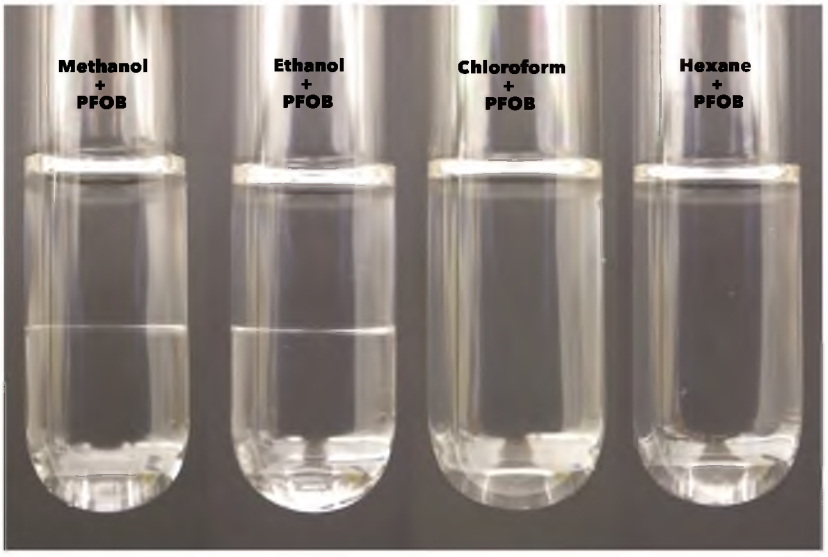

Figure 3.1 Methanol/PFOB, ethanol/PFOB, chloroform/PFOB, and hexane/PFOB mixtures. Methanol and ethanol are not miscible in PFOB so a clear boundary line can be seen in those mixtures. Due to higher density of PFOB, the top layer should be methanol and ethanol, respectively. Chloroform and hexane are miscible well with PFOB so no obvious boundary line can be found in those mixtures.

and ethanol-PFOB phases. Due to the density difference ($r_{methanol}$=0.792 g/ml, $r_{ethanol}$=0.789 g/ml, and r_{PFOB}=1.93 g/ml), the bottom layer is PFOB and the upper one is the cosolvent. It can be explained by viewing the dipole moment and polarity index of cosolvents. The dipole moment and polarity index of cosolvents could be found in previous reference [446, 447] (Methanol: 1.7 μ, 6.2; Ethanol: 1.69 μ, 5.2; Chloroform: 1.04 μ, 4.3; Hexane: 0 μ, 0). The chemical structure of PFOB is relative symmetrical; only bromine atom lies at the end of the structure. The electronegativity of bromine (2.96) and chlorine (3.16) is fairly close [448]. Hence, PFOB should be classified as a nonpolar solvent. Due to a higher polarity of methanol and ethanol, PFOB is immiscible with methanol and ethanol, but it is still miscible with chloroform.

3.5.2 Emulsion

Cosolvents (10 ml)/PFOB(1 ml) mixtures with added 1.0 g of lecithin at 20 °C are shown in Figure 3.2. Because PFOB has limited lipid solubility [449], most of the lecithin remained in the methanol and ethanol top layers, while a clear layer of PFOB remains in the bottom. Lecithin dispersed throughout the chloroform/PFOB mixture, forming a uniform transparent solution. Lecithin also dispersed throughout the hexane/PFOB but formed a uniform translucent solution.

The above four emulsions were allowed to rest overnight to observe any changes (Figure 3.3). Lecithin in the hexane/PFOB solvent separated into two layers, a clear layer on the top and a denser white layer on the bottom, while the other had no visible change. The clear layer contained hexane (determined by relative density compared to water) and

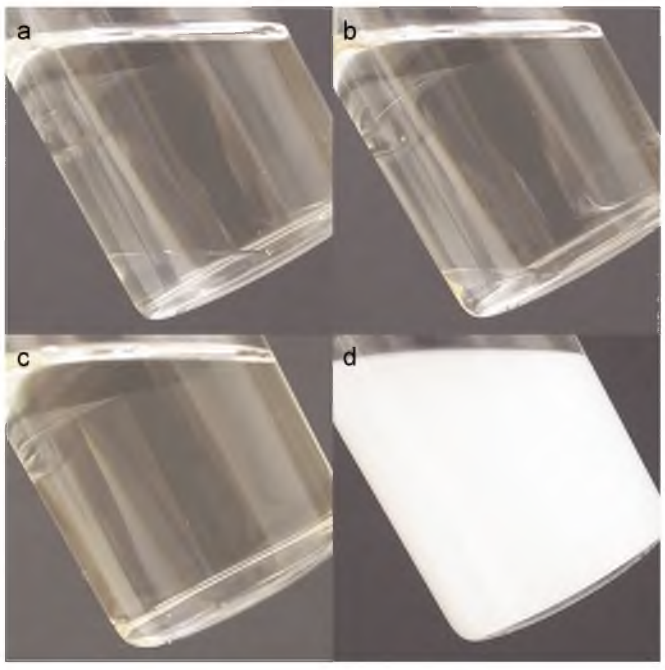

Figure 3.2 Lecithin dissolved in (a) methanol/PFOB, (b) ethanol/PFOB, (c) chloroform/PFOB, and (d) hexane/PFOB mixtures. Lecithin in chloroform/PFOB formed a uniform transparent solution, but lecithin in hexane/PFOB formed a uniform translucent solution.

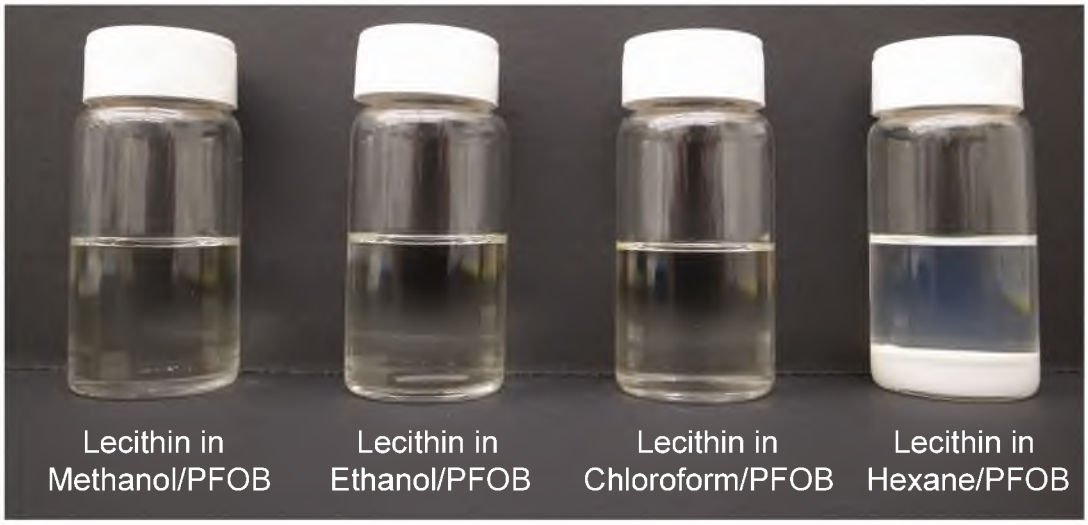

Figure 3.3 Four samples were allowed to rest overnight. From left to right: lecithin dissolved in methanol/PFOB, ethanol/PFOB, chloroform/PFOB, and hexane/PFOB. Only the latter produced a translucent emulsion that settled by gravity over time. The bottom layer of lecithin/PFOB/hexane should contain PFOB due to higher density.

some unused lecithin. The volume of the upper clear layer was similar to that of the amount of hexane added. Because of PFOB's higher relative density compared to hexane, the lower white layer should contain emulsion of lecithin-encapsulated PFOB. No droplets of clear PFOB were seen visibly.

To remove the higher volatility cosolvents and lower volatility unencapsulated PFOB from the emulsions, the four samples were dried by vacuum (about 0.25 atm) for 10 hours (Figure 3.4). Encapsulated PFOB is expected to be most resistant to vaporization. A light yellow solid material was generated in all four samples after the cosolvents were dried out. Cosolvent-dissolved lecithin gradually precipitated as cosolvent disappeared. In contrast, the sample prepared with hexane formed a uniform white solid (approximate volume: 2~3 ml) at the bottom of the vial.

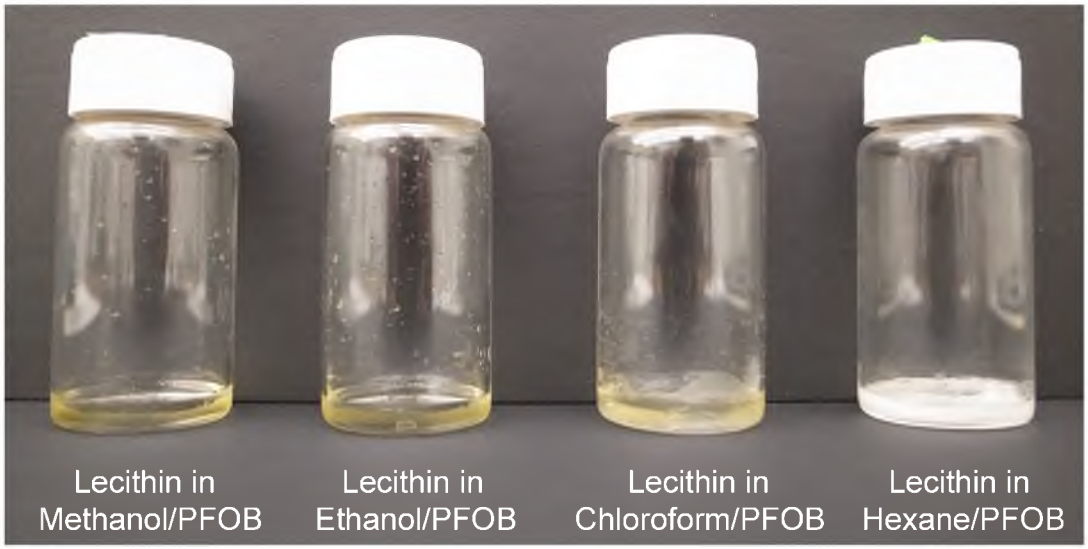

Figure 3.4 Samples prepared using the four cosolvents: methanol, ethanol, chloroform, and hexane, mixed with PFOB and vacuum-dried for 10 hours.

After the vaccum drying step, 5ml water was added and the suspension stirred at 300 rpm for 10 min to form a uniform phase. In Figure 3.5, four emulsions (MPL, EPL, CPL, and HPL emulsions) are shown after water resuspension.

The FTIR spectra of lecithin in water and PFOB are shown in Figure 3.6. Since PFOB shows peaks in the wavenumber range between 1000 to 1500 cm^{-1}, all subsequent scans focused on this region. Baseline-corrected FTIR spectra from MPL, EPL, CPL, and HPL emulsions (obtained by subtracting the spectra of lecithin in water from that of each sample and multiplying each by 20) are shown in the inset of Figure 3.7(a). MPL and EPL emulsions have no obvious peaks between the C-F bonds because almost all PFOB evaporated during vacuum. CPL emulsion had a small amount of PFOB retained and HPL the most. The absorbance at 1188 cm^{-1} versus polarity index in Figure 3.7(b) shows the PFOB retain rate has linear relation to the polarity index of the cosolvents. If the polarity

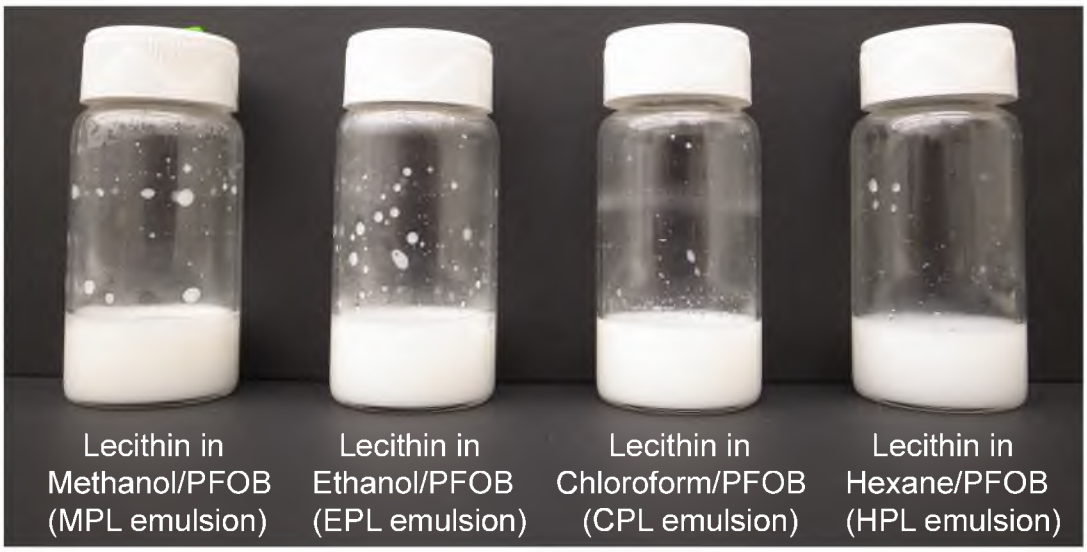

Figure 3.5 Water was added into each of the vacuum-dried samples. From left to right: lecithin dissolved in methanol/PFOB (MPL emulsion), ethanol/PFOB (EPL emulsion), chloroform/PFOB (CPL emulsion), and hexane/PFOB (HPL emulsion). It is difficult to tell the structure difference (liposome or emulsion) of these four samples so FTIR was applied to verify if PFOB was present after vacuuming.

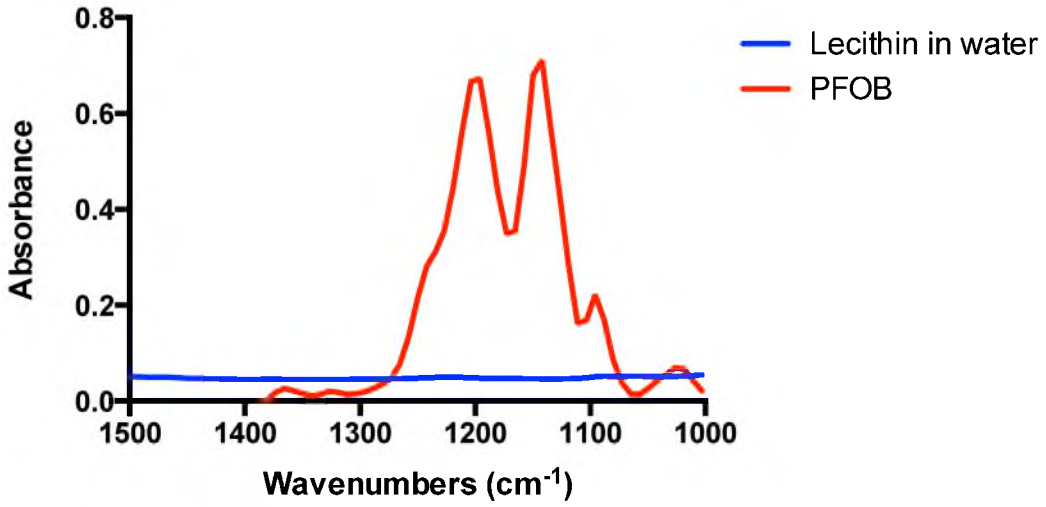

Figure 3.6 The FTIR spectra of lecithin in water and PFOB. Due to more than two fluorine atoms in the molecular structure of PFOB, the C-F strong peak would split into two peaks with symmetric and asymmetric modes at 1142 and 1196 cm^{-1}.

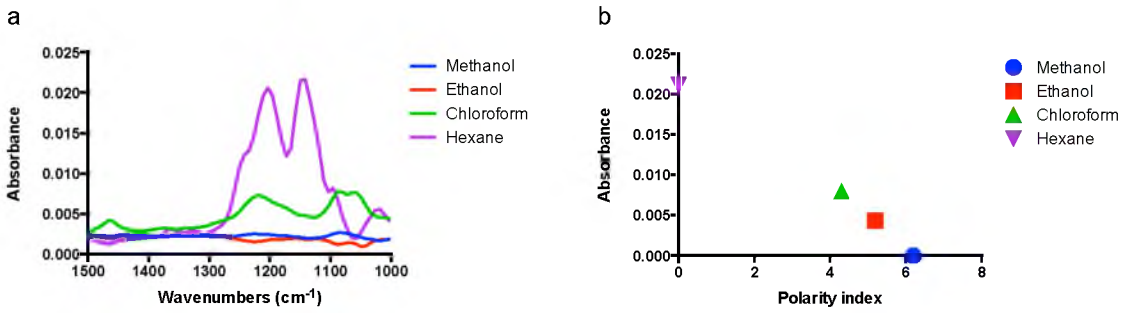

Figure 3.7 FTIR spectra of cosolvent and the curve of absorbance versus polarity index. (a) The FTIR spectra of MPL, EPL, CPL, and HPL emulsions. HPL retained the largest amount of PFOB. CPL emulsion only retained a small amount of PFOB but MPL and EPL emulsion shows no PFOB retained. (b) The curve of the absorbance at 1188 cm^{-1} versus polarity index shows PFOB retain rate has linear relation to polarity index. It shows that the polarity index of cosolvent is close to the polarity index of PFOB and can retain more PFOB during the new PFOB emulsion synthesis method.

index of cosolvent is close to the polarity index of PFOB, more PFOB can be retained. Quantitative evaluation of the amount retain is described later.

A standard curve of baseline-corrected FT-IR peak intensity at 1242 cm^{-1} corresponding to PFOB versus wt% of PFOB in hexane mixture was constructed in order to estimate the % of PFOB retained in the emulsion by this procedure (Table 3.3). Baselines were fitted by drawing a straight line across the two lowest sides of the peak (i.e., bottom) and subtracting. A trendline $y= 5.7265x - 0.3851$ with R^2 value of 0.98 was obtained. It can be found that the HPL emulsion has 72.0% PFOB retain rate by the cosolvent method.

3.5.3 Phase transition temperature (PTT)

To determine if temperature could be manipulated to increase the encapsulation efficiency for PFOB, HPL emulsions were prepared at several temperatures between 0 °C to 30 °C. It was found that the intermediate state containing hexane/PFOB lecithin before

Table 3.3 The standard FT-IR samples: Various ratios of hexane to PFOB (D_{PFOB}= 1.93g/ml and D_{hexane}= 0.66g/ml).

	Volume ratio: PFOB/Hexane	Weight ratio: PFOB/Hexane	PFOB weight portion: PFOB/total weight
50PFOB/50Hexane	50/50	96.5/32.7	0.747
30PFOB/70Hexane	30/70	57.9/45.8	0.558
20PFOB/80Hexane	20/80	38.6/52.4	0.424
10PFOB/90Hexane	10/90	19.3/58.9	0.247

vacuum drying had a different appearance depending on the temperature at which it was prepared. Below 24 ^{o}C, the mixture is translucent and above it, transparent. This transition point is easily shown by monitoring the UV-Vis spectrum at 525 nm as a function of temperature (Figure 3.8). It is also corroborated by DLS measurement, shown in Table 3.4.

To understand the significance of the difference in HPL synthesis between the two extremes of temperature, hexane/PFOB mixture at 0 °C and 30 °C were synthesized, respectively. After that, both samples were placed in vacuum at 4 °C for 10 hours and resuspended by 10 ml E-pure water. FT-IR spectra of these two samples in Figure 3.9 were measured after they were vacuumed dried and resuspended by water. For emulsion prepared at 30 °C, no PFOB was retained.

3.5.4 Fluorescence

During emulsion synthesis, it is inevitable for extra lipids to form liposomes mixed with the emulsion [181, 182]. To distinguish liposomes and emulsions generated by direct-

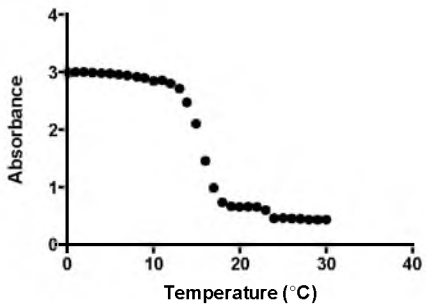

Figure 3.8 Phase transition temperate (PTT) of lecithin in PFOB/hexane measurement: UV-Vis measurement at 525 nm for lecithin in hexane/PFOB mixture before vacuum drying versus temperature. The first transition is between 13 °C and 19 °C, and the second around 22 °C to 24 °C.

Table 3.4 The particle size of lecithin in PFOB/hexane at 10 °C, 20 °C, and 30 °C. Because the particle size was too small if the applied temperature was 30 °C, the color of emulsion would be transparent.

Temperature (°C)	Particle size (nm)	Polydispersity Index (PDI)	Color of emulsion
10	344.7 ± 52.33	0.272	White
20	258.6 ± 39.33	0.366	White
30	54.1 ± 0.85	0.220	Transparent

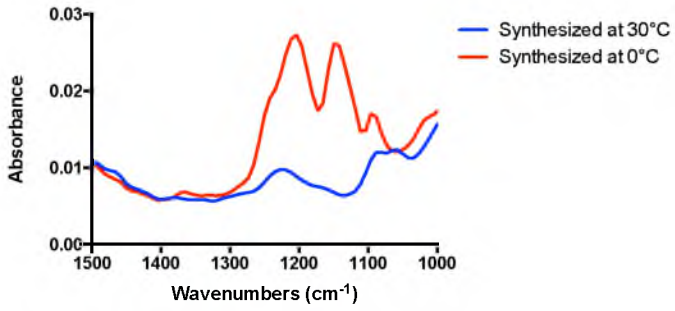

Figure 3.9 FT-IR spectra for HPL emulsions synthesized at 0 °C and 30 °C between 1000 and 1500 cm^{-1} show explicit details for PFOB bands.

emulsified and cosolvent methods, two added fluorescent dyes, fluorescein and pyrene, could be achieved. The relative solubility of fluorescein and pyrene in water and PFOB was first determined using fluorescence measurements (Figure 3.10). Fluorescein is essentially insoluble in PFOB. Pyrene is highly soluble in PFOB and partially in water. However, the spectra of pyrene is different in polar water and non-polar PFOB due to solvatochromic behavior [450], and this difference can be used to determine the partitioning between the two materials. An extra peak at 381nm of pyrene in PFOB could be used to decide where the fluorescence comes from.

Histograms presenting the change of fluorescent intensity at 518 nm for fluorescein and 394 nm for pyrene as a ratio of initial intensity (I_0) (measured before extrusion) to I (measured after extrusion) are shown in Figure 3.11. For HPL emulsion, less fluorescein is retained in the suspension after dialysis compared with DE emulsion. The large loss in fluorescein signal suggests that there are fewer fluorescein-friendly reservoirs (i.e., liposomes) in the HPL suspension. On the other hand, much more pyrene is retained in the

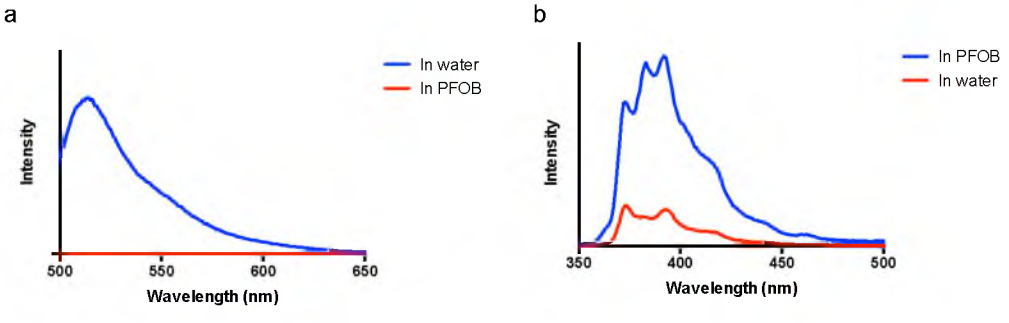

Figure 3.10 Fluorescence spectra. (a) The fluorescence spectra of fluorescein in water and PFOB: it shows fluorescein in water has a peak at 518 nm but no fluorescent intensity as fluorescein in PFOB. The excitation wavelength was applied for 480 nm. (b) The fluorescent spectra of pyrene in water and PFOB: there are three peaks at 372 nm, 381 nm, and 394 nm for pyrene in PFOB, but there are only two peaks at 372 nm and 394 nm for pyrene in water.

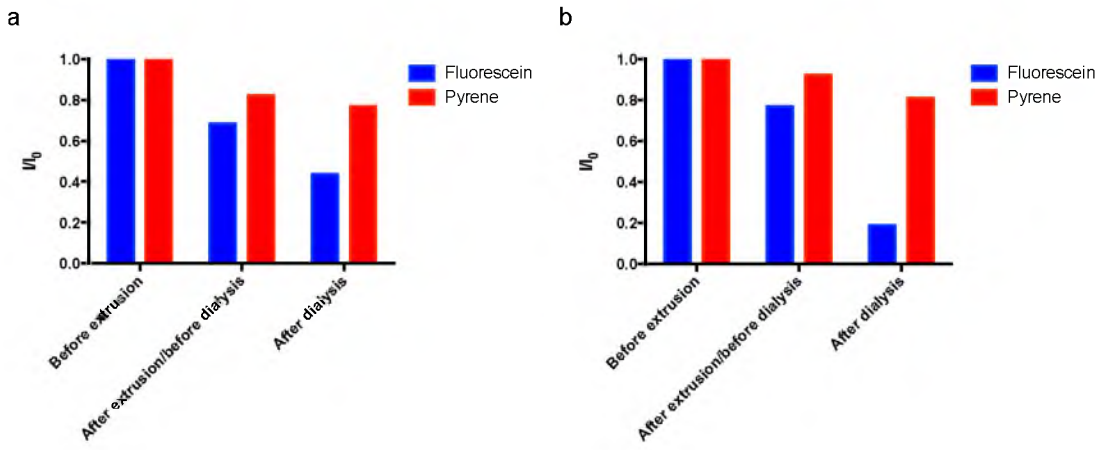

Figure 3.11 The ratio of fluorescent intensity is defined that the denominator is the intensity of fluorescein and pyrene in PFOB emulsion before extrusion (I_0) and the numerator is the intensity of fluorescein and pyrene in PFOB emulsion before extrusion, after extrusion but before dialysis, and after dialysis (I). The fluorescent intensity of fluorescein and pyrene is decided at 518 nm and 394 nm, respectively. (a) Fluorescent intensity ratios of fluorescein and pyrene in PFOB emulsion made by the direct-emulsified method. (b) Fluorescent intensity ratios of fluorescein and pyrene in PFOB emulsion made by the cosolvent method.

HPL emulsion and the pyrene spectrum reflects entrapment of the dye in a hydrophobic compartment.

3.5.5 Centrifugation

As another supporting evidence for the presence of a liposome phase in the extrusion-prepared suspension, centrifugation was used to separate the dense fraction in the suspension, and DLS used to characterize the supernatant. For suspension containing mainly high density PFOB O/W emulsions, the supernatant should have few particulates, whereas for a suspension with a mixture of liposome and high density emulsions, the supernatant should remain translucent and DLS indicates particulate structures are present. After 10 min of centrifugation at room temperature (25 °C) at 2000 rpm, only the HPL emulsion separated into two layers, but there is no separation found for DE emulsion. The

top layer is clear (transparent) and the bottom layer is opaque (white). The particle size of the opaque layer right layer by DLS (Fig 3.12(b)) was analyzed and possessed approximately 600 nm diameter particles, similar to the situation before centrifugation. FTIR analyses of supernatant and pellet also identify the pellet as the PFOB-rich phase in Fig 3.13 but not in the supernatant. It can be concluded that our cosolvent produces more PFOB emulsion than does the extrusion method.

3.5.6 Cryo-TEM

Two samples of emulsions prepared above and below were imaged in Figure 3.14 and 3.15. For emulsions made below PTT (Figure 3.14(a) and 3.14(b)), the darker and lighter structures are PFOB emulsion and water liposomes, respectively. The darker areas arise because PFOB has higher electron density than water. Layered structures and spherical emulsion particles of emulsions were also found (Figure 3.14(c)). It indicates that the morphology of emulsion could be altered during vacuum, which means round emulsion changes to layer-shaped emulsion for higher packing density if cosolvent is removed. From size measurement, the polydispersity index (PDI) of HPL emulsion without extrusion gave high value around 0.8~0.9 because its morphology has layer-liked structure. The layered structure can carry PFOB as seen in Figure 3.14(d). For emulsion made above PTT, there are also PFOB emulsions and water liposomes presented in Figure 3.15(b), 3.15(c), and 3.15(d). Layered structures were also formed in Figure 3.15(a) and 3.15(d). The lighter round area in the background is the hole on the carbon-coated copper grid and not part of the sample.

Also, the images of two samples, DE emulsion and extruded HPL emulsion in the centrifugation section, were obtained in Figure 3.16 and 3.17. It could be found that water

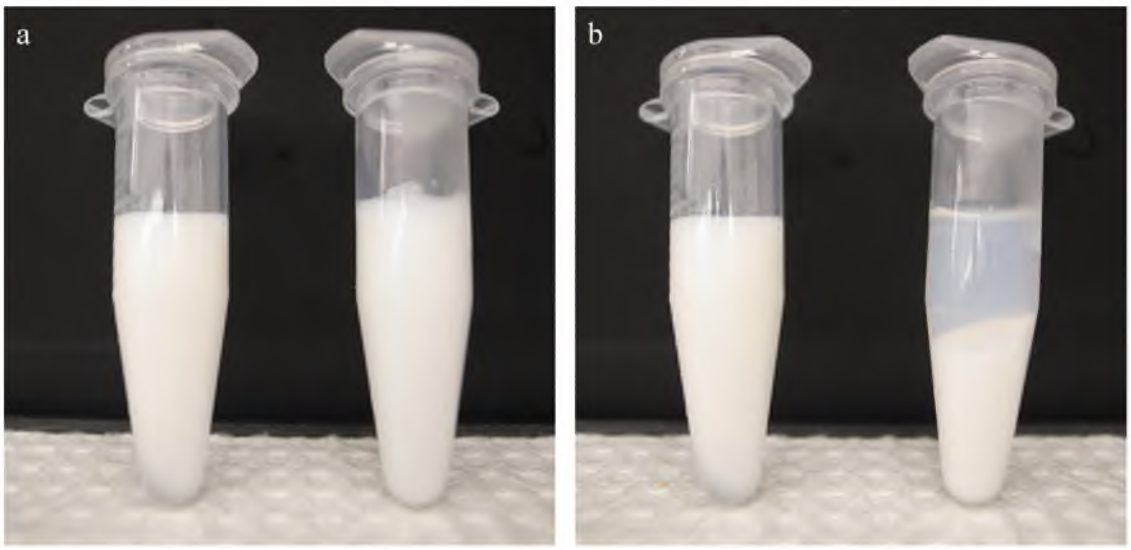

Figure 3.12 The results of centrifugation. (a) DE and HPL emulsion before centrifugation. (b) DE and HPL emulsion after centrifugation (2000 rpm, 10 min). There is a separation for HPL emulsion but not for DE emulsion. It shows HPL emulsion has PFOB emulsion with higher density than DE emulsion.

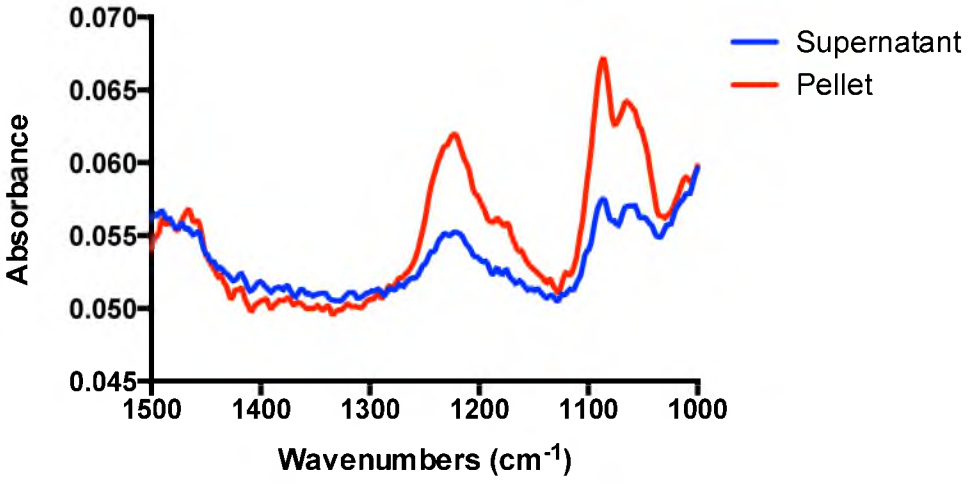

Figure 3.13 The FTIR spectra of supernatant and pellet of HPL emulsion after centrifugation. In the top layer, the spectrum is like only water or lecithin in water (in Figure 3.6). In bottom layer, the spectrum shows the peaks from C-F bonds (PFOB existence).

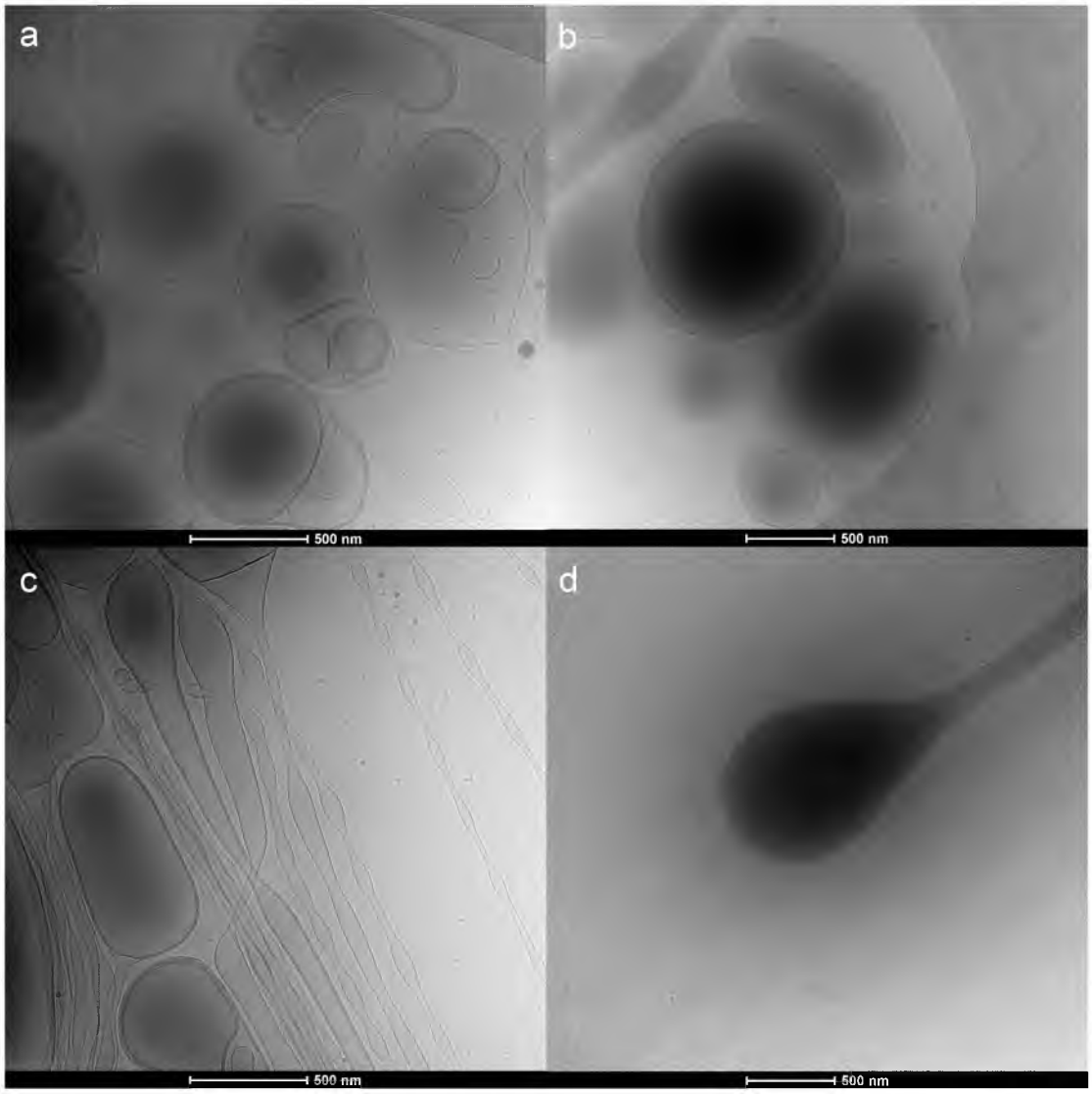

Figure 3.14 Typical cryo-TEM images of emulsions made by mixing lecithin/PFOB/hexane at 0 °C (smaller than PTT), vacuum at 4 °C for 10 hours and resuspended by water. The darker and lighter structures are PFOB emulsion and water liposomes, respectively. Spherical emulsion particles and layered structures were also found in Figure 3.14(c) and (d).

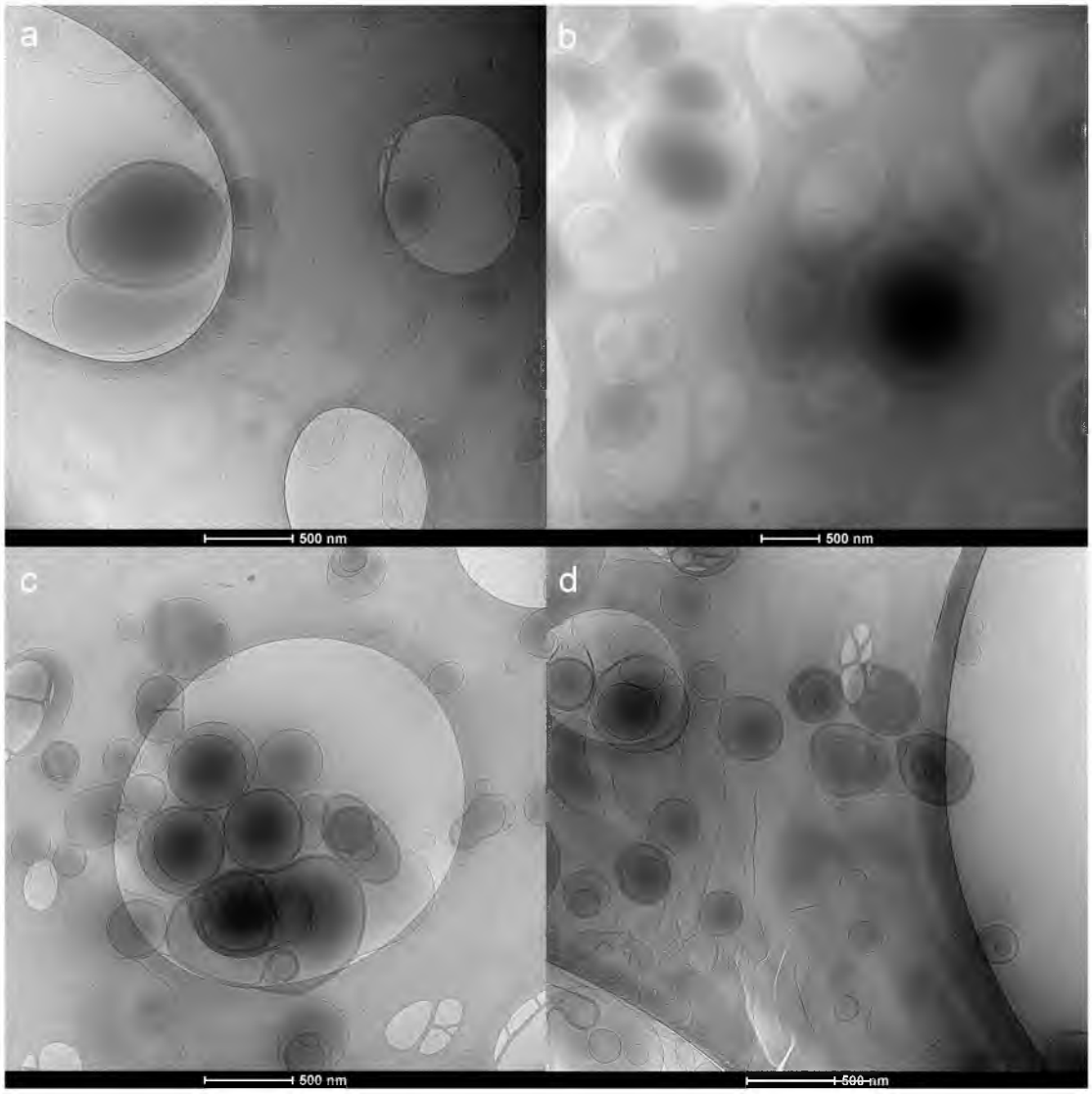

Figure 3.15 TEM images of emulsions made by mixing lecithin/PFOB/hexane at 30°C (larger than PTT), vacuum at 4°C for 10 hours and resuspended by water. The darker and lighter structures are PFOB emulsion and water liposomes, respectively.

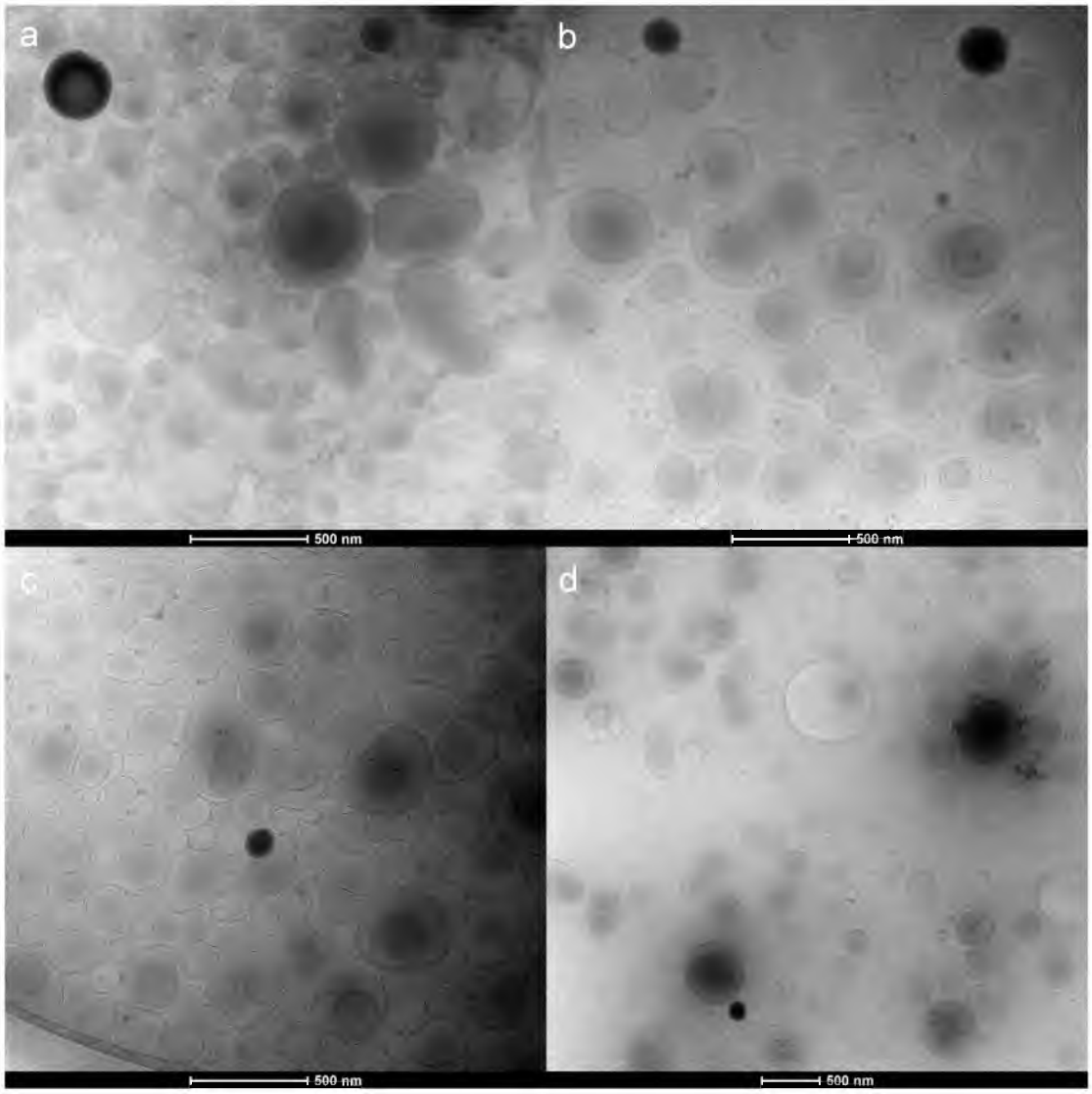

Figure 3.16 TEM images of DE emulsions: the darker and lighter structures are PFOB emulsion and water liposomes, respectively. Only few PFOB emulsions were present and most particles in the images were liposomes.

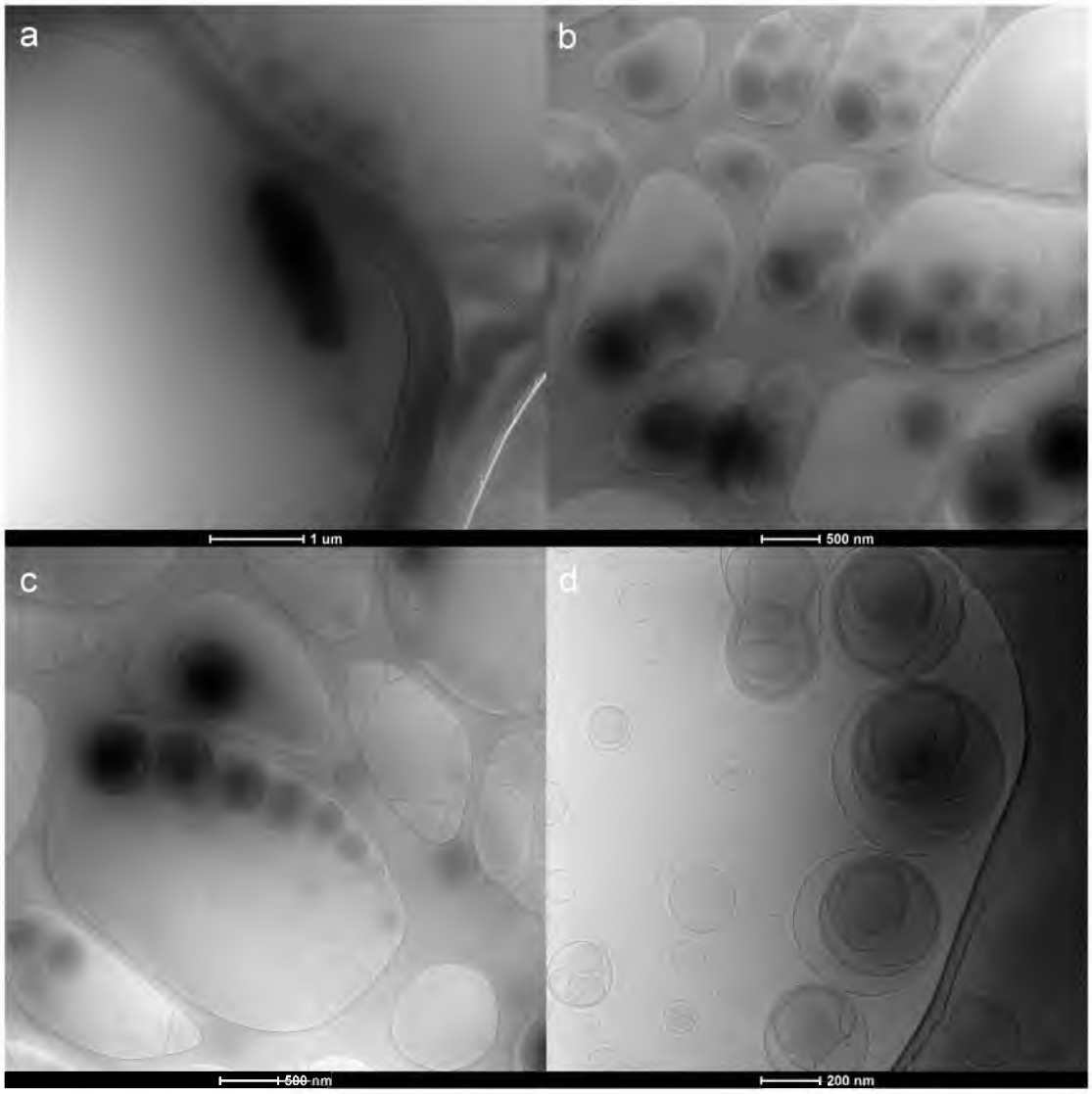

Figure 3.17 TEM images of HPL emulsion: the darker and lighter structures are PFOB emulsion and water liposomes, respectively. Compared to the image of DE emulsion, more PFOB emulsions were present in the images.

liposomes are the majority and there are only a few PFOB emulsions in Figure 3.16. Compared to Figure 3.17, more PFOB emulsions are made by the cosolvent method. In Figure 3.17(a), the layer structure-contained PFOB is also found even after extrusion. Identically, the light round background in Figure 3.17 is the hole on the carbon-coated copper grid.

3.6 Conclusion

In this study, four cosolvents were tested for their ability to increase the yield of PFOB emulsions. By FTIR, it was found that the use of hexane as cosolvent leads to significantly higher PFOB retention following vacuum drying. This is thought to be related to the fact that hexane dissolves lecithin and mixes with PFOB well. PFOB emulsion formation at various temperatures revealed a PTT above which poor PFOB retention was the case. Produced materials generally have a high polydispersity with a significantly large population of liposome structures. The cosolvent method described here reduces this problem and provides a means for producing highly concentrated emulsions. Such materials may find use in medicine or biotechnology [11, 214, 451-455] as they have excellent ability to dissolve physically significant amounts of oxygen (O_2) and carbon dioxide (CO_2) compared to water [456-458]. The technique described is not limited to 1-bromoperfluorooctane (PFOB), which was chosen as representative of a series of perfluorocarbon products [459].

CHAPTER 4

CONCLUSION AND FUTURE RESEARCH

The primary goal of the thesis project was to 1) understand the property and behaviors of coating materials assembled by electrostatic forces on the surface of PFOB emulsions, and 2) to improve the efficiency of producing uniform PFOB emulsions using a cosolvent method. Both these topics have been prepared for peer-reviewed publications.

In Chapter 1, a brief introduction of PFOB emulsion use as artificial blood substitutes and the related background of oil-in-water (O/W) systems were reviewed. Additionally, the synthesis and coating challenges for PFOB emulsions and the rationale behind material selection were discussed.

In the beginning of Chapter 2, a small amount (2%) of DOPA (an ionic surfactant) was mixed with lecithin (98%) (a nonionic surfactant) to increase surface charge of PFOB emulsions for advantageous electrostatic coating with other materials while permitting only minimal increase in production cost. The curves of zeta potential versus pH of the resulting 2D98L emulsions and lecithin-only emulsions were constructed and the isoelectric point identified. In the rest of Chapter 2, construction of polypeptide PLL and polysaccharide chitosan coatings on PFOB emulsions were studied in detail. Here is the summary of the conclusions:

1. Zeta potential changes versus pH: The relationship between the curves of zeta potential of the coating material and the PFOB emulsions was used to identify conditions where the coating material and emulsions have opposite electrical charge. Because the zeta potential of PLL and chitosan solution without pH titration is positive, they can be naturally coated on negatively charged emulsions via electrostatic force. The curve shape could be attributed to the phosphate head groups of the lipids.
2. Zeta potential, coating concentration, and size of emulsion at pH 7.2: As PLL coating concentration increases, zeta potential of coated emulsions becomes less negative and the particles tend toward electrical neutrality. Once the surface charge reached a critical minimum, as expected, flocculation, as evidenced by the size of PLL-coated emulsion, occurred. This effect was reversible. The zeta potential of chitosan-coated emulsions also became less negative but never approached neutrality so flocculation was avoided.
3. Zeta potential, coating concentration, and size of emulsion at various pH and temperature: Using MarvinSketch, the surfactant length and head group size of DOPA and lecithin were modeled in order to predict the size of the PFOB core of emulsion and the typical 2D98L emulsion concentration was calculated as 68.4 nM. From zeta potential measurement, a model relating surface charge density, coating, and the calculated emulsion concentration was used to calculate the concentration of bound coating materials, and the effective concentration of emulsion particles. The discrepancy between colorimetric/zeta potential back calculation of emulsion concentration and model calculation suggested a changing effective volume of the

coating molecules as a function of coating concentration. Using colorimetric and zeta potential measurements of the concentration of bound coating materials, a compression/expansion ratio (CER) can be defined and related to the conformation of molecules in the coating. If CER is smaller than one, it suggests that the coating materials have expanded as their accumulation on the emulsion surface progresses and vice versa. PLL appears to become more compressed, but chitosan becomes more expanded as coating concentration increases.

4. Fluorescent quenching and thermodynamic analysis: To prove the above hypothesis of compression/expansion without relying on assumptions inherent in the performed calculations, the conformation of PLL and chitosan on emulsions was probed by using iodide ions (I^-) to quench fluorescent dye pyrene trapped inside PFOB emulsion core. PLL exhibiting a compressed conformation had less fluorescent quenching than chitosan, consistent with the model. The predicted calculation and quenching-indicated conformation result also matched the thermodynamic analysis. The Gibbs free energy is lower as the compressed conformation of PLL and chitosan molecules on emulsions, which means the coating concentration of PLL and chitosan increases and decreases, respectively. The expanded conformation has higher free energy than the compressed one.
5. Overall: An easy and convenient method for conformation analysis of coating materials on submicron particles such as emulsions was developed. This procedure could be used to screen a wide range of coating materials and anticipate their conformation-based performance.

In Chapter 3, a novel method of emulsion production by cosolvent was proposed to address problems of side-product liposome formation inherent in emulsion production. This problem is most severe in systems where surfactant-oil and surfactant-water solubility has not been or cannot be optimized. The cosolvent helps the surfactant (i.e., lecithin) disperse with oil (i.e., PFOB) in the absence of water. After a uniform mixture is produced, the cosolvent is removed and replaced with water. This method is efficient, and avoids the need for lengthy mechanical agitation, extrusion, or homogenization. The emulsion made by the cosolvent method was compared to the emulsion made by the direct-emulsified method. Here is the summary of the conclusions:

1. Effect of cosolvent selection: Four organic solvents, methanol, ethanol, chloroform and hexane, were utilized as the cosolvents for the emulsion production. The polarity of cosolvent plays an important role to decide the mixing uniformity of oil and surfactant. PFOB retention is known by quantifying the specific C-F band in the FTIR spectrum. Hexane was the optimal cosolvent for the production of PFOB emulsion.
2. Phase transition temperature (PTT): Mixtures of hexane, surfactant, and PFOB possess two phase transitions, one around 13 to 19 °C and another at 22 to 24 °C. These were identified by UV-Vis spectrophotometry as a change in the translucency of the colorless mixture. Above the second transition temperature (24 °C), FTIR indicated little PFOB retention in the synthesized emulsion. Hence, it was decided to synthesize PFOB emulsion below the lower PTT (mixed at 0 °C and vacuumed at 4 °C) to maximize emulsion yield.

3. FTIR quantitative measurement: The maximum PFOB retention in the emulsion (prepared as 1.5 g lecithin dissolved in 15 ml hexane/ 1 ml PFOB at 0 °C, and vacuumed for 10 hours at 4 °C) was 72%.
4. Fluorescence: PFOB emulsions made by the direct-emulsified and the cosolvent method were compared, respectively, by adding two fluorescent dyes. Fluorescein only dissolves slightly in water but not at all in PFOB. Pyrene shows different spectra in water (two peaks) and in PFOB (three peaks). PFOB emulsion with fluorescein synthesized by the direct-emulsified method still exhibited significant fluorescent intensity after overnight dialysis. This suggests a significant population fluorescein encapsulated in water liposomes that are present when the emulsion is synthesized by the direct-emulsified method. PFOB emulsion with pyrene synthesized by the direct-emulsified method shows most PFOB was still retained after extrusion and dialysis. PFOB emulsion synthesized by the cosolvent method exhibited much lower fluorescein fluorescent intensity after dialysis, suggested significantly fewer liposomes were formed. Pyrene in the same system showed localization in PFOB and most of the PFOB was retained after extrusion and dialysis.
5. Density of emulsion: The densities of PFOB emulsions made by the two methods were compared relatively via centrifugation using 2000 rpm for 10 min. Only PFOB emulsion synthesized by the cosolvent method had visible pellet formation after centrifugation due to higher content of high density PFOB. The DLS diameters of DE and HPL emulsion in each material suspension were 534nm and 548nm, respectively. The pellet showed PFOB content by FTIR. There was no

obvious separation into pellet and supernatant for PFOB emulsion made by the direct-emulsified method, which suggests most of the sample is water-filled liposomes and multilamellar structures. Hence, liposomes could be avoided using the cosolvent method compared to the direct-emulsified method.

6. DLS: The cosolvent method provides a uniform emulsion with greatly reduced amounts of excess liposomes. The method is fairly simple and cheap because no special emulsification mixers/machines and homogenizers are needed. It would have a great potential and application for the production of emulsion in food, cosmetics and pharmaceutical industry.

For the future research, further confirmation of our model/analysis approach is needed as well as extension to other coating molecules. For example, PLL with long chain length/high molecular weight and chitosan with short chain length/low molecular weight at various pH and ionic strengths can be applied to observe if the observed phenomena is related only to chain length, or if the specific molecular structure is also important. In previous studies, the molecular conformation has been shown to be controlled by the proton concentration [460-462] and overall ionic strength [462-465]. For biomedical applications, other types of polypeptides, and polypeptide-sugar hybrids, could be used as a coating material. Similar molecules are know to have regulatory and signaling function in the body, and may result in the formation of bioactive emulsions for theranostic applications [466-469]. The developed analysis method for the conformation prediction could also be applied to the conjugation and surface coating of nanoparticles or multicomponent thin films like Langmuir-Blodgett films.

Following up on the cosolvent method, the amount of the surfactant, cosolvent, and oil could be adjusted to further reduce unreacted surfactant and to increase PFOB retention/eliminate liposome for the optimal recipe. The fluorescence signal of fluorescein trapped inside the liposomes formed by the extra surfactants would be reduced and the FTIR signal for PFOB increased. In addition, temperature and the vacuum-drying times for the mixing of surfactant, PFOB, and cosolvent could be optimized to maximize the retention of PFOB. Moreover, submicron size homogenization could be performed before vacuum-drying to reduce the size and improve the uniformity of the structures. This would have the benefit of avoiding size-homogenization at later stages. A membrane homogenizer could be set up in a cold room to keep the mixing of hexane, lecithin, and PFOB below PTT. After size homogenization and vacuum-drying, the size of PFOB emulsion can be measured to verify if better control over size is obtained.

REFERENCES

[1] L. T. Goodnough, M. E. Brecher, M. H. Kanter, and J. P. AuBuchon, "Transfusion medicine—blood transfusion," *New England Journal of Medicine,* vol. 340, pp. 438-447, 1999.

[2] J. F. Biebuyck, P. A. Schriemer, D. E. Longnecker, and P. D. Mintz, "The possible immunosuppressive effects of perioperative blood transfusion in cancer patients," *Anesthesiology,* vol. 68, p. 422, 1988.

[3] R. E. Voll, M. Herrmann, E. A. Roth, C. Stach, J. R. Kalden, and I. Girkontaite, "Immunosuppressive effects of apoptotic cells," *Nature,* vol. 390, pp. 350-351, 1997.

[4] M. Heiss, K. Jauch, C. Delanoff, G. Mayer, F. Schildberg, W. Mempel, *et al.*, "Beneficial effect of autologous blood transfusion on infectious complications after colorectal cancer surgery," *The Lancet,* vol. 342, pp. 1328-1333, 1993.

[5] S. D. ANNEMARIE WASLEY and M. J. Alter, "Epidemiology of hepatitis C: geographic differences and temporal trends," *Hepatitis C: State of the Art at the Millennium,* vol. 20, p. 1, 2000.

[6] L. O. Gostin, Z. Lazzarini, T. S. Jones, and K. Flaherty, "Prevention of HIV/AIDS and other blood-borne diseases among injection drug users," *JAMA: The Journal of the American Medical Association,* vol. 277, p. 53, 1997.

[7] M. P. Busch, S. H. Kleinman, and G. J. Nemo, "Current and emerging infectious risks of blood transfusions," *JAMA: The Journal of the American Medical Association,* vol. 289, p. 959, 2003.

[8] J. Gu, E. Gong, B. Zhang, J. Zheng, Z. Gao, Y. Zhong, *et al.*, "Multiple organ infection and the pathogenesis of SARS," *The Journal of Experimental Medicine,* vol. 202, p. 415, 2005.

[9] M. Finucane, P. Slovic, and C. Mertz, "Public perception of the risk ofblood transfusion," *Transfusion,* vol. 40, pp. 1017-1022, 2000.

[10] S. Sarkar, "Artificial blood," *Indian Journal of Critical Care Medicine: Peer-reviewed, Official Publication of Indian Society of Critical Care Medicine,* vol. 12, p. 140, 2008.

[11] J. E. Squires, "Artificial blood," *Science,* vol. 295, pp. 1002-1005, 2002.

[12] H. Oberman, "Early history of blood substitutes: Transfusion of milk," *Transfusion,* vol. 9, pp. 74-77, 1969.

[13] W. R. Amberson, J. J. Jennings, and C. M. Rhode, "Clinical experience with hemoglobin-saline solutions," *Journal of Applied Physiology,* vol. 1, pp. 469-489, 1949.

[14] L. C. Clark and F. Gollan, "Survival of mammals breathing organic liquids equilibrated with oxygen at atmospheric pressure," *Science,* vol. 152, pp. 1755-1756, 1966.

[15] J. Savitsky, J. Doczi, J. Black, and J. Arnold, "A clinical safety trial of stroma-free hemoglobin," *Clinical Pharmacology and Therapeutics,* vol. 23, p. 73, 1978.

[16] S. A. Gould, E. E. Moore, and D. B. Hoyt, "Blood substitutes: principles, methods, products, and clinical trials", T. M. S. Chang, Ed. Basel: Karger/ Texas: Landes Systems, 1998, pp. 12-28.

[17] T. M. S. Chang, "Artificial cells: biotechnology, nanomedicine, regenerative medicine, blood substitutes, bioencapsulation, and cell/stem cell therapy", vol. 1, Hackensack, NJ: World Scientific Publishing Company, 2007, pp. 95.

[18] J. G. Riess, "Oxygen Carriers ("Blood Substitutes") sRaison d'Etre, Chemistry, and Some," *Chem. Rev,* vol. 101, pp. 2797-2919, 2001.

[19] D. L. Schmidt, M. E. Pruitt, and K. I. Dismuke, "Perfluorocarbon-polymeric coatings having low critical surface tensions," U.S. Patent 4 344 993, August 17, 1982.

[20] D. L. Schmidt and R. F. Harris, "Perfluorocarbon based polymeric coatings having low critical surface tensions," U.S. Patent 4 592 930, June 3, 1986.

[21] D. L. Schmidt and D. Urchick, "Perfluorocarbon based polymeric coatings having low critical surface tensions," U.S. Patent 4 764 564, August 16, 1988.

[22] D. L. Schmidt, P. J. McCrackin, and C. E. Coburn, "Fluorocarbon containing, reactive polymeric surfactants and coating compositions therefrom," U.S. Patent 4 929 666 , May 29, 1990.

[23] D. L. Schmidt, C. E. Coburn, and P. J. McCrackin, "Fluorocarbon containing, reactive polymeric surfactants and coating compositions therefrom," U.S. Patent 5 006 624, April 9, 1991.

[24] Z. Liu and H. Xiao, "Soap-free emulsion copolymerisation of styrene with cationic monomer: effect of ethanol as a cosolvent," *Polymer,* vol. 41, pp. 7023-7031, 2000.

[25] E. Lorenceau, A. S. Utada, D. R. Link, G. Cristobal, M. Joanicot, and D. A. Weitz, "Generation of polymerosomes from double-emulsions," *Langmuir,* vol. 21, pp. 9183-9186, 2005.

[26] E. M. Ketcham and C. B. Cairns, "Hemoglobin-based oxygen carriers: development and clinical potential," *Annals of Emergency Medicine,* vol. 33, pp. 326-337, 1999.

[27] R. Spence, S. Swisher, and S. Kleinman, "Blood substitutes," *Clinical Practice of Transfusion Medicine. Third Edition. Petz LD, Swisher SN, Kleinman S, et al.(Eds). New York, Churchill Livingstone,* pp. 967-984, 1996.

[28] D. Partrick, E. Moore, C. Barnett, and C. Silliman, "Human polymerized hemoglobin as a blood substitute avoids transfusion-induced neutrophil priming," in *Surgical Forum Chicogo*, 1996, pp. 36-38.

[29] S. A. Gould and G. S. Moss, "Clinical development of human polymerized hemoglobin as a blood substitute," *World Journal of Surgery,* vol. 20, pp. 1200-1207, 1996.

[30] J. Simoni, G. Simoni, G. Newman, and M. Feola, "An improved blood substitute: in vivo evaluation of its hemodynamic effects," *ASAIO Journal,* vol. 42, pp. M773-781, 1996.

[31] J. R. Hess and R. F. Reiss, "Resuscitation and the limited utility of the present generation of blood substitutes," *Transfusion Medicine Reviews,* vol. 10, p. 276, 1996.

[32] R. J. Przybelski, E. K. Daily, J. C. Kisicki, C. Mattia-Goldberg, M. J. Bounds, and W. A. Colburn, "Phase I study of the safety and pharmacologic effects of diaspirin cross-linked hemoglobin solution," *Critical Care Medicine,* vol. 24, pp. 1993-2000, 1996.

[33] Z. S. Katušić, H. C. Lee, and E. T. Clambey, "Crosslinked hemoglobin inhibits endothelium-dependent relaxations in isolated canine arteries," *General Pharmacology: The Vascular System,* vol. 27, pp. 239-244, 1996.

[34] J. Hughes, E. J. Antal, P. K. Locker, S. F. Francom, W. J. Adams, and J. Jacobs, "Physiology and pharmacokinetics of a novel hemoglobin-based oxygen carrier in humans," *Critical Care Medicine,* vol. 24, pp. 756-764, 1996.

[35] R. F. Regan and S. S. Panter, "Neurotoxicity of hemoglobin in cortical cell culture," *Neuroscience Letters,* vol. 153, pp. 219-222, 1993.

[36] R. L. MacDonald and B. Weir, "A review of hemoglobin and the pathogenesis of cerebral vasospasm," *Stroke,* vol. 22, pp. 971-982, 1991.

[37] D. J. Cole, J. C. Nary, L. W. Reynolds, P. M. Patel, and J. C. Drummond, "Experimental Subarachnoid Hemorrhage in Rats: Effect of Intravenous α-α Diaspirin Crosslinked Hemoglobin on Hypoperfusion and Neuronal Death," *Anesthesiology,* vol. 87, pp. 1486-1493, 1997.

[38] R. Motterlini and V. W. Macdonald, "Cell-free hemoglobin potentiates acetylcholine-induced coronary vasoconstriction in rabbit hearts," *Journal of Applied Physiology,* vol. 75, pp. 2224-2233, 1993.

[39] G. Balla, G. Vercellotti, U. Muller-Eberhard, J. Eaton, and H. Jacob, "Exposure of endothelial cells to free heme potentiates damage mediated by granulocytes and toxic oxygen species," *Laboratory investigation; a Journal of Technical Methods and Pathology,* vol. 64, p. 648, 1991.

[40] J. Balla, K. Nath, G. Balla, M. Juckett, H. Jacob, and G. Vercellotti, "Endothelial cell heme oxygenase and ferritin induction in rat lung by hemoglobin in vivo," *American Journal of Physiology-Lung Cellular and Molecular Physiology,* vol. 268, pp. L321-L327, 1995.

[41] M. J. Broekman, A. M. Eiroa, and A. J. Marcus, "Inhibition of human platelet reactivity by endothelium-derived relaxing factor from human umbilical vein endothelial cells in suspension: blockade of aggregation and secretion by an aspirin-insensitive mechanism," *Blood,* vol. 78, pp. 1033-1040, 1991.

[42] S. B. Olsen, D. B. Tang, M. R. Jackson, E. R. Gomez, B. Ayala, and B. M. Alving, "Enhancement of platelet deposition by cross-linked hemoglobin in a rat carotid endarterectomy model," *Circulation,* vol. 93, pp. 327-332, 1996.

[43] J. Ning and T. Chang, "In vivo effects of stroma-free hemoglobin and polyhemoglobin on coagulation factors in rats," *The International Journal of Artificial Organs,* vol. 13, p. 509, 1990.

[44] S. A. Gould, E. E. Moore, D. B. Hoyt, P. M. Ness, E. J. Norris, J. L. Carson, *et al.*, "The life-sustaining capacity of human polymerized hemoglobin when red cells might be unavailable," *Journal of the American College of Surgeons,* vol. 195, pp. 445-452, 2002.

[45] K. Kipnis, N. M. King, and R. M. Nelson, "An open letter to institutional review boards considering Northfield Laboratories' PolyHeme® trial," *The American Journal of Bioethics,* vol. 6, pp. 18-21, 2006.

[46] J. Sprung, J. D. Kindscher, J. A. Wahr, J. H. Levy, T. G. Monk, M. W. Moritz, *et al.*, "The use of bovine hemoglobin glutamer-250 (Hemopure®) in surgical patients: results of a multicenter, randomized, single-blinded trial," *Anesthesia & Analgesia,* vol. 94, pp. 799-808, 2002.

[47] J. S. Jahr, M. Moallempour, and J. C. Lim, "HBOC-201, hemoglobin glutamer-250 (bovine), Hemopure®(Biopure Corporation)," *Expert Opinion on Biological Therapy,* vol. 8, pp. 1425-1433, 2008.

[48] L. Levien, "South Africa: clinical experience with Hemopure," *ISBT Science Series,* vol. 1, pp. 167-173, 2006.

[49] J. Freytag and D. Templeton, "Optro TM (recombinant human hemoglobin): A therapeutic for the delivery of oxygen and the restoration of blood volume in the treatment of acute blood loss in trauma and surgery," *Red Cell Substitutes: Basic Principles and Clinical Application. New York, Dekker,* pp. 325-334, 1997.

[50] R. Caspari, "Recent progress in the development of Optro®(Recombinant human hemoglobin, rHb 1.1)," in *Presented atthe VII International Symposium on Blood Substitutes, Tokyo*, 1997.

[51] K. Burhop and M. Doyle, "The development and preclinical testing of a second-generation recombinant hemoglobin solution, rHb2. 0 for injection," in *Microcircultory Effects of Hemoglobin solutions*, K. Messmer, K. Burhop, and J. Hutter, Ed. Basel: Karger, 2004, pp. 48-64.

[52] D. Cheng, C. Mazer, R. Martineau, A. Ralph-Edwards, J. Karski, J. Robblee, *et al.*, "A phase II dose-response study of hemoglobin raffimer (Hemolink) in elective coronary artery bypass surgery," *The Journal of Thoracic and Cardiovascular Surgery,* vol. 127, pp. 79-86, 2004.

[53] J. Adamson and C. Moore, "Hemolink, an o-raffinose crosslinked hemoglobin-based oxygen carrier," *Blood substitutes: Principles, Methods, Products and Clinical Trials,* vol. 2, pp. 62-81, 1998.

[54] D. Nelson, "Blood and HemAssist TM [DCLHb]: Potentially a complementary therapeutic team," *Blood Substitutes: Principles, Methods, Products and Clinical Trials. Basel, Karger,* vol. 2, pp. 39-57, 1998.

[55] J. Baron, J. Berridge, J. Brichant, R. Demeyere, M. Lamy, R. Larbuisson, *et al.*, "The HemAssist TM Cardiac Surgery Trial Collaborative Group. The use of diaspirin cross-linked hemoglobin (DCLHb) as an alternative to blood transfusion in cardiac surgery patients following cardiopulmonary bypass: a pivotal efficacy trial," *Anesthesiology,* vol. 87, p. A217, 1997.

[56] R. Banks and J. Tatlow, "Organofluorine Chemistry: Nomenclature and Historical Landmarks", in "*Organofluorine chemistry: principles and commercial applications*", R. Banks, B. Smart and J. Tatlow, New York: Springer, 1994, pp. 14-17

[57] M. Bibby and G. Carter, "C—F bond dissociation energies in perfluorocarbon gases using negative ion appearance potential data," *Transactions of the Faraday Society,* vol. 62, pp. 2637-2642, 1966.

[58] J. Heicklen and D. Saunders, "The reaction of oxygen atoms with perfluoropropene (Vapor phase oxidation of perfluorocarbons with reference to reactions of oxygen atoms with perfluoropropene)," in *Combustion INST, Wersten States Section, Spring Meeting, Hollywood, CA*, 1965, p. 1965.

[59] U. Gross, S. Rüdiger, and H. Reichelt, "Perfluorocarbons: chemically inert but biologically active?," *Journal of Fluorine Chemistry,* vol. 53, pp. 155-161, 1991.

[60] P. Monograph, "Fluosol® 20% Intravascular Perfluorochemical Emulsion,"," *Delivers Oxygen to Protect the Heart During PTCA," Alpha Therapeutic Corporation,* pp. 3-30.

[61] S. Rockwell, "Perfluorochemical emulsions and radiation therapy," *Artificial Cells, Blood Substitutes and Biotechnology,* vol. 22, pp. 1097-1108, 1994.

[62] B. Teicher, "Combination of perfluorochemical emulsions and carbogen breathing with cancer chemotherapy," *Artificial Cells, Blood Substitutes and Biotechnology,* vol. 22, pp. 1109-1120, 1994.

[63] B. Teicher, "An overview on oxygen carriers in cancer therapy," *Artificial Cells, Blood Substitutes and Biotechnology,* vol. 23, pp. 395-405, 1995.

[64] K. C. Lowe, "Perfluorochemical respiratory gas carriers: applications in medicine and biotechnology," *Science Progress,* vol. 80, p. 169, 1997.

[65] K. C. Lowe, M. R. Davey, and J. B. Power, "Perfluorochemicals: their applications and benefits to cell culture," *Trends in Biotechnology,* vol. 16, pp. 272-277, 1998.

[66] C. Rappaport, E. Trujillo, and L. Soong, "Novel oxygenation system supports multilayer growth of HeLa cells," *BioTechniques,* vol. 21, p. 672, 1996.

[67] T. H. Shaffer, M. R. Wolfson, and L. C. Clark, "Liquid ventilation," *Pediatric Pulmonology,* vol. 14, pp. 102-109, 1992.

[68] M. R. Wolfson, J. Greenspan, K. S. Deoras, S. D. Rubenstein, and T. H. Shaffer, "Comparison of gas and liquid ventilation: clinical, physiological, and histological correlates," *Journal of Applied Physiology,* vol. 72, pp. 1024-1031, 1992.

[69] S. G. Kramer, D. Hwang, G. A. Peyman, J. A. Schulman, and B. Sullivan, "Perfluorocarbon liquids in ophthalmology," *Survey of Ophthalmology,* vol. 39, pp. 375-395, 1995.

[70] K. Kobuch, D. Menz, H. Hoerauf, J. H. Dresp, and V.-P. Gabel, "New substances for intraocular tamponades: perfluorocarbon liquids, hydrofluorocarbon liquids and hydrofluorocarbon-oligomers in vitreoretinal surgery," *Graefe's Archive for Clinical and Experimental Ophthalmology,* vol. 239, pp. 635-642, 2001.

[71] K. Lowe, "Perfluorochemicals in vascular medicine," *Vascular Medcine Review,* vol. 5, pp. 15-15, 1994.

[72] R. F. Mattrey, "The potential role of perfluorochemicals (PFCs) in diagnostic imaging," *Artificial Cells, Blood Substitutes and Biotechnology,* vol. 22, pp. 295-313, 1994.

[73] E. G. Schutt, D. H. Klein, R. M. Mattrey, and J. G. Riess, "Injectable microbubbles as contrast agents for diagnostic ultrasound imaging: the key role of perfluorochemicals," *Angewandte Chemie International Edition,* vol. 42, pp. 3218-3235, 2003.

[74] A. M. Lincoff, J. J. Popma, S. G. Ellis, R. A. Vogel, and E. J. Topol, "Percutaneous support devices for high risk or complicated coronary angioplasty," *Journal of the American College of Cardiology,* vol. 17, pp. 770-780, 1991.

[75] K. C. Lowe, "Fluorinated blood substitutes and oxygen carriers," *Journal of Fluorine Chemistry,* vol. 109, pp. 59-65, 2001.

[76] E. Maevsky, G. Ivanitsky, L. Bogdanova, O. Axenova, N. Karmen, E. Zhiburt, *et al.*, "Clinical results of Perftoran application: Present and future," *Artificial Cells, Blood Substitutes and Biotechnology,* vol. 33, pp. 37-46, 2005.

[77] K. C. Lowe, "Second-generation perfluorocarbon emulsion blood substitutes," *Artificial Cells, Blood Substitutes and Biotechnology,* vol. 28, pp. 25-38, 2000.

[78] R. P. Mason, H. Shukla, and P. P. Antich, "Oxygent™; A Novel Probe of Tissue Oxygen Tension," *Artificial Cells, Blood Substitutes and Biotechnology,* vol. 20, pp. 929-932, 1992.

[79] P. E. Keipert, "Use of Oxygent™, a perfluorochemical-based oxygen carrier, as an alternative to intraoperative blood transfusion," *Artificial Cells, Blood Substitutes and Biotechnology,* vol. 23, pp. 381-394, 1995.

[80] M. P. Krafft, A. Chittofrati, and J. G. Riess, "Emulsions and microemulsions with a fluorocarbon phase," *Current Opinion in Colloid & Interface Science,* vol. 8, pp. 251-258, 2003.

[81] R. Kaufman, "The Results of a Phase I Clinical Trial of a 40% V/V Emulsion of HM (Oxyfluor)," *Art. Cells Blood Subst. Immobil. Biotechnol,* vol. 22, p. A112, 1994.

[82] J. C. Briceno, I. E. RINCÓN, J. F. Velez, I. Castro, M. I. Arcos, and C. E. Velasquez, "Oxygen transport and consumption during experimental cardiopulmonary bypass using oxyfluor," *ASAIO journal,* vol. 45, pp. 322-327, 1999.

[83] M. Winslow, Robert M, "New transfusion strategies: red cell substitutes," *Annual Review of Medicine,* vol. 50, pp. 337-353, 1999.

[84] L. Sacconi, D. Dombeck, and W. Webb, "Overcoming photodamage in second-harmonic generation microscopy: real-time optical recording of neuronal action potentials," *Proceedings of the National Academy of Sciences of the United States of America,* vol. 103, pp. 3124-3129, 2006.

[85] J. L. Richardson, R. A. Shivdasani, C. Boers, J. H. Hartwig, and J. E. Italiano, "Mechanisms of organelle transport and capture along proplatelets during platelet production," *Blood,* vol. 106, pp. 4066-4075, 2005.

[86] S. B. Shah, R. Nolan, E. Davis, G. B. Stokin, I. Niesman, I. Canto, *et al.*, "Examination of potential mechanisms of amyloid-induced defects in neuronal transport," *Neurobiology of Disease,* vol. 36, pp. 11-25, 2009.

[87] K. C. Lowe, "Engineering blood: synthetic substitutes from fluorinated compounds," *Tissue Engineering,* vol. 9, pp. 389-399, 2003.

[88] Z.-j. Yang, C. D. Price, G. Bosco, M. Tucci, N. S. El-Badri, D. Mangar, *et al.*, "The Effect of Isovolemic Hemodilution with Oxycyte®, a Perfluorocarbon Emulsion, on Cerebral Blood Flow in Rats," *PloS one,* vol. 3, p. e2010, 2008.

[89] M. Bullock, "Clinical Phase IIB Trial of Oxycyte Perflurocarbon in Severe Human Traumatic Brain Injury," MIAMI UNIV FL, 2011.

[90] T. C. Fabian, "Perfluorocarbons," *The Journal of Trauma and Acute Care Surgery,* vol. 70, pp. S42-S44, 2011.

[91] A. Vaddi, A. A. Iqbal, E. P. Chander, and R. Sunil, "Available at www. ijprronline. com A REVIEW ON: ARTIFICIAL BLOOD," *International Journal,* vol. 1, pp. 102-124, 2013.

[92] J. G. Riess, "Reassessment of Criteria for the Selection of Perfluorochemicals for Second-Generation Blood Substitutes: Analysis of Structure/Property Relationships," *Artificial Organs,* vol. 8, pp. 44-56, 1984.

[93] J. G. Riess, "Fluorous Materials for Biomedical Uses" in "*Handbook of Fluorous Chemistry*," J. A. Gladysz, D. P. Curran, and I. T. Horvath, Weinheim, Ed. Germany: Wiley, 2006, pp. 545.

[94] K. C. Lowe, "Fluorocarbon Emulsions as Blood Substitutes," in "*Blood Substitutes, Present and Future Perspectives*", E. Tsuchida, Switzerland: Elsevier Science, 1999, pp. 329-333

[95] S. F. Flaim, "Pharmacokinetics and side effects of perfluorocarbon-based blood substitutes," *Artificial Cells, Blood Substitutes and Biotechnology,* vol. 22, pp. 1043-1054, 1994.

[96] J. G. Riess and M. P. Krafft, "Advanced fluorocarbon-based systems for oxygen and drug delivery, and diagnosis," *Artificial Cells, Blood Substitutes and Biotechnology,* vol. 25, pp. 43-52, 1997.

[97] C. Sharts, H. Reese, K. A. Ginsberg, F. K. Multer, M. D. Nielson, A. G. Greenburg, *et al.*, "The solubility of oxygen in aqueous fluorocarbon emulsions," *Journal of Fluorine Chemistry,* vol. 11, pp. 637-641, 1978.

[98] T. F. Zuck, J. G. Riess, and G. Biro, "Current status of injectable oxygen carriers," *Critical Reviews in Clinical Laboratory Sciences,* vol. 31, pp. 295-324, 1994.

[99] M. R. Wolfson, N. E. Kechner, R. F. Roache, J.-P. Dechadarevian, H. E. Friss, S. D. Rubenstein, *et al.*, "Perfluorochemical rescue after surfactant treatment: Effect of perflubron dose and ventilatory frequency," *Journal of Applied Physiology,* vol. 84, pp. 624-640, 1998.

[100] A. S. Kabalnov and E. D. Shchukin, "Ostwald ripening theory: applications to fluorocarbon emulsion stability," *Advances in Colloid and Interface Science,* vol. 38, pp. 69-97, 1992.

[101] A. Kabal'Nov, A. Pertzov, and E. Shchukin, "Ostwald ripening in two-component disperse phase systems: Application to emulsion stability," *Colloids and Surfaces,* vol. 24, pp. 19-32, 1987.

[102] S. Davis, H. Round, and T. Purewal, "Ostwald ripening and the stability of emulsion systems: an explanation for the effect of an added third component," *Journal of Colloid and Interface Science,* vol. 80, pp. 508-511, 1981.

[103] A. Kabalnov, J. Weers, R. Arlauskas, and T. Tarara, "Phospholipids as emulsion stabilizers. 1. Interfacial tensions," *Langmuir,* vol. 11, pp. 2966-2974, 1995.

[104] J. G. Riess, "Perfluorocarbon-based oxygen delivery," *Artificial Cells, Blood Substitutes and Biotechnology,* vol. 34, pp. 567-580, 2006.

[105] M. J. Lawrence and G. D. Rees, "Microemulsion-based media as novel drug delivery systems," *Advanced Drug Delivery Reviews,* vol. 45, pp. 89-121, 2000.

[106] A. Kabalnov, T. Tarara, R. Arlauskas, and J. Weers, "Phospholipids as Emulsion Stabilizers: 2. Phase Behavior versus Emulsion Stability," *Journal of Colloid and Interface Science,* vol. 184, pp. 227-235, 1996.

[107] D. Morales, J. M. Gutiérrez, M. Garcia-Celma, and Y. Solans, "A study of the relation between bicontinuous microemulsions and oil/water nano-emulsion formation," *Langmuir,* vol. 19, pp. 7196-7200, 2003.

[108] H. E. Schaeffer and D. L. Krohn, "Liposomes in topical drug delivery," *Investigative Ophthalmology & Visual Science,* vol. 22, pp. 220-227, 1982.

[109] D. C. Litzinger and L. Huang, "Phosphatidylethanolamine liposomes: drug delivery, gene transfer and immunodiagnostic applications," *Biochimica et Biophysica Acta, MR. Reviews on Biomembranes,* vol. 1113, pp. 201-227, 1992.

[110] G. Gregoriadis, "*Liposomes as drug carriers: recent trends and progress",* Chichester, England: Wiley, 1988, pp. 34-76

[111] J. G. Riess, "Blood substitutes and other potential biomedical applications of fluorinated colloids," *Journal of Fluorine Chemistry,* vol. 114, pp. 119-126, 2002.

[112] R. Satterfield, V. Tarter, D. J. Schumacher, P. Tran, and R. F. Mattrey, "Comparison of different perfluorocarbons as ultrasound contrast agents," *Investigative Radiology,* vol. 28, p. 325, 1993.

[113] B. B. Goldberg, J.-B. Liu, and F. Forsberg, "Ultrasound contrast agents: a review," *Ultrasound in Medicine & Biology,* vol. 20, pp. 319-333, 1994.

[114] E. G. Schutt, T. J. Pelura, and R. M. Hopkins, "Osmotically stabilized microbubble sonographic contrast agents," *Academic Radiology,* vol. 3, p. S188, 1996.

[115] A. Kabalnov, D. Klein, T. Pelura, E. Schutt, and J. Weers, "Dissolution of multicomponent microbubbles in the bloodstream: 1. Theory," *Ultrasound in Medicine & Biology,* vol. 24, pp. 739-749, 1998.

[116] J.-M. Correas, L. Bridal, A. Lesavre, A. Méjean, M. Claudon, and O. Hélénon, "Ultrasound contrast agents: properties, principles of action, tolerance, and artifacts," *European Radiology,* vol. 11, pp. 1316-1328, 2001.

[117] I. Imagent, "AFO 150," *Adis International,* vol. 3, pp. 116-118, 2002.

[118] R. Weissleder, G. Elizondo, J. Wittenberg, C. Rabito, H. Bengele, and L. Josephson, "Ultrasmall superparamagnetic iron oxide: characterization of a new class of contrast agents for MR imaging," *Radiology,* vol. 175, pp. 489-493, 1990.

[119] U. Flögel, Z. Ding, H. Hardung, S. Jander, G. Reichmann, C. Jacoby, *et al.*, "In vivo monitoring of inflammation after cardiac and cerebral ischemia by fluorine magnetic resonance imaging," *Circulation,* vol. 118, pp. 140-148, 2008.

[120] Y.-X. J. Wang, S. M. Hussain, and G. P. Krestin, "Superparamagnetic iron oxide contrast agents: physicochemical characteristics and applications in MR imaging," *European Radiology,* vol. 11, pp. 2319-2331, 2001.

[121] G. Holland, P. Bottomley, and W. Hinshaw, "19F magnetic resonance imaging," *Journal of Magnetic Resonance,* vol. 28, pp. 133-136, 1977.

[122] Y. Jian-xin, V. D. Kodibagkar, C. Weina, and R. P. Mason, "19F: a versatile reporter for non-invasive physiology and pharmacology using magnetic resonance," *Current Medicinal Chemistry,* vol. 12, pp. 819-848, 2005.

[123] T. Jackson, "Fluorine: Benchmark Books", Tarrytown, New York: Marshall Cavendish, 2004, pp. 24.

[124] S. Laukemper-Ostendorf, A. Scholz, K. Bürger, C. P. Heussel, M. Schmittner, N. Weiler, *et al.*, "19F-MRI of perflubron for measurement of oxygen partial pressure in porcine lungs during partial liquid ventilation," *Magnetic Resonance in Medicine,* vol. 47, pp. 82-89, 2002.

[125] H. P. Shukla, R. P. Mason, N. Bansal, and P. P. Antich, "Regional myocardial oxygen tension: 19F MRI of sequestered perfluorocarbon," *Magnetic resonance in Medicine,* vol. 35, pp. 827-833, 1996.

[126] R. M. Judd, G. A. Rottman, J. R. Forder, F. C. Yin, and S. J. Blackband, "Feasibility of 19F imaging of perfluorochemical emulsions to measure myocardial vascular volume," *Magnetic Resonance in Medicine,* vol. 28, pp. 129-136, 1992.

[127] D. Lu, P. M. Joseph, J. H. Greenberg, R. Lin, B. Mukherji, and H. A. Sloviter, "Use of 19F magnetic resonance imaging to measure local cerebral blood volume," *Magnetic Resonance in Medicine,* vol. 29, pp. 179-187, 1993.

[128] R. P. Mason, P. P. Antich, E. E. Babcock, J. L. Gerberich, and R. L. Nunnally, "Perfluorocarbon imaging in vivo: A< sup> 19</sup> F MRI study in tumor-bearing mice," *Magnetic Resonance Imaging,* vol. 7, pp. 475-485, 1989.

[129] J. Bruneton, M. Falewee, E. Francois, P. Cambon, C. Philip, J. Riess, *et al.*, "Liver, spleen, and vessels: preliminary clinical results of CT with perfluorooctylbromide," *Radiology,* vol. 170, pp. 179-183, 1989.

[130] M. Behan, D. O'Connell, R. Mattrey, and D. Carney, "Perfluorooctylbromide as a contrast agent for CT and sonography: preliminary clinical results," *American Journal of Roentgenology,* vol. 160, pp. 399-405, 1993.

[131] N. PATRONAS, D. L. MILLER, and M. GIRTON, "Experimental comparison of EOE-13 and perfluoroctylbromide for the CT detection of hepatic metastases," *Investigative Radiology,* vol. 19, pp. 570-573, 1984.

[132] R. F. Mattrey, D. M. Long, W. W. Peck, R. A. Slutsky, and C. B. Higgins, "Perfluoroctylbromide as a blood pool contrast agent for liver, spleen, and vascular imaging in computed tomography," *Journal of Computer Assisted Tomography,* vol. 8, pp. 739-744, 1984.

[133] P. Freeny, W. Marks, J. Ryan, and J. Bolen, "Colorectal carcinoma evaluation with CT: preoperative staging and detection of postoperative recurrence," *Radiology,* vol. 158, pp. 347-353, 1986.

[134] P. Walstra, "Principles of emulsion formation," *Chemical Engineering Science,* vol. 48, pp. 333-349, 1993.

[135] P. Walstra, "Physical Chemistry of Foods", New York: Marcel Dekker Incorporated, 2002, pp. 355-390

[136] D. J. McClements, "Food emulsions: principles, practice, and techniques", vol. 5, Boca Raton, FL: CRC press, 1999, pp. 171-178

[137] D. J. Mcclements, "Critical review of techniques and methodologies for characterization of emulsion stability," *Critical Reviews in Food Science and Nutrition,* vol. 47, pp. 611-649, 2007.

[138] J. M. Chirgwin, A. E. Przybyla, R. J. MacDonald, and W. J. Rutter, "Isolation of biologically active ribonucleic acid from sources enriched in ribonuclease," *Biochemistry,* vol. 18, pp. 5294-5299, 1979.

[139] K. Uetani and H. Yano, "Nanofibrillation of wood pulp using a high-speed blender," *Biomacromolecules,* vol. 12, pp. 348-353, 2010.

[140] L. Moreau, H.-J. Kim, E. A. Decker, and D. J. McClements, "Production and characterization of oil-in-water emulsions containing droplets stabilized by β-lactoglobulin-pectin membranes," *Journal of Agricultural and Food Chemistry,* vol. 51, pp. 6612-6617, 2003.

[141] D. J. McClements, "Food Emulsions: Principles, Practice, and Techniques", Boca Raton, FL: CRC PressI Llc, 1999, pp. 174.

[142] S. Ando, M. Ando, and T. Ando, "HIGH-PRESSURE HOMOGENIZER," ed: WO Patent 2,009,054,041, July 7, 2010.

[143] G. Narsimhan and P. Goel, "Drop coalescence during emulsion formation in a high-pressure homogenizer for tetradecane-in-water emulsion stabilized by sodium dodecyl sulfate," *Journal of Colloid and Interface Science,* vol. 238, pp. 420-432, 2001.

[144] I. Burgaud, E. Dickinson, and P. Nelson, "An improved high-pressure homogenizer for making fine emulsions on a small scale," *International Journal of Food Science & Technology,* vol. 25, pp. 39-46, 1990.

[145] P. Paquin, "Technological properties of high pressure homogenizers: the effect of fat globules, milk proteins, and polysaccharides," *International Dairy Journal,* vol. 9, pp. 329-335, 1999.

[146] J. Davies, "Drop sizes of emulsions related to turbulent energy dissipation rates," *Chemical Engineering Science,* vol. 40, pp. 839-842, 1985.

[147] B. Zober, "Colloid mill," U.S. Patent 2 121 275, May 3, 1938.

[148] W. J. Goodwin, "Disc disperser-mixer," U.S. Patent 3 254 877, June 7, 1966.

[149] M. R. King and D. T. Leighton Jr, "Measurement of shear-induced dispersion in a dilute emulsion," *Physics of Fluids,* vol. 13, p. 397, 2001.

[150] H. Rashid, B. Tay, and M. Edirisinghe, "Dispersion of ceramic ink using an ultrasonic disruptor," *Journal of Materials Science Letters,* vol. 19, pp. 799-801, 2000.

[151] Y. Hwang, J.-K. Lee, J.-K. Lee, Y.-M. Jeong, S.-i. Cheong, Y.-C. Ahn, *et al.*, "Production and dispersion stability of nanoparticles in nanofluids," *Powder Technology,* vol. 186, pp. 145-153, 2008.

[152] Y. Hatate, H. Ohta, Y. Uemura, K. Ijichi, and H. Yoshizawa, "Preparation of monodispersed polymeric microspheres for toner particles by the Shirasu porous glass membrane emulsification technique," *Journal of Applied Polymer Science,* vol. 64, pp. 1107-1113, 1997.

[153] N. Aryanti, R. Hou, and R. A. Williams, "Performance of a rotating membrane emulsifier for production of coarse droplets," *Journal of Membrane Science,* vol. 326, pp. 9-18, 2009.

[154] N. M. van Os, J. R. Haak, and L. A. M. Rupert, "*Physico-Chemical Properties of Selected Anionic, Cationic and Nonionic Surfactants*", Amsterdan, Netherlands: Elsevier Science, 1993, pp. 9-376

[155] D. Zweytick, K. Athenstaedt, and G. Daum, "Intracellular lipid particles of eukaryotic cells," *Biochimica et Biophysica Acta (BBA)-Reviews on Biomembranes,* vol. 1469, pp. 101-120, 2000.

[156] J. L. Thewalt and M. Bloom, "Phosphatidylcholine: cholesterol phase diagrams," *Biophysical Journal,* vol. 63, pp. 1176-1181, 1992.

[157] R. Anderson, M. Kates, and B. Volcani, "Sulphonium analogue of lecithin in diatoms," *Nature,* vol. 263, pp. 51-53, 1976.

[158] C. Kent and G. M. Carman, "Interactions among pathways for phosphatidylcholine metabolism, CTP synthesis and secretion through the Golgi apparatus," *Trends in Biochemical Sciences,* vol. 24, pp. 146-150, 1999.

[159] P. Campbell, "Toxicity of some charged lipids used in liposome preparations," *Cytobios,* vol. 37, p. 21, 1983.

[160] D. D. Lasic, "Liposomes in Gene Delivery", Boca Raton, FL: CRC PressINC, 1997, pp. 61-65.

[161] D. D. Lasic and F. J. Martin, "Stealth Liposomes", Boca Raton, FL: CRC PressINC, 1995, pp. 173-210.

[162] R. Banerjee, "Liposomes: applications in medicine," *Journal of Biomaterials Applications,* vol. 16, pp. 3-21, 2001.

[163] D. D. Lasic, "Novel applications of liposomes," *Trends in Biotechnology,* vol. 16, pp. 307-321, 1998.

[164] E. Dickinson, ". Emulsions," *Annual Reports Section" C"(Physical Chemistry),* vol. 83, pp. 31-58, 1986.

[165] T. Tadros, "Application of rheology for assessment and prediction of the long-term physical stability of emulsions," *Advances in Colloid and Interface Science,* vol. 108, pp. 227-258, 2004.

[166] M. M. Robins, "Emulsions—creaming phenomena," *Current Opinion in Colloid & Interface Science,* vol. 5, pp. 265-272, 2000.

[167] E. Dickinson, "Food emulsions and foams: Stabilization by particles," *Current Opinion in Colloid & Interface Science,* vol. 15, pp. 40-49, 2010.

[168] To, Schematic of Mechanisms Leading, "Emulsion Stability and Testing," *Particle Sciences-Technical Brief,* vol. 2, 2011.

[169] P. Becher, "Emulsions: theory and practice," 3rd ed, Washington, DC: American Chemistry Society, 2001, pp. 119-303.

[170] P. Becher, "Encyclopedia of emulsion technology: Applications vol. 2," New York: Marcel Dekker, 1985, pp. 77-238.

[171] M. Shields, R. Ellis, and B. R. Saunders, "A creaming study of weakly flocculated and depletion flocculated oil-in-water emulsions," *Colloids and Surfaces A: Physicochemical and Engineering Aspects,* vol. 178, pp. 265-276, 2001.

[172] S. Reddy, D. Melik, and H. S. Fogler, "Emulsion stability—theoretical studies on simultaneous flocculation and creaming," *Journal of Colloid and Interface Science,* vol. 82, pp. 116-127, 1981.

[173] C. Cowell and B. Vincent, "Temperature-particle concentration phase diagrams for dispersions of weakly interacting particles," *Journal of Colloid and Interface Science,* vol. 87, pp. 518-526, 1982.

[174] R. Hogg, "Collision efficiency factors for polymer flocculation," *Journal of colloid and interface science,* vol. 102, pp. 232-236, 1984.

[175] S. Reddy and H. S. Fogler, "Emulsion stability: delineation of different particle loss mechanisms," *Journal of Colloid and Interface Science,* vol. 79, pp. 105-113, 1981.

[176] L. Skinner and J. Sambles, "The Kelvin equation—a review," *Journal of Aerosol Science,* vol. 3, pp. 199-210, 1972.

[177] G. Madras and B. J. McCoy, "Distribution kinetics theory of Ostwald ripening," *The Journal of Chemical Physics,* vol. 115, p. 6699, 2001.

[178] J. T. Edward, "Molecular volumes and the Stokes-Einstein equation," *Journal of Chemical Education,* vol. 47, p. 261, 1970.

[179] C. Wilke and P. Chang, "Correlation of diffusion coefficients in dilute solutions," *AIChE Journal,* vol. 1, pp. 264-270, 1955.

[180] R. J. Greff, M. L. Jones, and S. Evans, "Compositions for use in embolizing blood vessels," U.S Patents 5 667 767, September 16, 1997.

[181] C.-F. Hung, J.-K. Chen, M.-H. Liao, H.-M. Lo, and J.-Y. Fang, "Development and evaluation of emulsion-liposome blends for resveratrol delivery," *Journal of Nanoscience and Nanotechnology,* vol. 6, pp. 9-10, 2006.

[182] A. Amri, J. Chaumeil, S. Sfar, and C. Charrueau, "Administration of resveratrol: what formulation solutions to bioavailability limitations?," *Journal of Controlled Release,* vol. 158, pp. 182-193, 2012.

[183] T. F. Tadros, "Emulsion Formation and Stability," Hoboken: Wiley-VCH, 2013, pp. 1-73.

[184] T. J. Pedley, "The fluid mechanics of large blood vessels vol. 1," Cambridge, NY: Cambridge University Press, 1980.

[185] N. Resnick, H. Yahav, A. Shay-Salit, M. Shushy, S. Schubert, L. C. M. Zilberman, *et al.*, "Fluid shear stress and the vascular endothelium: for better and for worse," *Progress in Biophysics and Molecular Biology,* vol. 81, pp. 177-199, 2003.

[186] M. Zamir, "Shear forces and blood vessel radii in the cardiovascular system," *The Journal of General Physiology,* vol. 69, pp. 449-461, 1977.

[187] Y. Fung and S. Liu, "Elementary mechanics of the endothelium of blood vessels," *Journal of Biomechanical Engineering,* vol. 115, p. 1, 1993.

[188] T. Ziegler and R. M. Nerem, "Tissue engineering a blood vessel: regulation of vascular biology by mechanical stresses," *Journal of Cellular Biochemistry,* vol. 56, pp. 204-209, 1994.

[189] K. H. Keller, "Effect of fluid shear on mass transport in flowing blood," in *Federation Proceedings*, 1971, p. 1591.

[190] A. Grazioli, C. S. Alves, K. Konstantopoulos, and J. T. Yang, "Defective blood vessel development and pericyte/pvSMC distribution in< i> α4 integrin</i>-deficient mouse embryos," *Developmental Biology,* vol. 293, pp. 165-177, 2006.

[191] T. Nagel, N. Resnick, W. J. Atkinson, C. F. Dewey Jr, and M. A. Gimbrone Jr, "Shear stress selectively upregulates intercellular adhesion molecule-1 expression in cultured human vascular endothelial cells," *Journal of Clinical Investigation,* vol. 94, p. 885, 1994.

[192] R. F. Schmidt, F. Lang, and M. Heckmann, *Physiologie Des Menschen: Mit Pathophysiologie*: Springer London, Limited, 2005.

[193] J. Kreuter, "Evaluation of nanoparticles as drug-delivery systems. III: materials, stability, toxicity, possibilities of targeting, and use," *Pharmaceutica Acta Helvetiae,* vol. 58, p. 242, 1983.

[194] J. Kreuter, "Factors influencing the body distribution of polyacrylic nanoparticles," *Elsevier, Amsterdam,* p. 51, 1985.

[195] U. Häfeli, W. Schütt, J. Teller, and M. Zborowski, "Scientific and clinical applications of magnetic carriers," New York: Prenum Press, 1997, pp. 53-68.

[196] R. Van Furth, Z. Cohn, J. Hirsch, J. Humphrey, W. Spector, and H. Langevoort, "The mononuclear phagocyte system: a new classification of macrophages,

monocytes, and their precursor cells," *Bulletin of the World Health Organization,* vol. 46, p. 845, 1972.

[197] D. A. Hume, "The mononuclear phagocyte system," *Current Opinion in Immunology,* vol. 18, pp. 49-53, 2006.

[198] B. Hamm, T. Staks, A. Mühler, M. Bollow, M. Taupitz, T. Frenzel, *et al.*, "Phase I clinical evaluation of Gd-EOB-DTPA as a hepatobiliary MR contrast agent: safety, pharmacokinetics, and MR imaging," *Radiology,* vol. 195, pp. 785-792, 1995.

[199] E. Renkin and C. Crone, "Microcirculation and capillary exchange," *Comprehensive Human Physiology,* vol. 2, pp. 1965-1979, 1996.

[200] L. R. Johnson, "Essential Medical Physiology," Boston: Elsevier Academic Press, 2003, pp. 157-258.

[201] S. M. Moghimi, A. C. Hunter, and J. C. Murray, "Long-circulating and target-specific nanoparticles: theory to practice," *Pharmacological Reviews,* vol. 53, pp. 283-318, 2001.

[202] C. Chouly, D. Pouliquen, I. Lucet, J. Jeune, and P. Jallet, "Development of superparamagnetic nanoparticles for MRI: effect of particle size, charge and surface nature on biodistribution," *Journal of Microencapsulation,* vol. 13, pp. 245-255, 1996.

[203] Y. Okuhata, "Delivery of diagnostic agents for magnetic resonance imaging," *Advanced Drug Delivery Reviews,* vol. 37, pp. 121-137, 1999.

[204] M. W. Brightman, M. Hori, S. I. Rapoport, T. S. Reese, and E. Westergaard, "Osmotic opening of tight junctions in cerebral endothelium," *Journal of Comparative Neurology,* vol. 152, pp. 317-325, 1973.

[205] H. Wolburg, J. Neuhaus, U. Kniesel, B. Krauß, E.-M. Schmid, M. Ocalan, *et al.*, "Modulation of tight junction structure in blood-brain barrier endothelial cells. Effects of tissue culture, second messengers and cocultured astrocytes," *Journal of Cell Science,* vol. 107, pp. 1347-1357, 1994.

[206] B. Haraldsson, "Physiological studies of macromolecular transport across capillary walls. Studies on continuous capillaries in rat skeletal muscle," *Acta Physiologica Scandinavica. Supplementum,* vol. 553, p. 1, 1986.

[207] W. Paaske and P. Sejrsen, "Permeability of continuous capillaries," *Danish Medical Bulletin,* vol. 36, p. 570, 1989.

[208] G. G. Maul, "Structure and formation of pores in fenestrated capillaries," *Journal of Ultrastructure Research,* vol. 36, pp. 768-782, 1971.

[209] H. Friederici, "The tridimensional ultrastructure of fenestrated capillaries," *Journal of Ultrastructure Research,* vol. 23, pp. 444-456, 1968.

[210] Y. Kao and R. Juliano, "Interactions of liposomes with the reticuloendothelial system effects of reticuloendothelial blockade on the clearance of large unilamellar vesicles," *Biochimica et Biophysica Acta (BBA)-General Subjects,* vol. 677, pp. 453-461, 1981.

[211] K. Aterman, "The structure of the liver sinusoids and the sinusoidal cells," *The liver,* vol. 1, pp. 61-136, 1963.

[212] D. Napper and A. Netschey, "Studies of the steric stabilization of colloidal particles," *Journal of Colloid and Interface Science,* vol. 37, pp. 528-535, 1971.

[213] D.-H. Napper, "Steric stabilization," *Journal of Colloid and Interface Science,* vol. 58, pp. 390-407, 1977.

[214] M. Radisic, H. Park, F. Chen, J. E. Salazar-Lazzaro, Y. Wang, R. Dennis, *et al.*, "Biomimetic approach to cardiac tissue engineering: oxygen carriers and channeled scaffolds," *Tissue Engineering,* vol. 12, pp. 2077-2091, 2006.

[215] M. Radisic, H. Park, S. Gerecht, C. Cannizzaro, R. Langer, and G. Vunjak-Novakovic, "Biomimetic approach to cardiac tissue engineering," *Philosophical Transactions of the Royal Society B: Biological Sciences,* vol. 362, pp. 1357-1368, 2007.

[216] M. Radisic, W. Deen, R. Langer, and G. Vunjak-Novakovic, "Mathematical model of oxygen distribution in engineered cardiac tissue with parallel channel array perfused with culture medium containing oxygen carriers," *American Journal of Physiology-Heart and Circulatory Physiology,* vol. 288, pp. H1278-H1289, 2005.

[217] M. Radisic, A. Marsano, R. Maidhof, Y. Wang, and G. Vunjak-Novakovic, "Cardiac tissue engineering using perfusion bioreactor systems," *Nature Protocols,* vol. 3, pp. 719-738, 2008.

[218] M. L. Fabiilli, K. J. Haworth, I. E. Sebastian, O. D. Kripfgans, P. L. Carson, and J. B. Fowlkes, "Delivery of chlorambucil using an acoustically-triggered perfluoropentane emulsion," *Ultrasound in Medicine & Biology,* vol. 36, pp. 1364-1375, 2010.

[219] H.-J. Lehmler, "Perfluorocarbon compounds as vehicles for pulmonary drug delivery," *Expert Opinion on Drug Delivery,* vol.4, pp. 247-262, 2007.

[220] M. P. Krafft, "Fluorocarbons and fluorinated amphiphiles in drug delivery and biomedical research," *Advanced Drug Delivery Reviews,* vol. 47, pp. 209-228, 2001.

[221] J. G. Riess, "Fluorocarbon-Based in vivo Oxygen Transport and Delivery Systems," *Vox Sanguinis,* vol. 61, pp. 225-239, 1991.

[222] E. C. Unger, T. Porter, W. Culp, R. Labell, T. Matsunaga, and R. Zutshi, "Therapeutic applications of lipid-coated microbubbles," *Advanced Drug Delivery Reviews,* vol. 56, pp. 1291-1314, 2004.

[223] E. Takahashi, M. Furui, H. Seko, and T. Shibatani, "D-lysine production from L-lysine by successive chemical racemization and microbial asymmetric degradation," *Applied Microbiology and Biotechnology,* vol. 47, pp. 347-351, 1997.

[224] H. L. Holland, "Microbial transformations," *Current Opinion in Chemical Biology,* vol. 2, pp. 77-84, 1998.

[225] J. Hiraki, T. Ichikawa, S.-i. Ninomiya, H. Seki, K. Uohama, H. Seki, *et al.*, "Use of ADME studies to confirm the safety of ε-polylysine as a preservative in food," *Regulatory Toxicology and Pharmacology,* vol. 37, pp. 328-340, 2003.

[226] I. Geornaras and J. N. Sofos, "Activity of ε–Polylysine Against Escherichia coli O157: H7, Salmonella Typhimurium, and Listeria monocytogenes," *Journal of Food Science,* vol. 70, pp. M404-M408, 2005.

[227] H. Liu, H. Xu, M. Wang, L. Lang, and X. Xiu, "The sutdy of poly-lysine in food," *Journal of Northeast Agricultural University,* vol. 31, pp. 294-298, 2000.

[228] T. Yoshida and T. Nagasawa, "ε-Poly-l-lysine: microbial production, biodegradation and application potential," *Applied Microbiology and Biotechnology,* vol. 62, pp. 21-26, 2003.

[229] S. Shima, H. Matsuoka, T. Iwamoto, and H. Sakai, "Antimicrobial action of epsilon-poly-L-lysine," *The Journal of Antibiotics,* vol. 37, p. 1449, 1984.

[230] U. Food, "Drug Administration. 2004b. Agency response letter; GRAS Notice No. GRN 000135. Washington, DC: US Food and Drug Administration," ed, 2005.

[231] M. B. Najjar, D. Kashtanov, and M. Chikindas, "ε-Poly-l-lysine and nisin A act synergistically against Gram-positive food-borne pathogens Bacillus cereus and Listeria monocytogenes," *Letters in Applied Microbiology,* vol. 45, pp. 13-18, 2007.

[232] D. T. Curiel, S. Agarwal, E. Wagner, and M. Cotten, "Adenovirus enhancement of transferrin-polylysine-mediated gene delivery," *Proceedings of the National Academy of Sciences,* vol. 88, pp. 8850-8854, 1991.

[233] E. Wagner, K. Zatloukal, M. Cotten, H. Kirlappos, K. Mechtler, D. T. Curiel, *et al.*, "Coupling of adenovirus to transferrin-polylysine/DNA complexes greatly

enhances receptor-mediated gene delivery and expression of transfected genes," *Proceedings of the National Academy of Sciences,* vol. 89, pp. 6099-6103, 1992.

[234] D. W. Pack, A. S. Hoffman, S. Pun, and P. S. Stayton, "Design and development of polymers for gene delivery," *Nature Reviews Drug Discovery,* vol. 4, pp. 581-593, 2005.

[235] S. C. De Smedt, J. Demeester, and W. E. Hennink, "Cationic polymer based gene delivery systems," *Pharmaceutical Research,* vol. 17, pp. 113-126, 2000.

[236] K. R. Kamath and K. Park, "Biodegradable hydrogels in drug delivery," *Advanced Drug Delivery Reviews,* vol. 11, pp. 59-84, 1993.

[237] K. Crompton, J. Goud, R. Bellamkonda, T. Gengenbach, D. Finkelstein, M. Horne, *et al.*, "Polylysine-functionalised thermoresponsive chitosan hydrogel for neural tissue engineering," *Biomaterials,* vol. 28, pp. 441-449, 2007.

[238] J. L. Drury and D. J. Mooney, "Hydrogels for tissue engineering: scaffold design variables and applications," *Biomaterials,* vol. 24, pp. 4337-4351, 2003.

[239] M. Lutolf and J. Hubbell, "Synthetic biomaterials as instructive extracellular microenvironments for morphogenesis in tissue engineering," *Nature Biotechnology,* vol. 23, pp. 47-55, 2005.

[240] E. Lavik and R. Langer, "Tissue engineering: current state and perspectives," *Applied Microbiology and Biotechnology,* vol. 65, pp. 1-8, 2004.

[241] H. Andersson and A. Van Den Berg, "Microfabrication and microfluidics for tissue engineering: state of the art and future opportunities," *Lab Chip,* vol. 4, pp. 98-103, 2004.

[242] S. W. Ueng, S.-S. Lee, S.-S. Lin, E.-C. Chan, B. R.-S. Hsu, and K.-T. Chen, "Biodegradable alginate antibiotic beads," *Clinical Orthopaedics and Related Research,* vol. 380, pp. 250-259, 2000.

[243] T. M. Fahmy, R. M. Samstein, C. C. Harness, and W. Mark Saltzman, "Surface modification of biodegradable polyesters with fatty acid conjugates for improved drug targeting," *Biomaterials,* vol. 26, pp. 5727-5736, 2005.

[244] J. A. Hubbell, "Synthetic biodegradable polymers for tissue engineering and drug delivery," *Current Opinion in Solid State and Materials Science,* vol. 3, pp. 246-251, 1998.

[245] R. H. Garrett and C. M. Grisham, "Biochemistry," 5th ed, Belmont, CA: Brooks/ Cole Publishing Company, 2013, pp. 210-211.

[246] S. P. Davis, "Chitosan: Manufacture, Properties, and Usage," Hauppauge, NY: Nova Science Publishers, Incorporated, 2011, pp. 2-10.

[247] B. Ghosh and M. W. Urban, "Self-repairing oxetane-substituted chitosan polyurethane networks," *Science,* vol. 323, pp. 1458-1460, 2009.

[248] M. W. Urban, "Stratification, stimuli-responsiveness, self-healing, and signaling in polymer networks," *Progress in Polymer Science,* vol. 34, pp. 679-687, 2009.

[249] N. Saifuddin M and P. Kumaran, "Removal of heavy metal from industrial wastewater using chitosan coated oil palm shell charcoal," *Electronic Journal of Biotechnology,* vol. 8, pp. 43-53, 2005.

[250] C. L. Lasko and M. P. Hurst, "An investigation into the use of chitosan for the removal of soluble silver from industrial wastewater," *Environmental Science & Technology,* vol. 33, pp. 3622-3626, 1999.

[251] O. Amuda, A. Giwa, and I. Bello, "Removal of heavy metal from industrial wastewater using modified activated coconut shell carbon," *Biochemical Engineering Journal,* vol. 36, pp. 174-181, 2007.

[252] F. Shahidi and R. Abuzaytoun, "Chitin, chitosan, and co-products: chemistry, production, applications, and health effects," *Advances in Food and Nutrition Research,* vol. 49, pp. 93-135, 2005.

[253] M. Pittler, N. Abbot, E. Harkness, and E. Ernst, "Randomized, double-blind trial of chitosan for body weight reduction," *European Journal of Clinical Nutrition,* vol. 53, p. 379, 1999.

[254] C. N. Mhurchu, S. Poppitt, A. McGill, F. Leahy, D. Bennett, R. Lin, *et al.*, "The effect of the dietary supplement, Chitosan, on body weight: a randomised controlled trial in 250 overweight and obese adults," *International Journal of Obesity,* vol. 28, pp. 1149-1156, 2004.

[255] M. F. A. Goosen, "Applications of Chitin and Chitosan," Lancaster, PA: Technomic Publishing Company, 1997, pp. 16-18.

[256] J. C. Linden and R. R. Stoner, "Proprietary elicitor affects seed germination and delays fruit senescence," *Journal of Food Agriculture and Environment,* vol. 3, p. 184, 2005.

[257] T. Miyata, K. Kodaira, H. Higashijima, T. Kimura, and Y. Noishiki, "A biomaterial comprising a composite material of chitosan derivative and collagen and a process for the production of the same," U.S Patent 5 116 824 A, May 26, 1992.

[258] C. Hardy, E. L. Johnson, and P. Luksch, "Hemostatic material," U.S. Patents 7 981 872 B2, July 19, 2011.

[259] W. E. Roorda, J. A. McCoy, R. Seto, and E. T. Michal, "Stable chitosan hemostatic implant and methods of manufacture," U.S. Patents 0 311 608 A1, December 22, 2010.

[260] Y. Wan, X. Cao, Q. Wu, S. Zhang, and S. Wang, "Preparation and mechanical properties of poly (chitosan-g-DL-lactic acid) fibrous mesh scaffolds," *Polymers for Advanced Technologies,* vol. 19, pp. 114-123, 2008.

[261] K. Y. Lee, W. S. Ha, and W. H. Park, "Blood compatibility and biodegradability of partially< i> N</i>-acylated chitosan derivatives," *Biomaterials,* vol. 16, pp. 1211-1216, 1995.

[262] J. Berger, M. Reist, J. Mayer, O. Felt, N. Peppas, and R. Gurny, "Structure and interactions in covalently and ionically crosslinked chitosan hydrogels for biomedical applications," *European Journal of Pharmaceutics and Biopharmaceutics,* vol. 57, pp. 19-34, 2004.

[263] J. Berger, M. Reist, J. Mayer, O. Felt, and R. Gurny, "Structure and interactions in chitosan hydrogels formed by complexation or aggregation for biomedical applications," *European Journal of Pharmaceutics and Biopharmaceutics,* vol. 57, pp. 35-52, 2004.

[264] F. Chen, Z.-C. Wang, and C.-J. Lin, "Preparation and characterization of nano-sized hydroxyapatite particles and hydroxyapatite/chitosan nano-composite for use in biomedical materials," *Materials Letters,* vol. 57, pp. 858-861, 2002.

[265] E. Khor and L. Y. Lim, "Implantable applications of chitin and chitosan," *Biomaterials,* vol. 24, pp. 2339-2349, 2003.

[266] S. E. Kim, J. H. Park, Y. W. Cho, H. Chung, S. Y. Jeong, E. B. Lee, *et al.*, "Porous chitosan scaffold containing microspheres loaded with transforming growth factor-β1: implications for cartilage tissue engineering," *Journal of Controlled Release,* vol. 91, pp. 365-374, 2003.

[267] S. V. Madihally and H. W. Matthew, "Porous chitosan scaffolds for tissue engineering," *Biomaterials,* vol. 20, pp. 1133-1142, 1999.

[268] J.-K. Francis Suh and H. W. Matthew, "Application of chitosan-based polysaccharide biomaterials in cartilage tissue engineering: a review," *Biomaterials,* vol. 21, pp. 2589-2598, 2000.

[269] A. Di Martino, M. Sittinger, and M. V. Risbud, "Chitosan: a versatile biopolymer for orthopaedic tissue-engineering," *Biomaterials,* vol. 26, pp. 5983-5990, 2005.

[270] R. Jayakumar, M. Prabaharan, S. Nair, and H. Tamura, "Novel chitin and chitosan nanofibers in biomedical applications," *Biotechnology Advances,* vol. 28, pp. 142-150, 2010.

[271] J. Varshosaz, "The promise of chitosan microspheres in drug delivery systems," *Expert Opinion on Drug Delivery*, vol. 4, pp. 263-273, 2007.

[272] M. Phisalaphong and N. Jatupaiboon, "Biosynthesis and characterization of bacteria cellulose–chitosan film," *Carbohydrate Polymers,* vol. 74, pp. 482-488, 2008.

[273] M. Shimaoka, J. Takagi, and T. A. Springer, "Conformational regulation of integrin structure and function," *Annual Review of Biophysics and Biomolecular Structure,* vol. 31, pp. 485-516, 2002.

[274] H. Z. Streicher, I. J. Berkower, M. Busch, F. Gurd, and J. A. Berzofsky, "Antigen conformation determines processing requirements for T-cell activation," *Proceedings of the National Academy of Sciences,* vol. 81, pp. 6831-6835, 1984.

[275] E. Fanning and R. Knippers, "Structure and function of simian virus 40 large tumor antigen," *Annual Review of Biochemistry,* vol. 61, pp. 55-85, 1992.

[276] I. A. Wilson and R. L. Stanfield, "Antibody-antigen interactions: new structures and new conformational changes," *Current Opinion in Structural Biology,* vol. 4, pp. 857-867, 1994.

[277] K. Ryder, S. Silver, A. L. DeLucia, E. Fanning, and P. Tegtmeyer, "An altered DNA conformation in origin region I is a determinant for the binding of SV40 large T antigen," *Cell,* vol. 44, pp. 719-725, 1986.

[278] A. Ulman, "Langmuir-Blodgett Films," *The Handbook of Surface Imaging and Visualization,* p. 277, 1995.

[279] J. Zasadzinski, R. Viswanathan, L. Madsen, J. Garnaes, and D. Schwartz, "Langmuir-Blodgett films," *Science-AAAS-Weekly Paper Edition-including Guide to Scientific Information,* vol. 263, pp. 1726-1738, 1994.

[280] G. G. Roberts, "Langmuir-blodgett films," New York: Plenum press, 1990, pp. 1-16.

[281] M. C. Petty, "Langmuir-Blodgett films: an introduction," Cambridge, NY: Cambridge University Press, 1996, pp. 12-37.

[282] G. Roberts, "An applied science perspective of Langmuir-Blodgett films," *Advances in Physics,* vol. 34, pp. 475-512, 1985.

[283] B. Mui, L. Chow, and M. J. Hope, "Extrusion technique to generate liposomes of defined size," *Methods in Enzymology,* vol. 367, pp. 3-14, 2003.

[284] P. Muthukumarasamy, P. Allan-Wojtas, and R. A. Holley, "Stability of Lactobacillus reuteri in different types of microcapsules," *Journal of Food Science,* vol. 71, pp. M20-M24, 2006.

[285] F. Olson, C. Hunt, F. Szoka, W. Vail, and D. Papahadjopoulos, "Preparation of liposomes of defined size distribution by extrusion through polycarbonate membranes," *Biochimica et Biophysica Acta (BBA)-Biomembranes,* vol. 557, pp. 9-23, 1979.

[286] B. J. Berne and R. Pecora, "Dynamic light scattering: with applications to chemistry, biology and physics," Mineola: Dover Publications, 2000, pp. 83-85.

[287] R. Pecora, "Dynamic light scattering: applications of photon correlation spectroscopy," New York: Plenum press, 1985, pp. 96-100.

[288] W. Brown, "Dynamic light scattering: the method and some applications," New York: Oxford University Press, 1993, pp. 26-28

[289] B. E. Smart and R. E. Fernandez, "Fluorinated aliphatic compounds," *Kirk-Othmer Encyclopedia of Chemical Technology,* 1994.

[290] J. Coe and T. Godfrey, "Viscosity of water," *Journal of Applied Physics,* vol. 15, pp. 625-626, 1944.

[291] P. Schiebener, J. Straub, J. L. Sengers, and J. Gallagher, "Refractive index of water and steam as function of wavelength, temperature and density," Washington, DC: American Chemical Society, 1990, pp. 677-717

[292] D. Van Velzen, R. L. Cardozo, and H. Langenkamp, "A liquid viscosity-temperature-chemical constitution relation for organic compounds," *Industrial & Engineering Chemistry Fundamentals,* vol. 11, pp. 20-25, 1972.

[293] S. Hirayama, Y. Iuchi, F. Tanaka, and K. Shobatake, "Natural radiative lifetimes of anthracene derivatives and their dependence on refractive index," *Chemical Physics,* vol. 144, pp. 401-406, 1990.

[294] W. J. Wiscombe, "Improved Mie scattering algorithms," *Applied Optics,* vol. 19, pp. 1505-1509, 1980.

[295] R. J. Hunter, "Zeta potential in colloid science: principles and applications," New York: Academic press, 1981, pp. 1-386

[296] B. J. Kirby and E. F. Hasselbrink, "Zeta potential of microfluidic substrates: 1. Theory, experimental techniques, and effects on separations," *Electrophoresis,* vol. 25, pp. 187-202, 2004.

[297] D. Henry, "The cataphoresis of suspended particles. Part I. The equation of cataphoresis," *Proceedings of the Royal Society of London. Series A,* vol. 133, pp. 106-129, 1931.

[298] H. J. Butt, K. Graf, and M. Kappl, "Physics and Chemistry of Interfaces," 2nd ed, Weinheim, Germany: Wiley-VCH, 2006, pp. 42-79.

[299] K. S. Birdi, "Handbook of Surface and Colloid Chemistry," 3rd ed, Boca Raton, FL: CRC press/ Taylor & Francis, 2009, pp. 197-330

[300] H. Ohshima, "Electrophoretic mobility of soft particles," *Colloids and Surfaces A: Physicochemical and Engineering Aspects,* vol. 103, pp. 249-255, 1995.

[301] R. W. O'Brien and R. J. Hunter, "The electrophoretic mobility of large colloidal particles," *Canadian Journal of Chemistry,* vol. 59, pp. 1878-1887, 1981.

[302] R. Greenwood and K. Kendall, "Selection of suitable dispersants for aqueous suspensions of zirconia and titania powders using acoustophoresis," *Journal of the European Ceramic Society,* vol. 19, pp. 479-488, 1999.

[303] T. M. Riddick, "Control of colloid stability through zeta potential," *Blood,* vol. 10, p. 1, 1968.

[304] J. Harris and M. Hayes, "Acid dissociation constant," *IN: Handbook of Chemical Property Estimation Methods: Environmental Behavior of Organic Compounds. American Chemical Society, Washington, DC. 1990. p 6. 1-6. 28. 10 tab, 12 ref*, 1990.

[305] R. Chang, Physical Chemistry for the Chemical and Biological Sciences," Sausalito, CA: University Science Books, 2000, pp. 397-430.

[306] M. Clugston and R. Flemming, "Advanced Chemistry," Oxford: Oxford University press, 2000, pp. 194-195.

[307] F. A. Bettelheim, W. H. Brown, M. K. Campbell, and S. O. Farrell, "Introduction to General, Organic and Biochemistry," 9th ed, Boston, MA: Brooks/Cole, Cengage Learning, 2010, pp. 240-275

[308] H. N. Po and N. Senozan, "The Henderson-Hasselbalch equation: its history and limitations," *Journal of Chemical Education,* vol. 78, p. 1499, 2001.

[309] B. M. Weckhuysen, "Ultraviolet-visible spectroscopy," Stevenson Ranch, CA: American Scientific Publishers, 2004, pp. 255-270.

[310] J. R. Platt, "Ultra-violet and visible spectroscopy: chemical applications," *American Chemical Society,* vol. 84, pp. 3034-3034, 1962.

[311] M. Thomas, "Ultraviolet and visible spectroscopy," 2nd ed, New York: Wiley India Pvt. Limited, 2008, pp. 1-229.

[312] K. Fuwa and B. Valle, "The Physical Basis of Analytical Atomic Absorption Spectrometry. The Pertinence of the Beer-Lambert Law," *Analytical Chemistry,* vol. 35, pp. 942-946, 1963.

[313] D. Swinehart, "The beer-lambert law," *Journal of Chemical Education,* vol. 39, p. 333, 1962.

[314] F. P. Miller, A. F. Vandome, and J. McBrewster, "Beer-Lambert Law," Berlin: Germany :VDM Publishing, 2009, pp. 1-154

[315] W.-C. Shen, D. Yang, and H. J.-P. Ryser, "Colorimetric determination of microgram quantities of polylysine by trypan blue precipitation," *Analytical Biochemistry,* vol. 142, pp. 521-524, 1984.

[316] A. Grotzky, Y. Manaka, S. Fornera, M. Willeke, and P. Walde, "Quantification of α-polylysine: a comparison of four UV/Vis spectrophotometric methods," *Analytical Methods,* vol. 2, pp. 1448-1455, 2010.

[317] W. Shen, "Yang, and Ryser, HJP (1984) Colorimetric determination of microgram quantities of polylysine by trypan blue precipitation," *Analytical Biochemistry,* vol. 142, pp. 521-524.

[318] C. Wischke and H.-H. Borchert, "Increased sensitivity of chitosan determination by a dye binding method," *Carbohydrate Research,* vol. 341, pp. 2978-2979, 2006.

[319] M. Abou-Shoer, "A Simple Colorimetric Method for the Evaluation of Chitosan," *American Journal of Analytical Chemistry,* vol. 1, pp. 91-94, 2010.

[320] R. Muzzarelli, "Colorimetric determination of chitosan," *Analytical biochemistry,* vol. 260, p. 255, 1998.

[321] R. A. Muzzarelli, "Colorimetric determination of chitosan," *Analytical biochemistry,* vol. 260, pp. 255-257, 1998.

[322] J. R. Lakowicz, "Principles of fluorescence spectroscopy," New York: Springer, 2006, pp. 1-25.

[323] B. Valeur and J. C. Brochon, "New Trends in Fluorescence Spectroscopy: Applications to Chemical and Life Sciences," Berlin, Germany: Springer-Verlag GmbH, 2001, pp. 35-52.

[324] A. Sharma and S. G. Schulman, "Introduction to Fluorescence Spectroscopy," New York: Wiley, 1999, pp. 1-173.

[325] S. Strickler and R. A. Berg, "Relationship between absorption intensity and fluorescence lifetime of molecules," *The Journal of Chemical Physics,* vol. 37, p. 814, 1962.

[326] P. Andresen, A. Bath, W. Gröger, H. Lülf, G. Meijer, and J. t. Meulen, "Laser-induced fluorescence with tunable excimer lasers as a possible method for instantaneous temperature field measurements at high pressures: checks with an atmospheric flame," *Applied Optics,* vol. 27, pp. 365-378, 1988.

[327] D. Sheehan, "Physical Biochemistry: Principles and Applications," 2nd ed, Chichester, England: Wiley-Blackwell, 2010.

[328] B. Valeur and M. N. Berberan-Santos, "Molecular Fluorescence: Principles and Applications," Weinheim, Germany: Wiley, 2013, pp. 141-158.

[329] S. Phillips, L. Wilson, and R. Borkman, "Acrylamide and iodide fluorescence quenching as a structural probe of tryptophan microenvironment in bovine lens crystallins," *Current Eye Research,* vol. 5, pp. 611-620, 1986.

[330] M. R. Eftink, "Fluorescence quenching: theory and applications," *Topics in Fluorescence Spectroscopy,* vol. 2, pp. 53-126, 1991.

[331] M. R. Eftink, "Fluorescence quenching reactions," in *Biophysical and Biochemical Aspects of Fluorescence Spectroscopy*, New York: Pelnum press, 1991, pp. 1-41.

[332] H. Kautsky, "Quenching of luminescence by oxygen," *Transactions of the Faraday Society,* vol. 35, pp. 216-219, 1939.

[333] K. Kawaoka, A. Khan, and D. R. Kearns, "Role of singlet excited states of molecular oxygen in the quenching of organic triplet states," *The Journal of Chemical Physics,* vol. 46, p. 1842, 1967.

[334] D. R. Kearns, "Physical and chemical properties of singlet molecular oxygen," *Chemical Reviews,* vol. 71, pp. 395-427, 1971.

[335] M. Kasha, "Collisional Perturbation of Spin-Orbital Coupling and the Mechanism of Fluorescence Quenching. A Visual Demonstration of the Perturbation," *The Journal of Chemical Physics,* vol. 20, p. 71, 1952.

[336] G. Nelson and I. M. Warner, "Fluorescence quenching studies of cyclodextrin complexes of pyrene and naphthalene in the presence of alcohols," *Journal of Physical Chemistry,* vol. 94, pp. 576-581, 1990.

[337] M. Okamoto and H. Teranishi, "Effect of pressure on the external heavy atom quenching of pyrene fluorescence in fluid solution," *The Journal of Physical Chemistry,* vol. 88, pp. 5644-5646, 1984.

[338] M. Grätzel and J. Thomas, "Dynamics of pyrene fluorescence quenching in aqueous ionic micellar systems. Factors affecting the permeability of micelles," *Journal of the American Chemical Society,* vol. 95, pp. 6885-6889, 1973.

[339] O. Stern and M. Volmer, "Über die abklingzeit der fluoreszenz," *Physikalische Zeitschrift,* vol. 20, pp. 183-188, 1919.

[340] H. Boaz and G. Rollefson, "The quenching of fluorescence. Deviations from the Stern-Volmer law," *Journal of the American Chemical Society,* vol. 72, pp. 3435-3443, 1950.

[341] K. Hong and J. Noolandi, "Solution of the Smoluchowski equation with a Coulomb potential. II. Application to fluorescence quenching," *The Journal of Chemical Physics,* vol. 68, p. 5172, 1978.

[342] K. Hong and J. Noolandi, "Solution of the Smoluchowski equation with a Coulomb potential. I. General results," *The Journal of Chemical Physics,* vol. 68, p. 5163, 1978.

[343] A. Szabo, "Theory of diffusion-influenced fluorescence quenching," *The Journal of Physical Chemistry,* vol. 93, pp. 6929-6939, 1989.

[344] U. Christensen, "Convection with pressure-and temperature-dependent non-Newtonian rheology," *Geophysical Journal International,* vol. 77, pp. 343-384, 1984.

[345] N. B. Colthup, L. H. Daly, and S. E. Wiberley, "Introduction to infrared and Raman spectroscopy," Boston, MA: Academic press, 1990, pp. 1-74.

[346] B. H. Stuart, "Infrared Spectroscopy: Fundamentals and Applications," Hoboken, NJ: John Wiley and Sons, 2004, pp. 1-13.

[347] C. D. Slater, D. G. Nyberg, and J. Vikin, "Infrared spectroscopy," Boston, MA: W. Grant Press, 1974, pp. 1-56.

[348] N. Colthup, "Spectra-structure correlations in the infra-red region," *JOSA,* vol. 40, pp. 397-400, 1950.

[349] J. M. Hunt, M. P. Wisherd, and L. C. Bonham, "Infrared absorption spectra of minerals and other inorganic compounds," *Analytical Chemistry,* vol. 22, pp. 1478-1497, 1950.

[350] S. Krimm, "Infrared spectra of high polymers," Ann Arbor, Michigan: Harrison M. Randall Laboratory of Physics, University of Michigan, 1960. pp. 52-58.

[351] E. B. Wilson, "Molecular vibrations: the theory of infrared and Raman vibrational spectra," New York: Dover Publications, 1955, pp. 1-10.

[352] J. M. Hornback, "Organic Chemistry," 2nd ed, Belmont, CA: Thomson Brooks/Cole, 2006, pp. 532.

[353] D. R. Klein, "Organic Chemistry," Hoboken, NJ: John Wiley & Sons, 2011, pp. 688-694.

[354] J. W. Suggs, "Organic Chemistry," Hauppague, NY: Barrons Educational Series Incorporated, 2002, pp. 204-215.

[355] E. Castillo, J. Koenig, J. Anderson, C. Kliment, and J. Lo, "Surface analysis of biomedical polymers by attenuated total reflectance-Fourier transform infra-red," *Biomaterials,* vol. 5, pp. 186-193, 1984.

[356] K. Oberg, B. A. Chrunyk, R. Wetzel, and A. L. Fink, "Native-like Secondary Structure in Interleukin-1. beta. Inclusion Bodies by Attenuated Total Reflectance FTIR," *Biochemistry,* vol. 33, pp. 2628-2634, 1994.

[357] J. J. van Soest, H. Tournois, D. de Wit, and J. F. Vliegenthart, "Short-range structure in (partially) crystalline potato starch determined with attenuated total reflectance Fourier-transform IR spectroscopy," *Carbohydrate Research,* vol. 279, pp. 201-214, 1995.

[358] R. Potts, D. Guzek, R. Harris, and J. McKie, "A noninvasive, in vivo technique to quantitatively measure water concentration of the stratum corneum using attenuated total-reflectance infrared spectroscopy," *Archives of Dermatological Research,* vol. 277, pp. 489-495, 1985.

[359] K. A. Oberg and A. L. Fink, "A new attenuated total reflectance Fourier transform infrared spectroscopy method for the study of proteins in solution," *Analytical Biochemistry,* vol. 256, pp. 92-106, 1998.

[360] J. H. Simons, "Fluorine chemistry," New York: Academic Press, 1950, pp. 42

[361] D. Weiblen, "The infrared spectra of fluorocarbons and related compounds vol. 2," NewYork: Academic Press, 1954, pp. 458.

[362] G. Socrates and G. Socrates, "Infrared and Raman characteristic group frequencies: tables and charts," New York: Wiley, 2001, pp. 1-366.

[363] J. M. García-Martínez, O. Laguna, S. Areso, and E. Collar, "FTIR quantitative characterization of chemically modified polypropylenes containing succinic grafted groups," *Journal of Applied Polymer Science,* vol. 73, pp. 2837-2847, 1999.

[364] L. D. Tickanen, M. I. Tejedor-Tejedor, and M. A. Anderson, "Quantitative characterization of aqueous suspensions using variable-angle ATR-FTIR spectroscopy: Determination of optical constants and absorption coefficient spectra," *Langmuir,* vol. 13, pp. 4829-4836, 1997.

[365] F. B. Reig, J. Adelantado, and M. Moya Moreno, "FTIR quantitative analysis of calcium carbonate (calcite) and silica (quartz) mixtures using the constant ratio method. Application to geological samples," *Talanta,* vol. 58, pp. 811-821, 2002.

[366] P. Rasband and W. Hecker, "Catalyst characterization using quantitative FTIR: CO on supported Rh," *Journal of Catalysis,* vol. 139, pp. 551-560, 1993.

[367] T. Onfroy, G. Clet, and M. Houalla, "Quantitative IR characterization of the acidity of various oxide catalysts," *Microporous and Mesoporous Materials,* vol. 82, pp. 99-104, 2005.

[368] L. De Broglie, "The wave nature of the electron," *Nobel Lecture,* pp. 244-56, 1929.

[369] A. Einstein, "Quantum theory of the monoatomic ideal gas," *Sitzungsber. Preuss. Akad. Wiss,* p. 261, 1924.

[370] D. B. Williams and C. B. Carter, "The Transmission Electron Microscope: a textbook for materials science," 2nd ed, New York: Springer, 2009, pp. 4-8.

[371] A. Den Dekker and A. Van den Bos, "Resolution: a survey," *JOSA A,* vol. 14, pp. 547-557, 1997.

[372] L. Rayleigh, "XXXI. investigations in optics, with special reference to the spectroscope," *The London, Edinburgh, and Dublin Philosophical Magazine and Journal of Science,* vol. 8, pp. 261-274, 1879.

[373] B. S. Murty, P. Shankar, B. B. Rath, and J. Murday, "Textbook of Nanoscience and Nanotechnology," London: Springer, 2012, pp. 176-213.

[374] H. D. Espinosa and G. Bao, "Nano and Cell Mechanics: Fundamentals and Frontiers," Chichester, England: Wiley, 2012, pp. 115-119.

[375] S. Jennings, "The mean free path in air," *Journal of Aerosol Science,* vol. 19, pp. 159-166, 1988.

[376] D. B. Williams and C. B. Carter, "The Transmission Electron Microscope: a textbook for materials science," 2nd ed, New York: Springer, 2009, pp. 127-140.

[377] J. Kuo, "Electron Microscopy: Methods and Protocols," Totowa, NJ: Humana Press, 2007, pp. 35-45.

[378] J. J. Bozzola and L. D. Russell, "Electron Microscopy: Principles and Techniques for Biologists," Sudbury, MA: Jones and Bartlett Publishers, 1999, pp. 16-47.

[379] M. Adrian, J. Dubochet, J. Lepault, and A. W. McDowall, "Cryo-electron microscopy of viruses," *Nature*, vol. 308, pp. 32-36, 1984.

[380] K. McDonald, "Cryopreparation methods for electron microscopy of selected model systems," *Methods in Cell Biology,* vol. 79, pp. 23-56, 2007.

[381] R. A. Steinbrecht and K. Zierold, "Cryotechniques in Biological Electron Microscopy," New York: Springer-Verlag, 2011, pp. 175-191.

[382] V. Mittal and N. B. Matsko, "Analytical Imaging Techniques for Soft Matter Characterization," NewYork: Springer, 2012, pp. 18.

[383] H. Takeuchi, H. Yamamoto, and Y. Kawashima, "Mucoadhesive nanoparticulate systems for peptide drug delivery," *Advanced Drug Delivery Reviews,* vol. 47, pp. 39-54, 2001.

[384] H. Takeuchi, H. Yamamoto, T. Niwa, T. Hino, and Y. Kawashima, "Enteral absorption of insulin in rats from mucoadhesive chitosan-coated liposomes," *Pharmaceutical Research,* vol. 13, pp. 896-901, 1996.

[385] H.-S. Lee, D. M. Eckmann, D. Lee, N. J. Hickok, and R. J. Composto, "Symmetric pH-dependent swelling and antibacterial properties of chitosan brushes," *Langmuir,* vol. 27, pp. 12458-12465, 2011.

[386] M. M. Kaneda, S. Caruthers, G. M. Lanza, and S. A. Wickline, "Perfluorocarbon nanoemulsions for quantitative molecular imaging and targeted therapeutics," *Annals of Biomedical Engineering,* vol. 37, pp. 1922-1933, 2009.

[387] D. J. McClements, "Design of Nano-Laminated Coatings to Control Bioavailability of Lipophilic Food Components," *Journal of Food Science,* vol. 75, pp. R30-R42, 2010.

[388] M. Barea, M. Jenkins, M. Gaber, and R. Bridson, "Evaluation of liposomes coated with a pH responsive polymer," *International Journal of Pharmaceutics,* vol. 402, pp. 89-94, 2010.

[389] J. Jerobin, R. Sureshkumar, C. Anjali, A. Mukherjee, and N. Chandrasekaran, "Biodegradable polymer based encapsulation of neem oil nanoemulsion for controlled release of Aza-A," *Carbohydrate Polymers,* 2012.

[390] Y. Ohguchi, K. Kawano, Y. Hattori, and Y. Maitani, "Selective delivery of folate-PEG-linked, nanoemulsion-loaded aclacinomycin A to KB nasopharyngeal cells and xenograft: effect of chain length and amount of folate-PEG linker," *Journal of Drug Targeting,* vol. 16, pp. 660-667, 2008.

[391] K. S. Soppimath, T. M. Aminabhavi, A. R. Kulkarni, and W. E. Rudzinski, "Biodegradable polymeric nanoparticles as drug delivery devices," *Journal of Controlled Release,* vol. 70, pp. 1-20, 2001.

[392] P. P. Constantinides, M. V. Chaubal, and R. Shorr, "Advances in lipid nanodispersions for parenteral drug delivery and targeting," *Advanced Drug Delivery Reviews,* vol. 60, pp. 757-767, 2008.

[393] O. M. Koo, I. Rubinstein, and H. Onyuksel, "Role of nanotechnology in targeted drug delivery and imaging: a concise review," *Nanomedicine: Nanotechnology, Biology and Medicine,* vol. 1, pp. 193-212, 2005.

[394] P. Billsten, U. Carlsson, B. H. Jonsson, G. Olofsson, F. Höök, and H. Elwing, "Conformation of human carbonic anhydrase II variants adsorbed to silica nanoparticles," *Langmuir,* vol. 15, pp. 6395-6399, 1999.

[395] M. Lundqvist, I. Sethson, and B.-H. Jonsson, "Protein adsorption onto silica nanoparticles: conformational changes depend on the particles' curvature and the protein stability," *Langmuir,* vol. 20, pp. 10639-10647, 2004.

[396] L. Shang, Y. Wang, J. Jiang, and S. Dong, "pH-dependent protein conformational changes in albumin: gold nanoparticle bioconjugates: a spectroscopic study," *Langmuir,* vol. 23, pp. 2714-2721, 2007.

[397] T.-Q. Nguyen, V. Doan, and B. J. Schwartz, "Conjugated polymer aggregates in solution: Control of interchain interactions," *The Journal of Chemical Physics,* vol. 110, p. 4068, 1999.

[398] T. Tuomi, M. J. Rowley, W. J. Knowles, Q.-Y. Chen, T. McAnally, P. Z. Zimmet, *et al.*, "Autoantigenic properties of native and denatured glutamic acid decarboxylase: evidence for a conformational epitope," *Clinical Immunology and Immunopathology,* vol. 71, pp. 53-59, 1994.

[399] Y. Itoh, K. Itoh, M. B. Frank, and M. Reichlin, "Autoantibodies to the Ro/SSA autoantigen are conformation dependent II: antibodies to the denatured form of 52 kD Ro/SSA are a cross reacting subset of antibodies to the native 60 kD Ro/SSA molecule," *Autoimmunity,* vol. 14, pp. 89-95, 1992.

[400] N. C. Reich, P. Sarnow, E. Duprey, and A. J. Levine, "Monoclonal antibodies which recognize native and denatured forms of the adenovirus DNA-binding protein," *Virology,* vol. 128, pp. 480-484, 1983.

[401] H. Elwing, B. Nilsson, K.-E. Svensson, A. Askendahl, U. R. Nilsson, and I. Lundström, "Conformational changes of a model protein (complement factor 3) adsorbed on hydrophilic and hydrophobic solid surfaces," *Journal of Colloid and Interface Science,* vol. 125, pp. 139-145, 1988.

[402] C. G. Glabe, "Conformation-dependent antibodies target diseases of protein misfolding," *Trends in Biochemical Sciences,* vol. 29, pp. 542-547, 2004.

[403] J. Schurr, "Dynamic light scattering of biopolymers and biocolloids," *CRC Critical Reviews in Biochemistry,* vol. 4, p. 371, 1977.

[404] R. Tanner, B. Herpigny, S. H. Chen, and C. Rha, "Conformational change of protein sodium dodecylsulfate complexes in solution: A study of dynamic light scattering," *The Journal of Chemical Physics,* vol. 76, p. 3866, 1982.

[405] M. DATHE, H. FABIAN, K. GAST, D. ZIRWER, R. WINTER, M. BEYERMANN, *et al.*, "Conformational differences of ovine and human corticotrophin releasing hormone A CD, IR, NMR and dynamic light scattering study," *International Journal of Peptide and Protein Research,* vol. 47, pp. 383-393, 1996.

[406] G. D. Smith, D. Y. Yoon, R. L. Jaffe, R. H. Colby, R. Krishnamoorti, and L. J. Fetters, "Conformations and structures of poly (oxyethylene) melts from molecular dynamics simulations and small-angle neutron scattering experiments," *Macromolecules,* vol. 29, pp. 3462-3469, 1996.

[407] R. G. Kirste and H. G. Ohm, "The conformation of liquid‐crystalline polymers as revealed by neutron scattering," *Die Makromolekulare Chemie, Rapid Communications,* vol. 6, pp. 179-185, 1985.

[408] G. Lieser, E. Fischer, and K. Ibel, "Conformation of polyethylene molecules in the melt as revealed by small‐angle neutron scattering," *Journal of Polymer Science: Polymer Letters Edition,* vol. 13, pp. 39-43, 1975.

[409] P. I. Haris and D. Chapman, "The conformational analysis of peptides using Fourier transform IR spectroscopy," *Biopolymers,* vol. 37, pp. 251-263, 1995.

[410] K. Payne and A. Veis, "Fourier transform IR spectroscopy of collagen and gelatin solutions: deconvolution of the amide I band for conformational studies," *Biopolymers,* vol. 27, pp. 1749-1760, 1988.

[411] G. Kister, G. Cassanas, and M. Vert, "Effects of morphology, conformation and configuration on the IR and Raman spectra of various poly(lactic acid)s," *Polymer,* vol. 39, pp. 267-273, 1998.

[412] X. Chen, Z. Shao, N. S. Marinkovic, L. M. Miller, P. Zhou, and M. R. Chance, "Conformation transition kinetics of regenerated< i> Bombyx mori</i> silk fibroin membrane monitored by time-resolved FTIR spectroscopy," *Biophysical Chemistry,* vol. 89, pp. 25-34, 2001.

[413] K.-V. Schubert and E. Kaler, "Microemulsifying fluorinated oils with mixtures of fluorinated and hydrogenated surfactants," *Colloids and Surfaces A: Physicochemical and Engineering Aspects,* vol. 84, pp. 97-106, 1994.

[414] K. Kalyanasundaram, "Pyrene fluorescence as a probe of fluorocarbon micelles and their mixed micelles with hydrocarbon surfactants," *Langmuir,* vol. 4, pp. 942-945, 1988.

[415] W. E. Acree and M. H. Abraham, "Solubility predictions for crystalline polycyclic aromatic hydrocarbons (PAHs) dissolved in organic solvents based upon the Abraham general solvation model," *Fluid Phase Equilibria,* vol. 201, pp. 245-258, 2002.

[416] C. Washington, "Stability of lipid emulsions for drug delivery," *Advanced Drug Delivery Reviews,* vol. 20, pp. 131-145, 1996.

[417] D. Stuart and T. Allen, "A new liposomal formulation for antisense oligodeoxynucleotides with small size, high incorporation efficiency and good stability," *Biochimica et Biophysica Acta (BBA)-Biomembranes,* vol. 1463, pp. 219-229, 2000.

[418] Y. Lvov, K. Ariga, I. Ichinose, and T. Kunitake, "Assembly of multicomponent protein films by means of electrostatic layer-by-layer adsorption," *Journal of the American Chemical Society,* vol. 117, pp. 6117-6123, 1995.

[419] J. Pecher and S. Mecking, "Nanoparticles of conjugated polymers," *Chemical Reviews,* vol. 110, pp. 6260-6279, 2010.

[420] D. G. Dalgleish, "Adsorption of protein and the stability of emulsions," *Trends in Food Science & Technology,* vol. 8, pp. 1-6, 1997.

[421] R. Pal and E. Rhodes, "Viscosity/ Concentration Relationships for Emulsions," *Journal of Rheology,* vol. 33, p. 1021, 1989.

[422] D. L. Klass and T. W. Martinek, "Electroviscous fluids. I. Rheological properties," *Journal of Applied Physics,* vol. 38, pp. 67-74, 1967.

[423] Q. Gan, T. Wang, C. Cochrane, and P. McCarron, "Modulation of surface charge, particle size and morphological properties of chitosan–TPP nanoparticles intended for gene delivery," *Colloids and Surfaces B: Biointerfaces,* vol. 44, pp. 65-73, 2005.

[424] T. Imai, S. Ohyama, A. Kovalenko, and F. Hirata, "Theoretical study of the partial molar volume change associated with the pressure-induced structural transition of ubiquitin," *Protein Science,* vol. 16, pp. 1927-1933, 2007.

[425] R. S. Cantor, "Lateral pressures in cell membranes: a mechanism for modulation of protein function," *The Journal of Physical Chemistry B,* vol. 101, pp. 1723-1725, 1997.

[426] B. van den Berg, R. J. Ellis, and C. M. Dobson, "Effects of macromolecular crowding on protein folding and aggregation," *The EMBO Journal,* vol. 18, pp. 6927-6933, 1999.

[427] D. Homouz, M. Perham, A. Samiotakis, M. S. Cheung, and P. Wittung-Stafshede, "Crowded, cell-like environment induces shape changes in aspherical protein," *Proceedings of the National Academy of Sciences,* vol. 105, pp. 11754-11759, 2008.

[428] S. Martins, B. Sarmento, E. B. Souto, and D. C. Ferreira, "Insulin-loaded alginate microspheres for oral delivery–effect of polysaccharide reinforcement on physicochemical properties and release profile," *Carbohydrate Polymers,* vol. 69, pp. 725-731, 2007.

[429] P. C. Lee and D. Meisel, "Photophysical studies of pyrene incorporated in NAFION membranes," *Photochemistry and Photobiology,* vol. 41, pp. 21-26, 1985.

[430] W. E. Acree Jr and M. H. Abraham, "Solubility predictions for crystalline polycyclic aromatic hydrocarbons (PAHs) dissolved in organic solvents based upon the Abraham general solvation model," *Fluid Phase Equilibria,* vol. 201, pp. 245-258, 2002.

[431] M. W. Geiger and N. J. Turro, "Pyrene fluorescence lifetime as a probe for oxygen penetration of micelles," *Photochemistry and Photobiology,* vol. 22, pp. 273-276, 1975.

[432] R. Figueroa Jr, B. G. Harrison Jr, and J. P. SaNogueira, "Oil-in-water-in-silicone emulsion compositions," U.S. Patents 4 960 764, October 2, 1990.

[433] J.-W. Kim, Y.-G. Joe, and K.-D. Suh, "Poly (methyl methacrylate) hollow particles by water-in-oil-in-water emulsion polymerization," *Colloid and Polymer Science,* vol. 277, pp. 252-256, 1999.

[434] H.-J. Kim, K. A. Yoon, M. Hahn, E.-S. Park, and S.-C. Chi, "Preparation and in vitro evaluation of self-microemulsifying drug delivery systems containing

idebenone," *Drug Development and Industrial Pharmacy,* vol. 26, pp. 523-529, 2000.

[435] K. SUZUKI, I. SHUTO, and Y. HAGURA, "Characteristics of the membrane emulsification method combined with preliminary emulsification for preparing corn oil-in-water emulsions," *Food Science and Technology International, Tokyo,* vol. 2, pp. 43-47, 1996.

[436] D. McClements and E. Decker, "Lipid Oxidation in Oil¬in¬Water Emulsions: Impact of Molecular Environment on Chemical Reactions in Heterogeneous Food Systems," *Journal of Food Science,* vol. 65, pp. 1270-1282, 2000.

[437] R. Katoh, Y. Asano, A. Furuya, K. Sotoyama, and M. Tomita, "Preparation of food emulsions using a membrane emulsification system," *Journal of Membrane Science,* vol. 113, pp. 131-135, 1996.

[438] W. Peschel, F. Sánchez-Rabaneda, W. Diekmann, A. Plescher, I. Gartzía, D. Jiménez, *et al.*, "An industrial approach in the search of natural antioxidants from vegetable and fruit wastes," *Food Chemistry,* vol. 97, pp. 137-150, 2006.

[439] O. Regev, S. Ezrahi, A. Aserin, N. Garti, E. Wachtel, E. Kaler, *et al.*, "A study of the microstructure of a four-component nonionic microemulsion by cryo-TEM, NMR, SAXS, and SANS," *Langmuir,* vol. 12, pp. 668-674, 1996.

[440] H. Jeffery, S. Davis, and D. O'hagan, "The preparation and characterisation of poly (lactide-co-glycolide) microparticles. I: Oil-in-water emulsion solvent evaporation," *International Journal of Pharmaceutics,* vol. 77, pp. 169-175, 1991.

[441] K. Zhu, H. Jiang, X. Du, J. Wang, W. Xu, and S. Liu, "Preparation and characterization of hCG-loaded polylactide or poly (lactide-co-glycolide) microspheres using a modified water-in-oil-in-water (w/o/w) emulsion solvent evaporation technique," *Journal of Microencapsulation,* vol. 18, pp. 247-260, 2001.

[442] P. Fernandez, V. André, J. Rieger, and A. Kühnle, "Nano-emulsion formation by emulsion phase inversion," *Colloids and Surfaces A: Physicochemical and Engineering Aspects,* vol. 251, pp. 53-58, 2004.

[443] R. C. Pasquali, N. Sacco, and C. Bregni, "The Studies on Hydrophilic-Lipophilic Balance (HLB): Sixty Years after William C. Griffin's Pioneer Work (1949-2009)," *Latin American Journal of Pharmacy,* vol. 28, pp. 313-7, 2009.

[444] *Handbook of Chemistry and Physics,* 45th ed, Chemical Rubber Pub., Cleveland, OH, 1964.

[445] A. Waggoner, "Fluorescent labels for proteomics and genomics," *Current Opinion in Chemical Biology,* vol. 10, pp. 62-66, 2006.

[446] F. A. Carey and R. J. Sundberg, "Advanced Organic Chemistry: Structure and mechanisms," Norwell, MA: Springer, 2007, pp. 8-10.

[447] R. E. Schirmer, "Modern methods of pharmaceutical analysis," 2nd ed, Boca Raton, FL: CRC Press, 1991, pp. 305.

[448] A. L. Horvath, "Molecular design: chemical structure generation from the properties of pure organic compounds," New York: Elsevier, 1992, pp. 518.

[449] J. F. Ellena, V. V. Obraztsov, V. L. Cumbea, C. M. Woods, and D. S. Cafiso, "Perfluorooctyl bromide has limited membrane solubility and is located at the bilayer center. Locating small molecules in lipid bilayers through paramagnetic enhancements of NMR relaxation," *Journal of Medicinal Chemistry,* vol. 45, pp. 5534-5542, 2002.

[450] D. Karpovich and G. Blanchard, "Relating the polarity-dependent fluorescence response of pyrene to vibronic coupling. Achieving a fundamental understanding of the py polarity scale," *The Journal of Physical Chemistry,* vol. 99, pp. 3951-3958, 1995.

[451] D. M. Long, M.-s. Liu, P. S. Szanto, D. P. Alrenga, M. M. Patel, M. V. Rios, *et al.*, "Efficacy and toxicity studies with radiopaque perfluorocarbon," *Radiology,* vol. 105, pp. 323-332, 1972.

[452] R. Bucala, M. Kawakami, and A. Cerami, "Cytotoxicity of a perfluorocarbon blood substitute to macrophages in vitro," *Science,* vol. 220, pp. 965-967, 1983.

[453] G. M. Vercellotti, D. E. Hammerschmidt, P. R. Craddock, and H. S. Jacob, "Activation of plasma complement by perfluorocarbon artificial blood: probable mechanism of adverse pulmonary reactions in treated patients and rationale for corticosteroids prophylaxis," *Blood,* vol. 59, pp. 1299-1304, 1982.

[454] S. Chang, "Perfluorocarbon liquids in vitreoretinal surgery," *International Ophthalmology Clinics,* vol. 32, pp. 153-163, 1992.

[455] W. G. Hundley, A. M. Kizilbash, I. Afridi, F. Franco, R. M. Peshock, and P. A. Grayburn, "Administration of an intravenous perfluorocarbon contrast agent improves echocardiographic determination of left ventricular volumes and ejection fraction: comparison with cine magnetic resonance imaging," *Journal of the American College of Cardiology,* vol. 32, pp. 1426-1432, 1998.

[456] B. P. Fuhrman, P. R. Paczan, and M. Defrancisis, "Perfluorocarbon-associated gas exchange," *Critical Care Medicine,* vol. 19, pp. 712-722, 1991.

[457] C. L. Leach, B. P. Fuhrman, F. C. Morin III, and M. G. Rath, "Perfluorocarbon-associated gas exchange (partial liquid ventilation) in respiratory distress syndrome A prospective, randomized, controlled study," *Critical Care Medicine,* vol. 21, pp. 1270-1278, 1993.

[458] A. S. Tütüncü, N. S. Faithfull, and B. Lachmann, "Intratracheal perfluorocarbon administration combined with mechanical ventilation in experimental respiratory distress syndrome: Dose-dependent improvement of gas exchange," *Critical Care Medicine,* vol. 21, pp. 962-969, 1993.

[459] C. Sharts, A. Reese Kenneth, F. K. Multer, M. D. Nielson, and A. G. Greenburg, "The solubility of oxygen in aqueous fluorocarbon emulsions," *Journal of Fluorine Chemistry,* vol. 11, pp. 637-641, 1978.

[460] S. Yasui and T. Keiderling, "Vibrational circular dichroism of polypeptides. 8. Poly (lysine) conformations as a function of pH in aqueous solution," *Journal of the American Chemical Society,* vol. 108, pp. 5576-5581, 1986.

[461] P. M. Claesson and B. W. Ninham, "pH-dependent interactions between adsorbed chitosan layers," *Langmuir,* vol. 8, pp. 1406-1412, 1992.

[462] S. Lee and N. D. Spencer, "Adsorption properties of poly (L-lysine)-graft-poly (ethylene glycol)(PLL-g-PEG) at a hydrophobic interface: influence of tribological stress, pH, salt concentration, and polymer molecular weight," *Langmuir,* vol. 24, pp. 9479-9488, 2008.

[463] J. Cho, M.-C. Heuzey, A. Bégin, and P. J. Carreau, "Viscoelastic properties of chitosan solutions: Effect of concentration and ionic strength," *Journal of Food Engineering,* vol. 74, pp. 500-515, 2006.

[464] S. Boddohi, C. E. Killingsworth, and M. J. Kipper, "Polyelectrolyte multilayer assembly as a function of pH and ionic strength using the polysaccharides chitosan and heparin," *Biomacromolecules,* vol. 9, pp. 2021-2028, 2008.

[465] T. J. Yu, J. L. Lippert, and W. L. Peticolas, "Laser Raman studies of conformational variations of poly-L-lysine," *Biopolymers,* vol. 12, pp. 2161-2176, 1973.

[466] K. Shiraishi, R. Endoh, H. Furuhata, M. Nishihara, R. Suzuki, K. Maruyama, *et al.*, "A facile preparation method of a PFC-containing nano-sized emulsion for theranostics of solid tumors," *International journal of pharmaceutics,* vol. 421, pp. 379-387, 2011.

[467] B. Sumer and J. Gao, "Theranostic nanomedicine for cancer," *Nanomedicine,* vol. 3, pp. 137-140, 2008.

[468] R. Bardhan, S. Lal, A. Joshi, and N. J. Halas, "Theranostic nanoshells: from probe design to imaging and treatment of cancer," *Accounts of Chemical Research,* vol. 44, pp. 936-946, 2011.

[469] D. Pan, S. D. Caruthers, G. Hu, A. Senpan, M. J. Scott, P. J. Gaffney, *et al.*, "Ligand-directed nanobialys as theranostic agent for drug delivery and manganese-based magnetic resonance imaging of vascular targets," *Journal of the American Chemical Society,* vol. 130, pp. 9186-9187, 2008.